JPRS L/9795

18 June 1981

USSR Report

PHYSICS AND MATHEMATICS

(FOUO 5/81)

Investigations of the Gas-Phase Cavity-Type Nuclear Reactor

FBIS FOREIGN BROADCAST INFORMATION SERVICE

NOTE

JPRS publications contain information primarily from foreign newspapers, periodicals and books, but also from news agency transmissions and broadcasts. Materials from foreign-language sources are translated; those from English-language sources are transcribed or reprinted, with the original phrasing and other characteristics retained.

Headlines, editorial reports, and material enclosed in brackets [] are supplied by JPRS. Processing indicators such as [Text] or [Excerpt] in the first line of each item, or following the last line of a brief, indicate how the original information was processed. Where no processing indicator is given, the information was summarized or extracted.

Unfamiliar names rendered phonetically or transliterated are enclosed in parentheses. Words or names preceded by a question mark and enclosed in parentheses were not clear in the original but have been supplied as appropriate in context. Other unattributed parenthetical notes within the body of an item originate with the source. Times within items are as given by source.

The contents of this publication in no way represent the policies, views or attitudes of the U.S. Government.

APPROVED FOR RELEASE: 2007/02/09: CIA-RDP82-00850R000400020034-8

JPRS L/9795

18 June 1981

USSR REPORT

PHYSICS AND MATHEMATICS

(FOUO 5/81)

INVESTIGATIONS OF THE GAS-PHASE CAVITY-TYPE NUCLEAR REACTOR

CONTENTS

UDC 621.039.52

SOME RESULTS OF INVESTIGATIONS OF THE GAS-PHASE CAVITY-TYPE NUCLEAR REACTOR

Moscow IZVESTIYA AKADEMII NAUK SSSR: ENERGETIKA I TRANSPORT in Russian No 6, 1977 pp 24-31

[Article by V. M. Iyevlev, Moscow]

[Text] The diagram and characteristic features of a new type nuclear reactor--the gas-phase cavity-type nuclear reactor--are described briefly. The principle factors which determine the prospects for using this reactor in power engineering are indicated. Some results of investigating the main processes in a gas-phase reactor are presented.

Many papers have been devoted to research on gas-phase reactors (see, for example [1-3]). Our investigations in this direction were carried out in parallel and to a considerable extent independently. A brief survey of the results of these investigations is presented in the article.*

We are talking about a reactor (Figure 1) in which gaseous nuclear fuel (UF6) or, at higher temperatures, uranium plasma) is located in the center of a cavity surrounded by a moderator-coolant. Another gas--the working substance--flows near the walls. Special measures are undertaken to produce mixing of the working substance and the uranium. The heat released during the nuclear reaction is dissipated from the uranium zone mainly by means of thermal radiation.

Radiation heats the darkened working substance in layers to significantly higher temperatures than can be achieved when the gas is heated from the walls; a relatively cold gas layer remains near the wall in this case. The radiation from

*The materials outlined in the article were reported at the 11th Conference on Energy Conversion in the United States in September 1976.

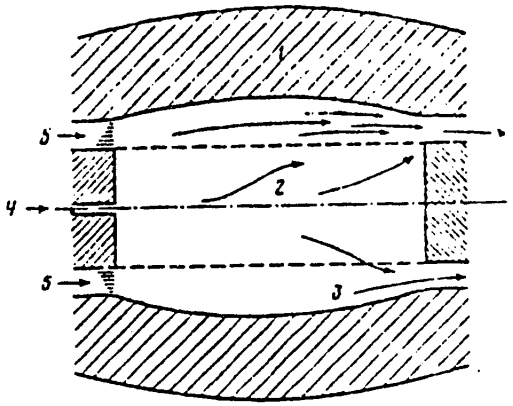

Figure 1. Diagram of Gas-Phase Cavity-Type Nuclear Reactor: 1--moderator-coolant; 2--gaseous fission zone; 3--working substance flow zone; 4--delivery of fissionable material; 5--delivery of working substance

the uranium zone can be dissipated at low output outside the reactor by means of a corresponding reflecting system.

The prospects of a gas-phase reactor for many areas of application--for heavy-duty electric power plants, high-temperature production systems, space power plants and engines, to produce very high neutron fluxes and so on--are noted in the American literature. The conclusions from our investigations are the same. A simplified diagram of an electric power plant with output of $6 \cdot 10^6$ kW, which includes a gas-phase reactor, MHD generator, working substance and uranium circulating circuits, separation, purification, heat-dumping systems and so on, is presented as one of the considered examples in Figure 2.

Analysis made it possible to determine the main advantages of electric power plants with gas-phase reactor: they include:

1) High efficiency (up to approximately 60-70 percent when using combination schemes). This improves the use of nuclear fuel and, which is especially important, reduces thermal pollution of the environment.

2) The possibility of increasing the heat-dump temperature (due to the very high temperature of heating the working substance in the reactor) without severe deterioration of efficiency and in this regard of providing economic heat removable to the atmosphere rather than into water.

3) The possibility of achieving considerably higher nuclear fuel conversion coefficients than in the presently used thermal neutron power engineering reactors. This is explained by the small amount of construction materials in the gas-phase reactor compared to an ordinary reactor of the same output. Breeding (conversion

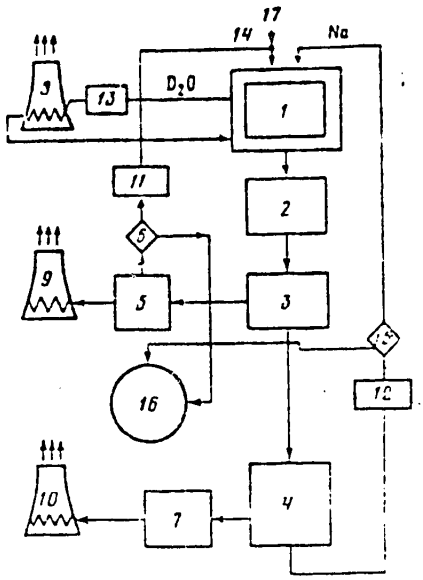

Figure 2. Diagram of Electric Power Plant With Gas-Phase Reactor: 1--gas-phase reactor, thermal output of 10^4 MW; 2--MHD generator with electric output of $4 \cdot 10^3$ MW; 3--separator for separation of working substance and nuclear fuel; 4--heat exchanger-steam generator; 5--heat exchanger; 6--nuclear fuel purification system; 7--steam-turbogenerator part of electric power plant with electric output of $2 \cdot 10^3$ MW; 8-10--"dry cooling towers" with thermal output of $1.5 \cdot 10^3$, $0.5 \cdot 10^3$ and $2 \cdot 10^3$ MW, respectively; 11-13--pumps; 14--nuclear fuel circulating line; 15--working substance purification system; 16--fission byproducts collector; 17--nuclear fuel feed

factor of approximately 1.05-1.07) can be achieved in U-233 (the thorium cycle) and the conversion factor comprises 0.8-0.9 in U-235.

4) The low uranium load to the reactor (tens of kilograms).

5) The permissibility of limiting oneself to relatively low-level purification of the circulating media of fission fragments since purification should prevent only reactor slagging. This permits one to hope that special plants for processing fuel elements required for ordinary reactors will be replaced by a purification system located in the circuit and will provide complete combustion of the uranium delivered to the reactor.

6) Reduction of the danger of emergency situations and facilitating repair operations with regard to continuous removal of fission byproducts from the circuits.

It should be noted that investigations in power engineering based on a gas-phase reactor are in good agreement with a number of trends of the thermonuclear program.

These and other prospects are intriguing and determination of the principle problems of the feasibility of processes in a gas-phase reactor should precede detailed development of any kind of designs.

Let us briefly present the results of some investigations in this direction.

One of the determining problems is reducing the mixing of the working substance and the gaseous uranium and thus reducing the uranium flow rate through the reactor. This is important not only for open-type installations but also for closed-type installations since an increase of uranium flow rate complicates development of the circuit, makes it difficult to control the reactor due to a reduction of delayed neutrons with short presence of their predecessors in the reactor and so on. Moreover, it is imporatnt to force the uranium away from the walls.

Three methods of affecting turbulent mixing and generally on the flow in the reactor cavity were investigated: suppression of initial perturbations and special profiling of the flow rate, twisting of the flow and the effects of a magnetic field.

The principles of jet flows (to which the flow in the reactor cavity is similar) with developed turbulence have been thoroughly studied. However, the effect of initial disturbances and the initial velocity profile on transition to turbulence in the jets and on the principles of mixing have as yet been little investigated. This was also the subject of the investigations in the first of the directions indicated above (some results have been published in [4, 5]). The initial velocity profile in coaxial flows was formed by means of a honeycomb and variation of the shape of the input channel. The dimensions of the honeycomb cells and the thickness of the edges varied. Transition to turbulence occurs very rapidly at the input with sharp, intermittent variation of velocity on the boundary; the transition can be drawn out very much even at high Reynolds numbers with smooth variation of velocity in the initial cross-section. The Reynolds number affects transition in the entire investigated range. The length of the transition section is strongly and nonmonotonically dependent on the size of the honeycomb cells, reaching a maximum at a certain size.

The laminar flow mode is retained at a length equal to tens of initial thicknesses of the layer with variable flow rate with optimum selection of parameters.

However, the effectiveness of using only this method of reducing gas mixing in the reactor cavity is limited by the development of free convection in the low-velocity zone. A good means of stabilizing the flow is twisting it if the density of the medium increases with an increase of radius, i. e., if a sufficiently heavy working substance can be used (although twisting may also occur with a light working substance in some zones of the reactor cavity).

The magnetic field has a very strong effect on the flow of conducting gases at high temperatures (see, for example [6, 7]). A longitudinal field whose lines of force are approximately parallel to the mean flow rate and the uranium-working substance interface should be used in the reactor.

[Figure 3 not available]

It is known that one of the effects of a longitudinal magnetic field is suppression of turbulence. This is illustrated in Figure 4 on the example of simple flows. Quenching of uniform lattice turbulence in molten metal in a magnetic field and a decrease of the resistance coefficient during flow of molten metal in a tube in a longitudinal magnetic field are presented here. The effect of this field on molten-metal and plasma flows, mixing of which is sharply reduced, is shown in Figure 5. The results of theoretical calculations, which agree quite satisfactorily with experiment, are also presented in Figures 4 and 5.

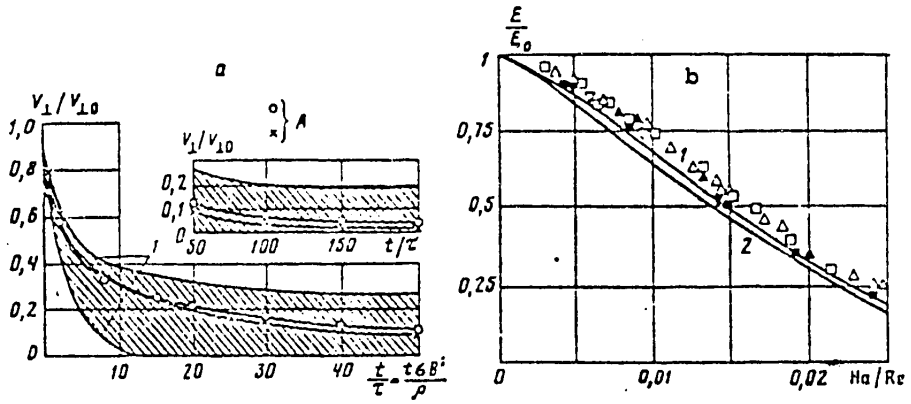

Figure 4. Effect of Magnetic Field on Turbulent Flows: a--quenching of uniform turbulence; v--pulsating velocity component perpendicular to direction of magnetic field; A--experimental data [8]; 1--calculation of limiting cases from [7]; b--coefficient of resistance ξ during flow of molten metal in a tube in a longitudinal magnetic field (ξ_0 is the value of ξ without a field); experimental data of [9]; 1 and 2--calculation from [7] for limiting parameters in experiments.

Besides affecting turbulence, a strong magnetic field permits one to suppress free convection and is an efficient stabilizing factor with respect to possible thermoacoustic oscillations in some cases [12].

However, use of a magnetic field also has a number of negative aspects, which include:

1) The complexity and cumbersomeness of the magnetic systems.

2) Inefficiency of field utilization at very low temperatures (below approximately 10,000 K).

3) The obligatory presence of wall sections intersected by the lines of force of the field passing through the uranium zone. It is very difficult to cool these sections.

4) Twisting the gas in the uranium mixing zone with the working substance due to interaction of the thermoelectric flows in a plasma with magnetic field. Twisting in a light working substance may lead to an increase of turbulization and mixing. Very high field intensities--up to $(70\text{-}100)\cdot10^3$ Oe--are necessary to eliminate turbulization in this case.

5) High resistance, occurring upon intersection of the conducting gas of the magnetic field at the reactor output. The radial and possible azimuth irregularities of this resistance have a strong reverse effect on flow in the reactor cavity.

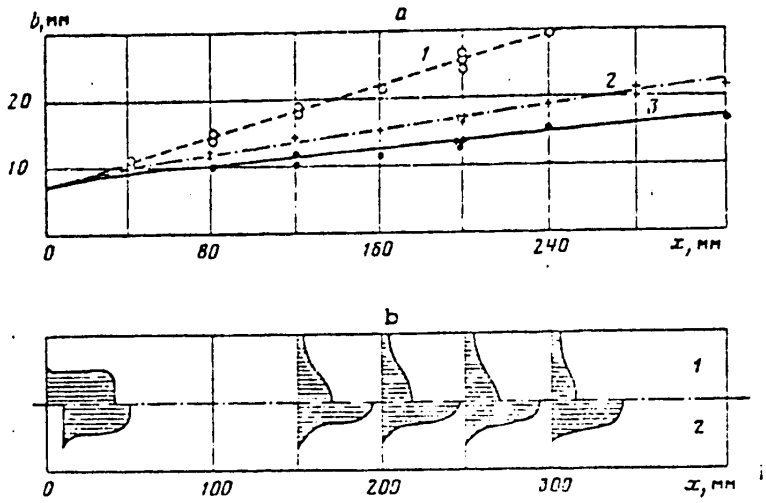

Figure 5. Effect of Longitudinal Magnetic Field on Jet Flows: a--example of dependence of width of mixing zone (b) on x for jet of molten metal [10, 11]; 1--H = 0; 2--H = 3,400 Oe; 3--H = 5,000 Oe; b--concentration profiles for jet and plasma in accompanying flows; 1 (the dot-dash line above)--in the presence of a magnetic field; 2 (the dot-dash line below)--in the presence of a magnetic field (the Stewart number for the jet mixing zone is close to 3)

These difficulties should be taken into account, but despite them, a magnetic field can be regarded as one of the effective means of affecting flow in a gas-phase reactor.

Various types of flow stabilization among the methods indicated above can be used as a function of the amount of working substance, temperature and flow rate of the gas. Good results are found with complex use of different methods.

The properties of the working media must be known to investigate and calculate the gas-dynamic, thermal and neutron-physical processes in a gas-phase reactor.

The thermodynamic, some transition and the optical properties of various substances, including uranium and uranium hexafluoride, were investigated. The investigations were carried out theoretically and experimentally on various types of laboratory installations: in shock tubes, in arcs with stationary and pulsed discharges, during explosions of wires; they were carried out for relatively low temperatures in a bomb, in heated-tubes and so on. Many of the results have been published (for example [13-21]). However, the accuracy of knowledge and the methods of calculating all the properties, especially optical properties, may be regarded as sufficient only in the first approximation, i. e., for the beginning of investigations.

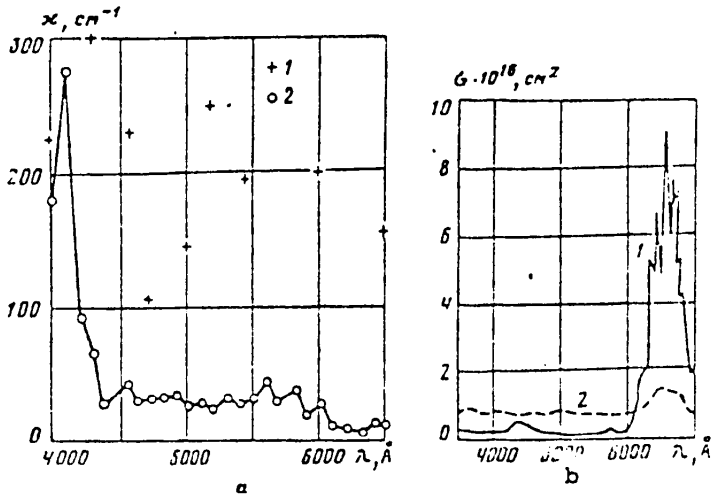

Figure 6. Optical Properties of Working Media: a--absorption coefficient (×) of uranium plasma as a function of radiation wavelength (λ); p ≈ 5.0 MPa and T ≈ 10^4 K; 1--experimental data; 2--theory; b--experimental data on effective cross-sections (σ) of radiation absorption by potassium atoms for helium-potassium vapor mixture (T = 700-950 K; 1--PHe ≈ 0.7 MPa; 2--7 MPa)

Some experimental data and the results of various calculations for optical properties (absorption coefficient) of the uranium plasma are presented in Figure 6. Data on the absorption coefficient at low temperatures of one of the possible working substances--potassium-helium mixtures--are presented here as an example. The circumstance that the spectral lines are broadened to such

an extent that absorption is continuous for the entire spectrum and is very intense even at low temperatures with an increase of pressure is noteworthy. This provides good shielding of the walls against radiation. The results of calculating the absorption coefficient as a function of radiation frequency for hydrogen with darkening additive of potassium are given in Figure 7 as an example. The different curves of Figure 7 are related to different processes studied.

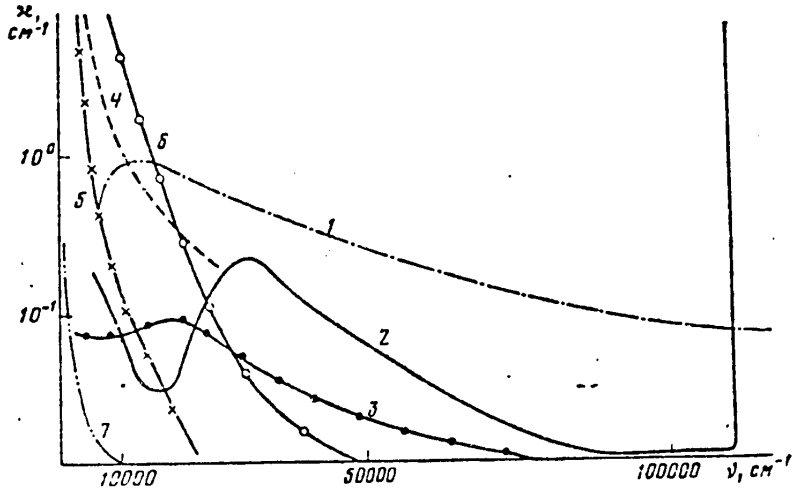

Figure 7. Example of Results of Calculating the Absorption Coefficient (×) as a Function of Inverse Wavelength ($\nu = 1/\lambda$) for Hydrogen With Addition of 3 Percent (Mole) Potassium Vapor; p ≈ 20.0 MPa, T = 12,000 K; 1--photoremoval of electron from H^-; 2--photoionization of H (from different levels); 3--photoionization of K (from different levels); 4-7--absorption during free-free electron transitions in H, K^+, H^+ and H_2^+ fields, respectively.

Data on the properties of media were used in two-dimensional numerical calculations of the flow in hte reactor cavity. Transition of radiation was described in approximation of radiant thermoconductivity; accurate formulas were used in the thin layer near the wall. Hydrodynamic and thermal calculations were carried out jointly with neutron-physical calculations of the reactor for which the Monte-Carlo method was used with special consideration of making the spectrum of thermal neutrons more rigid due to scattering in the working substance and because of the preferred "corrosion" of the soft part of the spectrum in gaseous uranium.

The complex thermal, gas-dynamic, neutron-physical and other calculations confirm the possibility of achieving parameters of a gas-phase reactor promising for various applications.

The results described briefly in the given article, a number of other investigations and the materials of published papers provide the basis to develop further investigations on gas-phase reactors--one of the most promising trends for future power engineering.

BIBLIOGRAPHY

1. Research on Uranium Plasmas and Their Technological Applications. The Proceedings of a Symposium, held January 7-8, 1970 in Gainesville, Florida (edited by K. Thom and R. T. Schneider), Washington, NASA, 1971.

2. Second Symposium on Uranium Plasmas. Research and Applications, Atlanta, Georgia, November 15-17, 1971.

3. "Dinamika i upravleniye atomnym raketnym dvigatelem" [The Dynamics and Control of Nuclear Rocket Engines], edited by B. N. Petrov, Atomizdat, 1972.

4. Navoznov, O. I. and A. A. Pavel'yev, "Transition to Turbulence in Accompanying Jets," IZV. AN SSSR, MEKHANIKA ZHIDKOSTI I GAZA, No 6, 1969.

5. Navoznov, O. I., A. A. Pavel'yev and A. V. Yatsenko, "Transition to Turbulence in Blunt and Accompanying Jets," IZV. AN SSSR, MEKHANIKA ZHIDKOSTI I GAZA, No 4, 1972.

6. Shurcliff, J., "Kurs magnitnoy gidrodinamiki" [A Course in Magnetic Hydrodynamics], Mir, 1967.

7. Iyevlev, V. M., "Turbulentnoye dvizheniye vysokotemperaturnykh sploshnykh sred" [Turbulent Motion of High-Temperature Compact Media], Nauka, 1975.

8. Volkov, A. V., "Experimental Investigation of the Effect of the Magnetic Field on Turbulence Behind a Screen," MAGNITNAYA GIDRODINAMIKA, No 4, 1975.

9. Levin, V. B. and I. A. Chinenkov, "Experimental Investigation of the Effect of a Longitudinal Magnetic Field on the Hydraulic Drag During Turbulent Flow of a Conducting Fluid in a Tube, MAGNITNAYA GIDRODINAMIKA, No 3, 1970.

10. Preobrazhenskiy, S. S. and I. A. Chinenkov, "Experimental Investigation of the Effect of a Longitudinal Magnetic Field on Turbulent Flows of a Conducting Fluid," MAGNITNAYA GIDRODINAMIKA, No 2, 1970.

11. Baushev, B. N., Ye. Yu. Krasil'nikov, V. G. Lushchik and I. G. Panevin, "Displacement of Accompanying Flows in a Longitudinal Magnetic Field," IZV. AN SSSR, MEKHANIKA ZHIDKOSTI I GAZA, No 5, 1972.

12. Artamonov, K. I., "Thermoacoustic Stability of a High-Temperature Heat-Dissipating Gas," DOKL. AN SSSR, Vol 231, No 3, 1976.

13. Kazanskiy, K. A. and V. N. Novikov, "The Thermal and Electrophysical Properties of UF_6 in the Temperature Range of $(1-11)\cdot 10^3$ K and at Pressures of 0.1-100 Atm," TEPLOFIZIKA VYSOKIKH TEMPERATUR, Vol 14, No 3, 1976.

14. Gryaznov, V. K. and I. L. Iosilevskiy, "Some Problems of Thermodynamic Calculation of a Multicomponent Nonideal Plasma," in "Teplofizicheskiye svoystva nizkotemperaturnoy plazmy" [The Thermophysical Properties of a Low-Temperature Plasma], Nauka, 1976.

15. Norman, G. E. and A. N. Starostin, "The Thermodynamics of a Nonideal Plasma," TEPLOFIZIKA VYSOKIKH TEMPERATUR, Vol 8, No 2, 1970.

16. Fortov, V. Ye., A. A. Leont'yev, A. N. Dremin and V. K. Gryaznov, "Generation of a Nonideal Plasma by Powerful Shock Waves," ZHURNAL EKSPERIMENTALNOY I TEORITECHISKOY FIZIKI, Vol 71, No 7, 1976.

17. Pavlov, G. A. and E. Ye. Son, "Diffusion in Multicomponent Gas Mixtures and Models of Local Thermodynamic Equilibrium," ZHURNAL PRIKLADNOY MATEMATIKI I TEKHNICHESKOY FIZIKI, No 4, 1975.

18. Kucherenko, V. I., G. A. Pavlov and E. Ye. Son, "Effective Transfer Coefficients in a Plasma in Approximation of Local Thermodynamic Equilibrium," TEPLOFIZIKA VYSOKIKH TEMPERATUR, Vol 14, No 5, 1976.

19. Ivanov, Yu. V., V. B. Mintsev, V. Ye. Fortov and A. N. Dremin, "Electrical Conductivity of a Nonideal Plasma," ZHURNAL EKSPERIMENTALNOY I TEORITECHISKOY FIZIKI, Vol 71, No 7, 1976.

20. Chertoprud, V. Ye., "An Infrared Molecular Potassium Absorption System," TEPLOFIZIKA VYSOKIKH TEMPERATUR, Vol 14, No 1, 1976.

21. Nesterov, Ye. V., "Study of an Arc Plasma of Inert Gases at High Pressures," in "Teplofizicheskiye svoystva nizkotemperaturnoy plazmy" edited by V. M. Iyevlev, Nauka, 1976.

6521
CSO: 8144/155

UDC 533.17

MIXING OF ACCOMPANYING GAS JETS

Moscow IZVESTIYA AKADEMII NAUK SSSR: ENERGETIKA I TRANSPORT in Russian No 2, 1968 pp 52-57

[Article by O. I. Navoznov and A. A. Pavel'yev, Moscow]

[Text] The authors experimentally determine how the average flow parameters and dimensions of the mixing zones of two coaxial jets of incompressible gas depend on initial conditions. The initial conditions were varied by placing fine-mesh grids in the initial section of the flow. When screens with mesh size of 0.07 mm are used, the ordinate of the inner boundary of the mixing zone falls off linearly right up to a velocity ratio of accompanying flows of $m = 0.95$, whereas in the absence of screens at the nozzle tip, mixing ceases to depend on the velocity ratio starting with $m = 0.5$, and is entirely determined by the magnitudes of the boundary layers on the nozzle wall that separates the two streams.

A relation is found for the way that mixing depends on the density ratio when submerged jets of different densities are discharged into different media. The density ratio ranged from 7 (air jet into a helium atmosphere) to 30 (helium jet into a Freon-12 atmosphere). Figures 7, references 4.

Existing semi-empirical theories of free turbulent flows [Ref. 1-3] are essentially differential methods of processing experimental data, but measurements of turbulence structure do not confirm the models on which these theories are based. Therefore they cannot be used in cases that have not been experimentally studied beforehand. Some information on flows can be obtained by using dimensional analysis, symmetry considerations, conservation laws and experimental data on turbulence structure of a more general nature. But only a properly designed experiment can give the complete picture. In view of the large number of parameters that influence mixing in a specific experiment and the simultaneous variation of these parameters, it is not always possible to single out the dependence on a single parameter such as velocity ratio. Much of the research on jet flows does not take consideration of changes in initial conditions, and this leads to different semi-empirical relations. For example, some papers give data that characterize the magnitudes of boundary layers on the separating jet of the nozzle

surface, but do not indicate flow velocities, and since the boundary layers change with changing velocity, the given data are insufficient for obtaining dependences on the ratio of velocities and densities.

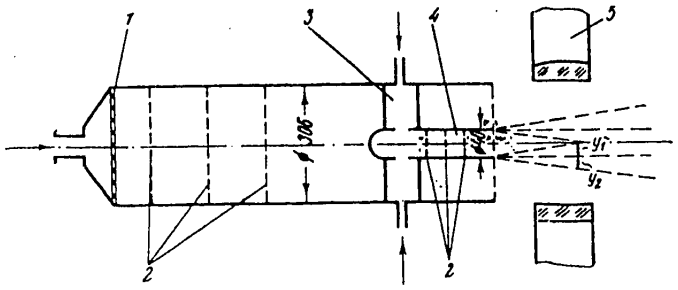

Fig. 1. Drilled grating and felt; 2--fine-mesh grids; 3--pylon; 4--central nozzle; 5--IAB-451 schlieren camera

Fig. 1 shows a diagram of the working section. Central nozzles 40 and 30 mm in diameter with edge thickness of 0.4 mm were fastened on two pylons in tubes 300 and 120 mm in diameter respectively. To deturbulize the flows and vary conditions at the inlet, fine-mesh grids with mesh size from 0.07 to 0.3 mm and porosity from 0.35 to 0.5 respectively were installed in the accompanying flow and in the central nozzle. Measurements of the coefficient of turbulent diffusion D_T in the airstream behind such grids from expansion of the thermal wake behind a heated wire 0.03 mm in diameter at an air velocity of 15 m/s at normal temperature showed that this parameter is close to the coefficient of molecular transfer D_M. Fig. 2 shows the dimensionless coefficient of turbulent diffusion $\bar{D}_T = D_T/Vd_{tube}$ as a function of the dimensionless axial coordinate x/d and the dimensionless distance from the wall $\xi = (r_{tube} - r)/r_{tube}$ in a tube 100 mm in diameter at an air velocity of V = 15 m/s. The broken line shows the dimensionless coefficient of molecular diffusion $\bar{D}_M$. It should be noted that the corresponding coefficient of turbulent diffusion when turbulence is fully developed in the tube is 10 times the D_T found in the experiment with the above-mentioned screens. Turbulence intensity was less than 1%.

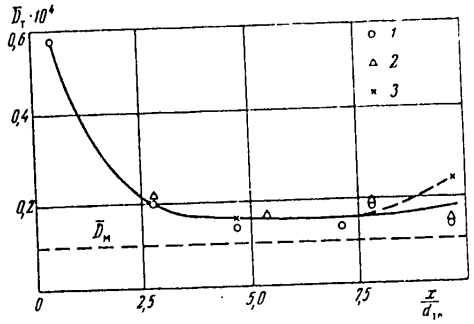

Fig. 2. 1--ξ =1; 2--ξ = 0.6; 3--ξ = 0.4

The installation of a common screen (or a stack of two or three screens) at the nozzle tip in the working section (Fig. 1) effectively equalized the velocity profiles in the boundary layers on the edge. The dimensions of boundary layers on the tip could be varied by the installation of screens at different distances from the edge.

The geometric characteristics of the flow (width of the mixing zone, length of the core) were determined from measurements of temperature profiles and velocity

heads. The boundaries of the mixing zone were taken as the points of the profiles where the relative excess temperatures ΔT_*, velocity heads $\Delta(\rho V^2/2)_*$ and velocities ΔV_* are equal to 0.97 and 0.03. One of the streams was heated for measurement of the temperature profiles. The temperature differential between streams was no more than 50 K. The temperature fields in the flow were measured by Chromel-Copel thermocouples assembled into a "comb" of 30 units with spacing of 3 mm. The thermocouple junction was about 0.1 mm in diameter. The thermocouple readings were recorded by the EPP-09 [chart-recording potentiometer]. A time of 15 s was required for taking one profile. The profiles of velocity heads were measured by a comb of 25 Pitot tubes with readings indicated on an inclined manometer bank. In addition, the schlieren method or a Töpler tube was used to photograph the gas flows of different density at the tip of the working section. The velocities varied over a range of 10-50 m/s. Air, helium and Freon-12 were used as working fluids.

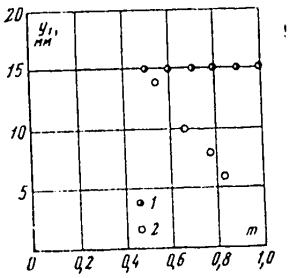

Fig. 3. 1--without a screen on the tip; 2--with screen on the tip

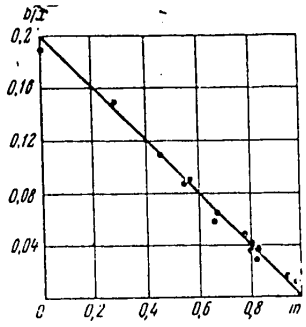

Fig. 4

The influence of boundary layers on the tip is illustrated by Fig. 3, which shows how the ordinate of the inside boundary of the mixing zone y_1 (with respect to a relative velocity of $\bar{V} = 0.03$) depends on the velocity ratio $m = V_1/V_2$ of two air jets at a distance of $x/d = 7.5$ from the tip. In the first case there was no grid on the tip, and the boundary layer accumulated to a length of 250 mm on the outer wall of the central nozzle. In the second case, a screen with mesh of 0.07 mm and porosity of 0.35 was installed on the tip. This figure shows that without a screen the mixing ceases to depend on the velocity ratio beginning with $m = 0.5$. However, this quantity is different for different distances from the edge, and increases with increasing distance. This is explained by the fact that the transfer properties of a mixing layer with constant difference between flow velocities increase with distance from the edge, whereas the transfer properties determined by the initial conditions remain constant with respect to length, or decrease. Therefore mixing will be determined mainly by the local velocity difference beginning with some distance from the edge for any initial conditions. And the more strongly the flow is turbulized, and the larger the boundary layers, the farther from the edge will the influence of the initial conditions be felt. This reasoning holds for a flat mixing zone and initial jet section. It should be noted that mixing on the initial section of axisymmetric jets, in view of the

usually short mixing length, either takes place under conditions of transition to developed turbulent flow, or is determined by the initial conditions.

The dependence of the width of the mixing zone on the velocity ratio in the case of weak influence of initial conditions was studied with grids installed on the nozzle tip. The thickness of the boundary layers in this case was less than 1 mm on each side of the edge. The corresponding dependence of the width b/x of the mixing zone determined from the relative excess velocity as a function of the velocity ratio m is shown in Fig. 4 (here $b = y_1 + y_2$, $n = \rho_1/\rho_2 = 1$). It can be seen that the experimental results are described by a linear function $b/x = 0.2(1-m)$ up to $m = 0.95$. In deriving this function, consideration was taken of the fact that on a considerable portion of the initial section of the jet the flow is markedly periodic or tending to turbulence; this section is eliminated from consideration. The length of this section was determined from schlieren photographs of the flow.

In connection with the above-mentioned strong influence of initial conditions (including the relative misalignment of the two streams), as well as the lack of necessary data on these conditions in different research papers, it is difficult to compare the various experimental results. A number of relations are proposed in the literature for the width of the mixing zone as a function of the ratios of velocities m and densities n derived with a variety of assumptions regarding the flow pattern in the mixing layer. For example it is suggested in Ref. 1, 4 that the ratio of the width of the mixing zone to the distance from the edge is proportional to the ratio of two velocities: transverse mixing is proportional to the absolute value of the difference in velocities of the two flows $\Delta u = |u_1 - u_2|$, while longitudinal mixing is proportional to some average velocity over the mixing zone

$$U^* = \int \rho u dy / \int \rho dy.$$

Then $b/x \approx \Delta U/U^*$. For mixing of homogeneous flows, this leads to the relation $b/x \sim (1-m)/(1+m)$, which has not been confirmed by the experiments of the authors of the present paper. Nor has the implied dependence of mixing on density ratio for submerged jets found confirmation. The relation implies that when a jet mixes in an atmosphere of lighter gas, the core cannot be increased to more than twice its length in the case of mixing of homogeneous streams. In experiments done with mixing of a submerged jet of Freon in an air atmosphere, the length of the core increases by a factor of approximately 2.5.

It was proposed in Ref. 1 that the mixing intensity is determined by the difference of velocity heads rather than velocities, and that minimum mixing is observed when the velocity heads of the streams are equal. This assumption has not been experimentally confirmed, and it has no sound theoretical basis.

Both the above-mentioned assumptions imply that mixing depends differently on n for different m, i. e. mixing differs for the same Δu when the absolute velocities are different. But it is more natural to assume that the particulars of interaction of two streams will be determined only by their relative motion if only the mixing is not affected by initial irregularities of velocity and initial turbulence. These assumptions together with the experimental results make the above-mentioned relations untenable.

Assuming that absolute velocities have no effect on the way that mixing depends on the density ratio for the same velocity difference, we get for the width of the mixing zone

$$b = (x - x_0) f(m) \varphi(n),$$

where x_0 is the effective coordinate origin determined by the conditions of transition to turbulent flow, while f(m) and $\phi(n)$ are given functions.

Dimensional analysis tells us that a flat mixing zone implies linear dependence on x, but gives us no information whatever on the form of functions f(m) and $\phi(n)$. However, if we assume that mixing is entirely determined by the velocity difference, and that the lower velocity shifts the flow pattern in the direction of flow, then we get

$$b = (x - x_0)(1 - m)\varphi(n).$$

It was assumed in deriving this formula that the dimensions of mixing zones for flows with different absolute velocities are equal for the same velocity difference at the same values of the coordinates $x - x_0$ where we have equal longitudinal mixing of undisturbed particles of one flow relative to the undisturbed particles of the other flow. The linear dependence of the width of the mixing zone on the velocity ratio that is obtained with such assumptions is confirmed well by experiment (Fig. 4). We find from these same assumptions that the dependence of the width of the mixing zone on the density ratio is the same for any velocity ratio. Therefore the function can be experimentally determined with any velocity ratio, including for submerged jets (m = 0), as was done by the authors (Fig. 5).

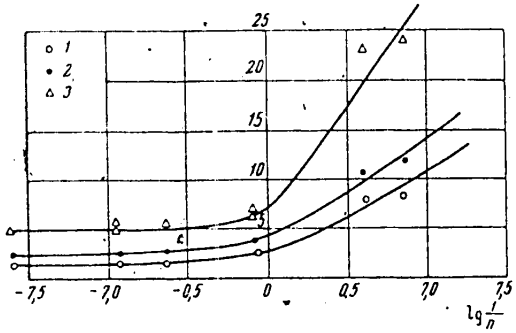

Fig. 5. 1--$\Delta x/\Delta b$; 2--$\Delta x/\Delta y_1$; 3--$\Delta x/\Delta y_2$

Studies were done at density ratios n ranging from 1/7 (air jet in a helium atmosphere) to 30 (helium jet in a Freon atmosphere). The central jet was heated, and the width of the mixing zone was determined from the temperature profiles. To reduce heat exchange and temperature boundary layers on the edge, the flows were thermally isolated by placing a heat-insulating jacket over the central nozzle. Measurements were made in each cross section on the end of the tube. Fig. 5 shows the way that the width of the mixing zone depends on the density ratio $n = \rho_{atm}/\rho_{jet}$. In individual experiments, m was somewhat greater than 0, but never exceeded 0.05. As we can see from Fig. 5, the intensity of mixing of a heavy jet in a light gas atmosphere drops sharply as compared with the mixing intensity of homogeneous flows ($\lg(1/n) = 0$), but when the jet density is reduced in comparison with the accompanying flow, the mixing intensity shows a very weak

increase. This can be attributed to the fact that the mixing intensity is determined by processes on the interface between the turbulent and nonturbulent fluids, where the density ratio changes sharply when a heavy jet is injected into an atmosphere of lighter gas, and changes weakly in the opposite case.

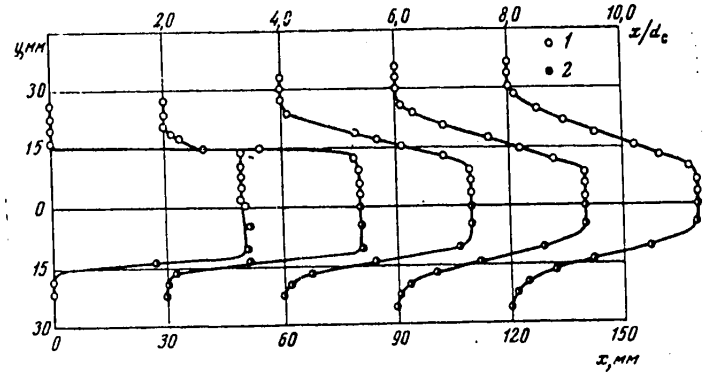

Fig. 6. $1-\Delta T_* = \frac{T-T_2}{T_1-T_2}$; $2-\Delta\left(\frac{\rho V^2}{2}\right)_* = \frac{\rho_1 V_1^2-\rho_2 V_2^2}{\rho_1 V_1^2-\rho_2 V_2^2}$

Fig. 6 shows profiles of relative velocity heads and temperatures for a Freon jet in an atmosphere of air at $V_1 = 10.4$ m/s, $T = 310$ K. It can be seen that the velocity head profile is narrower than the temperature profile in the outer part of the mixing zone, whereas their boundaries coincide in the inner section, i. e. the velocity profile is also narrower than the temperature profile, the boundaries of which coincide with those of the concentration profile. Consequently the velocity profile is narrower than the concentration profile in the case of different densities as well. This leads to a nonmonotonic change in the velocity head profile in the zone of mixing of two streams of different density with slightly different velocity heads even in the case where the velocity head of the light gas is greater than that of the heavier gas. Fig. 7 shows profiles of the velocity heads and temperatures in the zone of mixing of a jet of helium with an accompanying flow of air at equal velocity heads ($x = 102$ mm, $V_{air} = 14.2$ m/s) These results confirm coincidence of the boundaries of the temperature and density profiles.

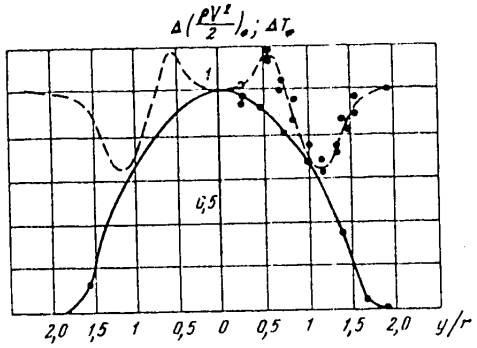

Fig. 7

It should be noted that calculation of the profile of average velocity from the measured profiles of velocity heads and concentrations may be very inexact since density pulsations in the zone of mixing of two flows of different density are not small compared with the average, and in isolated instances even exceed the average. With flow of a heavy jet in an atmosphere of light gas there is a strong reduction in the intensity of mixing turbulence if the ratio of the width of the mixing zone to the distance from the edge is taken as the characteristic of

turbulence intensity. In this case at low jet velocities molecular transport processes may be appreciable, and as a consequence mixing will be dependent on the absolute velocity.

The results of this research do not apply to the case of flow of two jets with equal velocities since the flow has a structure similar to the wake behind a body when m = 1.

Conclusions. 1. A relation is found for the width of the zone of accompanying gas jets as a function of the velocity ratio.

2. A relation has been experimentally found for the width of the mixing zone of submerged jets as a function of the density ratio of the gases being mixed.

3. The velocity head in the zone of mixing of accompanying jets of different density varies nonmonotonically with respect to radius.

REFERENCES

1. Vulis, L. A. and Kashkarov, V. P., "Teoriya struy vyazkoy zhidkosti" [Theory of Jets of Viscous Fluid], Nauka, 1965.

2. Abramovich, G. N., "Teoriya turbulentnykh struy" [Theory of Turbulent Jets], Fizmatgiz, 1960.

3. Bai Shi-yi, "Teoriya struy" [Theory of Jets], Fizmatgiz, 1960.

4. Yakovlevskiy, O. V., "Concerning the Question of the Thickness of the Zone of Turbulent Intermixing on the Interface Between Two Flows of Different Velocity and Density," IZVESTIYA AKADEMII NAUK SSSR, OTDELENIYE TEKHNICHESKIKH NAUK, No 10, 1958.

6610
CSO: 1862/137

UDC 532.517.4.532.518.532.526.001.5

WAKE FORMED BEHIND A PLATE UPON MERGING OF TWO FLOWS OF INCOMPRESSIBLE FLUID WITH DIFFERENT DENSITIES

Moscow IZVESTIYA AKADEMII NAUK SSSR: ENERGETIKA I TRANSPORT in Russian No 6, 1969 pp 122-132

[Article by O. I. Navoznov and A. A. Navel'yev, Moscow]

[Text] A theoretical and experimental study is done on the averaged characteristics of turbulent flow in the wake formed behind the edge of a plate upon merging of two flows of incompressible fluid with different densities ρ_1 and ρ_2.

Based on dimensional analysis and certain hypotheses concerning motion of the interface between the turbulent wake and the potential flow outside the wake, expressions are derived that describe the change in width b of the wake and its displacement relative to the plane of the plate with respect to longitudinal coordinate as a function of the density ratio $n = \rho_1/\rho_2$.

The experimental technique and procedure are described.

The authors present the results of measurements in the wake that arises upon merging of flows of the same gas (air-air), and also when streams of air and helium merge.

The appendix gives the method of calculating the concentration profile from the temperature profile measured by thermocouples. Figures 8, References 5.

1. Dimensional Analysis. Consider a two-dimensional wake formed when two incompressible fluids merge behind a plate, assuming that molecular transport is insignificant and that turbulence is small in both fluid streams. Then it can be assumed that far from the edge, where the velocity defect U* is small compared with the velocity of the unperturbed flow (i. e. $U^*/U_\infty \ll 1$), the specific form of loss of momentum P on the initial section of the wake is unimportant, the flow being determined only by the absolute value of P without dependence on the Reynolds number. The controlling parameters for such a flow are

$$U_\infty, \rho_1, \rho_2, P, b, x. \tag{1.1}$$

The following dimensionless numbers can be made up from these controlling parameters

$$n=\frac{\rho_1}{\rho_2};\quad \frac{b}{x^{1/2}(P/\rho U_\infty^2)^{1/2}};\quad \frac{P}{\rho U_\infty^2 x};\quad \frac{b}{x}. \tag{1.2}$$

Formula (1.2) shows us that as in the case of a wake in a homogeneous fluid, dimensional analysis does not give the dependence of the width b of the wake on the longitudinal coordinate, and does not show self-similarity of motion. However, it is known that in all investigated cases self-similarity is realized if the corresponding equations of motion permit self-similar solutions. In the boundary layer approximation the equations of continuity, motion and diffusion for averaged values of isothermal incompressible fluids in the wake are written in the following form:

$$\frac{\partial \bar{u}}{\partial x}+\frac{\partial \bar{v}}{\partial y}=0,$$

$$U_\infty\frac{\partial \bar{u}}{\partial x}+\frac{\partial \overline{u'v'}}{\partial y}+\frac{\overline{\rho'v'}}{\rho}\frac{\partial \bar{u}}{\partial y}=0, \tag{1.3}$$

$$U_\infty\frac{\partial \bar{\rho}}{\partial x}+\frac{\partial \overline{\rho'v'}}{\partial y}=0.$$

To these equations we must add the condition of conservation of momentum in the wake

$$\int_{-\infty}^{+\infty}\rho U_\infty \bar{U}^*\,dy=\text{const}. \tag{1.4}$$

In these equations u', v', ρ' are respectively the pulsations of longitudinal and transverse velocity and of density. In equations (1.3), we can introduce concentration c in place of density. Then at T = const

$$c=\frac{\bar{\rho}-\rho_2}{\rho_1-\rho_2};\quad c'=\frac{\rho'}{\rho_1-\rho_2}.$$

Then let us represent $\bar{U}^*$, $\bar{c}$, $\overline{c'v'}$ and $\overline{u'v'}$ in the following form:

$$\begin{aligned}&\bar{U}^*=x^p f_1(y/x^q);\quad \overline{u'v'}=x^{2p}f_3(y/x^q);\\ &\bar{c}=x^h f_2(y/x^q);\quad \overline{c'v'}=x^{h+p}f_4(y/x^q)\end{aligned} \tag{1.5}$$

and substitute them in equations (1.3) and (1.4). After transformations we get

$$\begin{aligned}&U_\infty(pf_1+q\eta f_1')=-\left(f_3'+\frac{f_4 f_1'}{f_2+\frac{x^{-h}}{n+1}}\right)x^{p+q+1},\\ &U_\infty(kf_2+q\eta f_2')=-f_4' x^{p+q+1},\\ &x^{p+h-q}U_\infty\int_{-\infty}^{+\infty}f_1 f_2\,d\eta+x^{p-q}\frac{1}{n+1}U_\infty\int_{-\infty}^{+\infty}f_1\,d\eta=\text{const},\end{aligned} \tag{1.6}$$

where $\eta = y/x^q$.

System of equations (1.6) does not depend on x if p, q and k satisfy the following equalities:

$$p+q+1=0;\quad p-q+k=0;\quad k=0. \tag{1.7}$$

Then we get

$$q=p=-\frac{1}{2},$$

$$\bar{U}^{*}=\frac{1}{x^{1/2}}f_1\left(\frac{y}{x^{1/2}}\right),\quad \overline{u'v'}=\frac{1}{x}f_3\left(\frac{y}{x^{1/2}}\right), \tag{1.8}$$

$$\bar{c}=f_2\left(\frac{y}{x^{1/2}}\right),\quad \overline{c'v'}=\frac{1}{x^{1/2}}f_4\left(\frac{y}{x^{1/2}}\right).$$

Finally the system can be written as

$$\frac{1}{2}U_\infty(f_1+\eta f_1')=f_3'+\frac{f_4 f_1'}{f_2+\frac{1}{n+1}}, \tag{1.9}$$

$$U_\infty \eta f_2'=2f_4'.$$

System (1.9) permits self-similar solutions, but here we have only two equations for determination of the four functions f_1-f_4. Closure requires certain additional assumptions. The most extensively used assumption of this kind is introduction of coefficients of eddy viscosity ε_v and eddy diffusion ε_ρ that are used to show the dependences of u'v' and ρ'v' on the gradients of the averaged quantities

$$\tau_v=-\rho\overline{u'v'}\Big/\frac{\partial\bar{u}}{\partial y}\text{ and }\varepsilon_\rho=-\overline{\rho'v'}\Big/\frac{\partial\bar{\rho}}{\partial y}.$$

Then equations (1.3) will be written as

$$U_\infty\frac{\partial\bar{u}}{\partial x}=\frac{\partial}{\partial y}\left(\varepsilon_v\frac{\partial\bar{u}}{\partial y}\right)+\frac{\varepsilon_\rho}{\rho}\frac{\partial\bar{\rho}}{\partial y}\frac{\partial\bar{u}}{\partial y}, \tag{1.10}$$

$$U_\infty\frac{\partial\bar{\rho}}{\partial x}=\frac{\partial}{\partial y}\left(\varepsilon_\rho\frac{\partial\bar{\rho}}{\partial y}\right), \tag{1.11}$$

and the solution of the diffusion equation is found in explicit form:

$$\frac{2\bar{\rho}-(\rho_1+\rho_2)}{\rho_1+\rho_2}=\operatorname{erf}\left\{\frac{y-y_{0,5}}{2\left(\varepsilon_\rho\frac{x-x_0}{U_\infty}\right)^{1/2}}\right\}, \tag{1.12}$$

where $y_{0.5}$ is the coordinate where $\rho=(\rho_1+\rho_2)/2$, and ε_ρ is determined from dimensional analysis:

$$\varepsilon_\rho=c\frac{P}{1/2(\rho_1+\rho_2)U_\infty^2}\xi(n),$$

where $\xi(n)$ is an experimental function.

On the basis of dimensional analysis, the quantities U* and ρ can be written as functions of the coordinates in the following form:

$$U^* = \left[\frac{P}{\rho(x-x_0)}\right]^{1/3} F_1\left\{\frac{y}{\left[\frac{P}{\rho U_\infty{}^2}(x-x_0)\right]^{1/3}}; \frac{\rho_1}{\rho_2}; \frac{U^*}{U_\infty}\right\}, \tag{1.13}$$

$$\frac{\rho-\rho_1}{\rho_2-\rho_1} = F_2\left\{\frac{y}{\left[\frac{P}{\rho U_\infty{}^2}(x-x_0)\right]^{1/3}}; \frac{\rho_1}{0}; \frac{\left[\frac{P}{\rho(x-x_0)}\right]^{1/3}}{U_\infty}\right\}. \tag{1.14}$$

As noted above, dimensional analysis does not yield self-similar relations. However, considering that the equations of motion permit self-similar solutions, we can assume that at some distance from the edge where $\frac{U^*}{U_\infty} \ll 1$ and

$$\left[\frac{P}{\rho(x-x_0)}\right]^{1/3} \Big/ U_\infty \ll 1,$$

these dimensionless parameters are unimportant, and self-similar relations are realized.

As the characteristic density ρ_{eff} let us take the arithmetic average density of the two flows $(\rho_1+\rho_2)/2$. Then, defining the boundary of the wake as the value of y at which $(\rho-\rho_1)/(\rho_2-\rho_1)$ takes some fixed value, we get the following expression for the width of the wake:

$$b = \left(P\Big/\frac{\rho_1+\rho_2}{2}U_\infty{}^2\right)^{1/3} (x-x_0)^{1/3}\varphi(n). \tag{1.15}$$

The function $\phi(n)$ shows up as a consequence of the arbitrary definition of the effective density ρ_{eff} as the arithmetic average density of the two flows. If relation (1.12) is considered valid for the distribution of concentrations, then such a definition corresponds to a content of equal volumes of fluids being mixed within the width of the wake. It can be assumed that in this case the function $\phi(n)$ will be weakly dependent on the density ratio.

Relation (1.15) will have a different appearance if the effective density is defined as

$$\rho_{eff} = \rho_1\alpha + (1-\alpha)\rho_2, \tag{1.16}$$

where α is some average value taken over the wake of the volumetric concentration of fluid with density ρ_1. In this case

$$b = c\left\{\frac{P}{[\rho_1\alpha+(1-\alpha)\rho_2]U_\infty{}^2}\right\}^{1/3}(x-x_0)^{1/3}. \tag{1.17}$$

The value of α in (1.17) can be experimentally determined from measurement of the width of the wake at some known loss of momentum P. It should be noted that

momentum losses in fluids of different densities affect the width of the wake differently. If the thickness of the edge is small, then

$$p = U_\infty^2(\rho_1\delta_1^* + \rho_2\delta_2^*),$$

where δ_1^* and δ_2^* are the thicknesses of the loss of momenta on the edge in boundary layers of the fluids with densities ρ_1 and ρ_2 respectively.

Substituting this expression in (1.17) we get

$$b = c\left(\frac{n\delta_1^* + \delta_2^*}{na + 1 - a}\right)^{1/2}(x - x_0)^{1/2}. \tag{1.18}$$

The thickness of loss of momentum of fluid 1 appears in this expression with a factor n, and if $n \ll 1$, the thickness of loss of momentum in the light fluid does not play an appreciable part.

2. Boundary of the Turbulent Region. Dimensional analysis cannot provide any information relative to displacement of the wake, i. e. the asymmetry of its boundaries on the side of the light and heavy fluid relative to the plane of the plate. Such information can be obtained by resorting to certain additional hypotheses.

Measurements that have been made so far, and especially visual observations of the interface between a turbulent wake and the potential flow outside of the wake [Ref. 1, 2], suggest that the instability of this boundary is instability of the Helmholtz type, i. e. it is determined by the flow parameters close to the boundary. This applies in particular to the influence of the density ratio of the mixing flows as well. From this standpoint, let us consider the propagation of a submerged jet in a space filled with a fluid of another density. As the light gas moves in an atmosphere of the heavy gas, the density ratio on each side of the boundary of the turbulence region is not too far from unity. This is explained by the fact that the heavy gas is located on one side, while a mixture of heavy and light gases is located on the other side. Thus the sought density ratio cannot be less than the volumetric fraction of heavy gas in the mixture. On the other hand, when the heavy gas is moving in the light one, this ratio may be very large. Hence it can be concluded that when the light gas moves in the heavier one, mixing should not be very different from that in the case of propagation of a submerged jet in a medium of the same gas. Contrariwise, mixing during motion of a heavy gas in a light one ought to have distinguishing features. These qualitative conclusions agree with experimental data. Further assumptions are required to get quantitative estimates.

Frames taken by a motion picture camera moving at the velocity of the flow show that perturbations develop cyclically, i. e. perturbations appear, increase, and after reaching a certain magnitude they break down, encompassing the nonturbulent fluid. Then after a certain rest period, perturbations arise once more, but now on a larger scale. It is known from experiments that transverse displacements of the boundary are of the order of the perturbation wavelength, i. e. of order k^{-1}, and that the ratio between the time of development of the perturbations and the time of rest is about the same for each period.

Let us assume that at some initial instant the interface is straight, velocity changes abruptly at this boundary by an amount ΔV, and the densities are different

on the different sides of the interface. Let us denote the density of the flow moving with greater velocity by $\rho_б$, and with lesser velocity--by $\rho_м$. In this case, perturbations of the type considered in Ref. 3 develop on the interface:

$$b = b_0 \exp i(kx - ct), \tag{2.1}$$

where

$$c = \frac{k\Delta V \rho_б}{\rho_б + \rho_м} + ik\Delta V \frac{\sqrt{\rho_б \rho_м}}{\rho_б + \rho_м}. \tag{2.2}$$

We assume further that the quantity $\gamma = k\Delta V \sqrt{\rho_б \rho_м}/(\rho_б + \rho_м)t$ is the same for each period of perturbation, and does not depend on the density ratio. This means that the initial perturbation increases in each period by the same factor regardless of the density ratio.

Hence the period is

$$T \sim \frac{\gamma}{k\Delta V \frac{\sqrt{\rho_б \rho_м}}{\rho_б + \rho_м}}.$$

In this time the crests of the perturbation wave shift relative to the stationary fluid by an amount proportional to

$$\frac{\Delta V \rho_б/(\rho_м + \rho_б)}{k\Delta V \sqrt{\rho_б \rho_м}/(\rho_м + \rho_б)} = k^{-1}\left(\frac{\rho_б}{\rho_м}\right)^{1/2}.$$

Thus the ratio of transverse to longitudinal displacement, i. e. db/dx, is proportional to $(\rho_м/\rho_б)^{1/2}$:

$$\frac{db}{dx} = \beta\left(\frac{\rho_м}{\rho_б}\right)^{1/2}, \tag{2.3}$$

where $\beta = db/dx$ for equal densities.

The application of expression (2.3) to the mixing layer must be considered in addition, since here there are two interfaces between the turbulent and nonturbulent flows--on the side of the fluid with lesser density and on the side of the fluid with greater density--and the use of expression (2.3) for estimates on these two boundaries leads to different results. Experimental data on the initial section of an axisymmetric jet coincide with these estimates if the formula is applied to the outside boundary of the jet.

If expression (2.3) is applied to the outside boundary of an axisymmetric submerged jet, then in this case $\rho_м$ is the density of the ambient medium, while $\rho_б = \alpha\rho_{jet} + (1 - \alpha)\rho_{med}$ is some effective density intermediate between that of the medium ρ_{med} and that of the jet ρ_{jet}. Thus, as applied to the mixing zone of a submerged jet, expression (2.3) should be written as

$$\frac{b}{x-x_0}=c\left[\frac{n}{a+(1-a)n}\right]^{1/2}, \tag{2.4}$$

where a is an experimental constant equal to 0.75, and $n=\rho_{med}/\rho_{jet}$.

Generally speaking, a may depend on n, and then the value of expression (2.4) is reduced, but as experiments have shown, for a wide range of density ratios the data are well described with $a=\text{const}$. It can be assumed that similar reasoning is applicable to all kinds of shear flows that have interfaces between turbulent and nonturbulent fluids.

Based on the results of theoretical and experimental consideration, the following model can be proposed for the averaged flow in the turbulent part of a wake (shown schematically in Fig. 1) where the smooth profiles of density and velocity

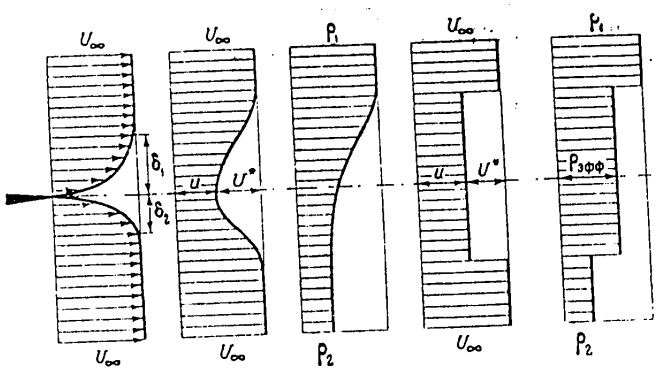

Fig. 1. Flow scheme in the wake behind an edge

are replaced by discontinuities with respect to some average position of the boundary surface. At some average effective density ρ_{eff} within the wake on the side of its boundary with the heavy liquid ρ_T, the velocity of the fluid with greater density is higher ($\rho_T > \rho_{eff}$, $U_T = U_\infty > U_{eff}$), while on the other side the fluid with lower density has higher velocity. Then from relation (2.3) we can get the ratio of coordinates of the two boundaries, i. e. the displacement of the wake relative to the plane of the plate:

$$\frac{dy_л}{dx}=\beta\left(\frac{\rho_{эфф.\,л}}{\rho_л}\right)^{1/2};\quad \frac{dy_т}{dx}=\beta\left(\frac{\rho_{эфф.\,т}}{\rho_т}\right)^{1/2}.$$

Whence

$$\frac{y_л}{y_т}=\left(\frac{\rho_т}{\rho_л}\right)^{1/2}\left(\frac{\rho_{эфф.\,л}}{\rho_{эфф.\,т}}\right)^{1/2}, \tag{2.5}$$

where the subscripts л and т refer to the light and heavy gases respectively, $\rho_{эфф.л}$ and $\rho_{эфф.т}$ are some average effective densities inside the wake on the side of the light and heavy fluids.

Thus dimensional analysis gives the dependence of the width of the wake on the longitudinal coordinate and initial loss of momentum, while a few hypotheses on motion of the interface give the displacement of the wake relative to the plane of the plate as a function of the density ratio.

3. Experimental Technique and Procedure. Flow in the wake behind the edge with merging of inhomogeneous fluids was studied in a working section with a channel of rectangular cross section measuring 160 x 160 mm (see Fig. 2). Air and helium

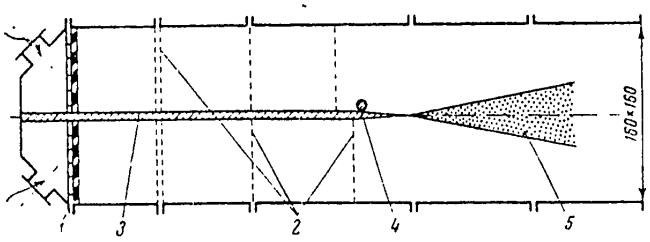

Fig. 2. 1--perforated grating and felt; 2--fine-mesh screens; 3--partition; 4--cylinder; 5--wake

were fed into the two halves of the channel separated by a horizontal partition. Flow velocities were equalized and turbulence was reduced by using a set of fine screens with mesh of M = 0.1 mm. The horizontal partition terminated in a sharp edge 0.3 mm thick. In the upper cavity there was a screen 40 mm from the edge, while in the lower cavity a creen was 50 mm from the edge. They minimized the thickness of the boundary layer on the edge (<1 mm) and reduced the coefficient of turbulent diffusion.

In the experiments the velocity heads and temperatures were measured simultaneously over the whole cross section. This was done by using a comb of Pitot tubes 1 mm in diameter, and a comb of Chromel-Copel thermocouples with diameters of about 0.5 mm. In the course of the experiments, one of the gases could be heated by 30-50°C over the other.

The width of the wake was determined with respect to coordinates corresponding to values of 0.95 and 0.05 respectively for the relative excess velocity heads $\Delta(\rho U^2/2)_* = (\rho U^2 - \rho_1 U_1^2)/(\rho_2 U_2^2 - \rho_1 U_1^2)$, temperature $\Delta T_* = (T - T_1)/(T_2 - T_1)$ and velocity $\Delta U_* = (U - U_1)/(U_2 - U_1)$. In a number of cases an estimate was made of the distribution of volumetric concentrations with respect to the known temperature field in accordance with the method presented in the Appendix.

In addition, the width and displacement of the wake were determined from photographs of the flow taken with the IAB-451 schlieren camera at an exposure of $\sim 10^{-4}$ s.

4. Experimental Results and Their Analysis. Fig. 3 shows the results of measurement of the relative angles of flare $(\Delta b/\Delta x)_{n=1}/(\Delta b/\Delta x)_{n=var}$ of zones of mixing of axisymmetric submerged jets (m = 0) and of flat layers with mixing of flows of different density as a function of the ratio of the jet density to the density of the medium or the density of the flow with lower velocity. Some of these data have already been given in a preceding paper by the authors [Ref. 4], which also

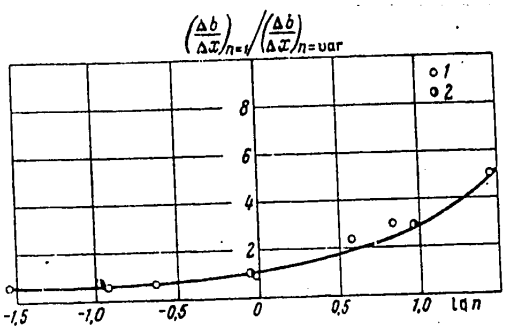

Fig. 3. 1--m = 0; 2--m = 0.4

contains a detailed description of the experimental conditions. Different combinations of three working gases (helium, air and Freon-12) enabled investigation of this relationship in the range of density ratios n from $^1/_{30}$ (helium jet in Freon atmosphere) to 30 (Freon jet in helium atmosphere). As we can see from these data, the intensity of mixing when jets of higher density are discharged into a medium of lower density decreases sharply as compared with mixing of homogeneous jets, whereas the change is weak for jets with lower density in a heavier medium. This result agrees with the qualitative conclusions of the hypothesis discussed above concerning the mechanism of mixing of flows with displacement. The theoretical curve plotted from relation (2.4) at $\alpha = 0.75$ (Fig. 3) satisfactorily describes the experimental data. Within the framework of the proposed mixing model, this means that in mixing of flows of different density, α is defined in the same way for the whole investigated range of n, which leads in turn to the conclusion that the concentration profile is independent of the density ratio. However, the latter statement requires further verification.

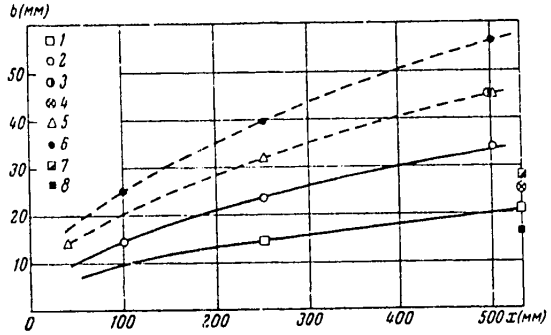

Fig. 4. 1--air-air; 2--air-air, diameter 1.2 mm in air; 3--air-air, diameter 2.5 mm in air; 4--air-helium; 5--air-helium, diameter 2.5 mm in air; 6--air-helium, diameter 1.2 mm in air; 7--air helium, diameter 1.2 mm in helium; 8--air-air, $U_\infty = 24.5$ m/s

All the experimental data on flow in the wake were obtained in the self-similar region at fairly remote distances from the edge.

Fig. 4 gives data on the behavior of the width b of the wake as a function of distance x from the edge at a low level of turbulence in an unperturbed flow of fluid. The width of the wake was determined from the temperature profile; the velocity of the unperturbed flow $U_\infty = 11$ m/s. To vary the initial loss of momentum, cylinders with diameters of 1.2 and 2.5 mm were placed in one of the streams along the entire edge, the larger cylinder being placed at a height of 2 mm above the surface separating the plates, while the smaller cylinder was put right on the surface. Both cylinders were held 30 mm from the edge.

The experimental points relating to homogeneous wakes (solid lines) are satisfactorily described by a parabola $b = c(x - x_0)^{1/2}$. With an increase in velocity ($U_\infty = 24.5$ m/s) the width of the wake decreases.

The same figure shows experimental data relating to the wake formed when flows of different density (air and helium) merge behind the plate. The density ratio was varied from 6.5 to 9.0 by heating the air or the helium. These data are also satisfactorily described by a parabolic relation (broken lines) $b \sim (x - x_0)^{1/2}$. In this case the width of the wake is greater than for wakes in a like fluid with placement of identical cylinders in the air stream.

It should be noted that placement of the cylinder in the light gas (helium) leads to a slight increase in the width of the wake, while placement of the same cylinder in the heavy gas (air) considerably increases the width of the wake.

Since the loss of momentum in the light gas remains unchanged when the cylinder is placed in the heavy gas, the value of α can be determined from relation (1.17) by measuring the width of the wake. In accordance with the assumptions of Section 2, the value of α is taken as 0.5, which corresponds to expression (1.15), where the form of function $\phi(n)$ depends on the definition of ρ_{eff}. Calculation by the data of Fig. 4 gives $\alpha = 0.435$. Thus the value of ρ_{eff} in the wake is close to the arithmetic mean density of the mixing gases. The difference between this value of α and the previously suggested value of $\alpha = 0.5$ corresponds to a difference in the width of the wake of 5%.

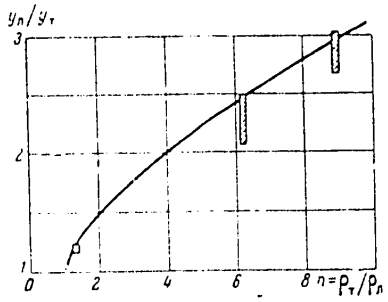

Fig. 5

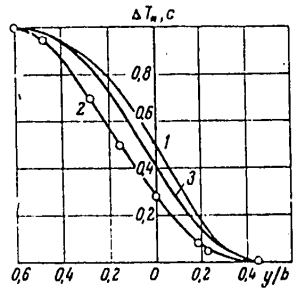

Fig. 6. 1--c (calculation); 2--ΔT_* (experiment); 3--error curve

Fig. 5 shows data on the change in the ratio of coordinates $y_Л/y_T$ of the wake boundary on the heavy and light gas sides reckoned from the plane of the plate as a function of the density ratio n. The disposition of experimental points is

shown by the shaded rectangles. Displacement of the wake was determined from the distribution of concentrations calculated from the experimental temperature field and from photographs of the flow at a distance x = 200 mm from the edge and with a cylinder of 1.2 mm diameter placed in the air stream. It should be noted that the displacement of the wake in the given case could have been influenced by flow conditions outside the wake, for example by the conditions of discharge from the working section.

Fig. 6 shows the profile of relative excess temperature ΔT_* ($T_{hel} < T_{air}$) in the wake with a helium-air flow, and the concentration profile calculated from this curve. For purposes of comparison, this figure also gives the Gauss curve that coincides with the concentration profile at points 0.95 and 0.05. Considering that the helium concentrations are understated in calculating the concentrations by the method presented in the Appendix, which assumes absence of molecular mixing, we can take it that the given profile is close to Gaussian distribution.

Schlieren photographs of the wakes behind the edge of a plate are shown in Fig. 7 [photo not reproduced]. These photographs show an increase in the width of the wake in a heterogeneous flow as compared with the wake in a medium with uniform density, and also displacement of the wake relative to the plate.

Conclusions. Based on dimensional analysis and some hypotheses concerning the mechanism of motion of the boundaries of the turbulent region of a wake, relations are found for the way that the width of the wake and its displacement depend on the ratio of densities of the mixing flows. Experimental data are obtained that agree with the results of the theoretical analysis.

APPENDIX

Thermocouple Measurement of Temperature in Flows with Density Gradient. Fluctuation of both concentration and temperature takes place in turbulent flows with a density gradient. This fluctuation may have a considerable effect on thermocouple readings, since they are determined by the conditions of junction heat exchange. In the zone of turbulent mixing of flows, pulsations of concentration are commensurate with the average value, but in some cases they may be several times the average. Since the exact level of pulsations is unknown, it is of interest to determine the relation between thermocouple readings and concentration in two extreme cases.

In the first case, it is assumed that the concentration and relative excess temperature vary from 0 to 1 during flow around the thrmocouple junction, and the average of the readings is determined by the frequency of alternating immersion of the junction in one fluid or the other.

The second extreme assumption is that the fluids are intermixed up to the molecular level, and that the corresponding temperatures and concentrations have been reached. However, this assumption is admittedly not realized in most free turbulent flows.

We will assume that the thermocouple responds sluggishly, so that its temperature does not vary when there are temperature pulsations in the incident flow. We will assume moreover that the difference in temperatures of the flows is small in

comparison with the average temperature of the mixture ($\Delta T/T \ll 1$), and in evaluating the parameters the temperature can be taken as constant. Then the heat applied to the thermocouple when the temperature of the flow exceeds that of the thermocouple should equal the heat carried away from the thermocouple when the flow temperature is less than that of the thermocouple. This heat balance is written as

$$\alpha_1(T_1 - T_T)t_1 = \alpha_2(T_T - T_2)t_2, \tag{A.1}$$

where t_1 and t_2 are the respective times during which the thermocouple is in fluids 1 and 2; α_1 and α_2 are heat transfer coefficients, T_T is the temperature of the thermocouple.

In this case, the concentration of fluid 1 is $c = t_1/(t_1 + t_2)$. Introducing $\gamma = \alpha_1/\alpha_2$; $T_* = (T_T - T_2)/(T_1 - T_2)$, we get

$$c = \frac{T_*}{\gamma + T_*(1-\gamma)}. \tag{A.2}$$

The coefficient of heat transfer of the junction is determined from the dimensionless relation

$$\mathrm{Nu} = A + B\,\mathrm{Re}^n\mathrm{Pr}^m. \tag{A.3}$$

At high Reynolds numbers, the first term in the right-hand member of (A.3) is insignificant. Then we get the following expression for γ:

$$\gamma = \frac{\alpha_1}{\alpha_2} = \frac{\lambda_1}{\lambda_2}\left(\frac{\nu_2}{\nu_1}\right)^n\left(\frac{\mathrm{Pr}_1}{\mathrm{Pr}_2}\right)^m. \tag{A.4}$$

In deriving this expression it was assumed that fluids 1 and 2 flow around the thermocouple junction at equal velocities. Let us take $n = 0.56$ and $m = 0.36$ [Ref. 5]. Then we can indicate the values of γ in the two cases: $A \gg B\,\mathrm{Re}^n\mathrm{Pr}^m$ and $A \ll B\,\mathrm{Re}^n\mathrm{Pr}^m$. For the first case, $\sigma_{air}/\sigma_{hel} = 0.17$, $\sigma_{air}/\sigma_{Fr} = 2.88$; for the second case, $\sigma_{air}/\sigma_{hel} = 0.545$, $\sigma_{air}/\sigma_{Fr} = 0.98$. In the experiments, γ was usually closer to the values typical of the second case. Therefore it can be assumed that when the temperature is measured by thermocouple, the distribution of relative temperatures in the zone of mixing of Freon with air is close to the distribution of concentrations.

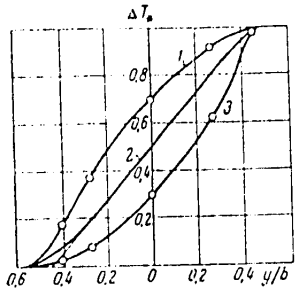

Fig. 8. 1--$V_{hel} > V_{air}$; $T_{hel} > T_{air}$; 2--$V_{Fr} > V_{air}$; $T_{Fr} > T_{air}$; 3--$V_{air} > V_{hel}$; $T_{air} > T_{hel}$

Fig. 8 shows the profiles of temperatures on the initial section of accompanying axisymmetric jets of air in helium, helium in air, and Freon in air. In the experiments the temperature of the jet was always higher than the temperature of the accompanying flow, while the jet velocities were always greater than the velocity of the accompanying flow. The resultant profiles differ strongly from one another. At the same time, the dimensionless profiles of temperatures of submerged jets of Freon in air, air in Freon and air in air practically coincide. Since in this case $\gamma \approx 1$, this coincidence of temperature profiles should be observed as well if

the concentration profiles in these cases are similar. When the temperature profiles typical of jets of helium in air and air in helium are recalculated with respect to the corresponding parameter γ, the resultant concentration profiles also approach the profiles of concentrations (temperatures) in a jet of air in air. It should be noted that recalculating by the proposed method should lead to systematic deviation of the calculated profile from the true profile since no consideration is taken of molecular transport.

REFERENCES

1. Townsend, A. A., "Struktura turbulentnogo potoka s poperechnym sdvigom" [Structure of Turbulent Flow with Transverse Shear], Foreign Literature Publishers, 1959.

2. Townsend, A. A., "The Mechanism of Entrainment in Free Turbulent Flows", JOURNAL OF FLUID MECHANICS, Vol 26, Part 4, 1966.

3. Landau, L. D. and Livshits, Ye. M., "Mekhanika sploshnykh sred" [Mechanics of Continuous Media], Gostekhizdat, 1953.

4. Navoznov, O. I. and Pavel'yev, A. A., "Mixing of Accompanying Gas Jets", IZVESTIYA AKADEMII NAUK SSSR: ENERGETIKA I TRANSPORT, No 2, 1968.

5. Kutateladze, S. S. and Borishanskiy, V. M., "Spravochnik po teploperedache" [Handbook on Heat Transfer], Leningrad, Gosenergoizdat, 1959.

6610
CSO: 1862/138

TRANSITION TO TURBULENCE IN ACCOMPANYING JETS

Moscow IZVESTIYA AKADEMII NAUK SSSR: MEKHANIKA ZHIDKOSTI I GAZA in Russian No 6, 1969 pp 131-136

[Article by O. I. Navoznov and A. A. Pavel'yev, Moscow]

[Text] An experimental investigation was made of the transition to turbulence for flow of an axisymmetric helium jet in an accompanying stream of air in the case where the velocity on their boundary in the initial cross section was varied in a layer of finite thickness produced by cross sectionally variable hydraulic drag--a honeycomb with tube length varying along the radius. Velocity and temperature profiles were measured, and photographs were taken by the Töpler method.

It is known that flow with transverse shift of velocity is unstable, and even near the nozzle one observes periodic perturbations that increase with respect to length, and the flow rapidly becomes turbulent. The absolute instability of the surface of tangential discontinuity of velocity has been rigorously proved by von Helmholtz, and an analysis done by Rayleigh on the stability of flow in a laminar layer with velocity shift (which corresponds to a laminar zone of mixing of plane-parallel flows) within the framework of linear stability has shown that such a flow is likewise unstable [Ref. 1].

More recent research [Ref. 2] has shown that a laminar mixing layer is unstable at all Reynolds numbers, and that this result is weakly dependent on the form of velocity profile [Ref. 3]. However, the development of perturbations apparently conforms to linear theory only near the nozzle, and further out the mechanisms described by nonlinear theory become appreciable. The nonlinear transition phase was studied in papers by Schade [Ref. 4] and Lin [Ref. 5]. It is shown in Ref. 5 that nonlinear effects on the transition section may lead to "survival" of perturbations of some single wavelength, and that there should be eddies with the axis directed along the flow. In Ref. 4 an attempt is made to establish the limits of applicability of linear stability theory.

It is shown below that in the absence of tangential discontinuity of velocity on the boundary of the jets and at low Reynolds numbers of flow around the edges of the outlet face of the honeycomb, the transition to turbulent flow is extended to distances from the nozzle greater than 14 initial diameters of the jet, and the mixing level on this section is close to laminar. In this case the Reynolds

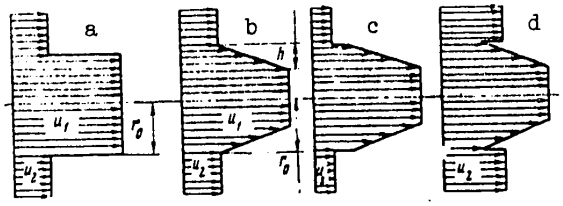

Fig. 1

number defined with respect to the initial diameter of the jet and the difference between the velocities of the accompanying flows was equal to ~5000, whereas according to the linear theory of hydrodynamic stability the critical Reynolds number for flows of this kind is <10. The experimental technique is described.

1. An experimental study of transition to turbulence was done on the initial section of accompanying axisymmetric jets when the velocity profiles shown in Fig. 1 were set up in the initial cross section. The following quantities were the controlling parameters in the research: u_1, u_2--flow velocities outside of the shear layer, u_1^*--velocity on the jet boundary in the initial section, ρ_1, ρ_2--flow densities, ν_1, ν_2--kinematic viscosities of the working fluids, h--thickness of the shear layer, r_0--radius of the central jet, R_0--radius of the accompanying stream, M_1, M_2--dimensions of the honeycomb cells and screen mesh, ψ_1, ψ_2--porosity of honeycomb and screen.

The flows were taken as isothermal, and the initial nonuniformities of the velocity profile determined by the boundary layers and edges were taken as small. We can form 11 dimensionless numbers from the above-mentioned quantities:

$$m = \frac{u_1}{u_2}, \quad m^* = \frac{u_1^*}{u_1}, \quad n = \frac{\rho_1}{\rho_2}, \quad f = \frac{\nu_1}{\nu_2}, \quad h^* = \frac{h}{r_0}, \quad r^* = \frac{r_0}{R_0}$$
$$R = \frac{h(u_1 - u_2)}{\nu_1}, \quad R_1 = \frac{M_1 u_1}{\nu_1}, \quad R_2 = \frac{M_2 u_2}{\nu_2}, \quad \psi_1, \psi_2$$

In experiments with tangential velocity discontinuity (Fig. 1a), the parameters m* and h* are eliminated. When helium and air are used as the working fluids, n and 1/f are approximately equal, since the dynamic viscosities of the fluids are approximately equal. In experiments with velocity shear where the construction of the working section is predetermined, m*, h*, r*, ψ_1, ψ_2 remained constant and the flow was studied as a function of the behavior of parameter m and Reynolds numbers R, R_1 and R_2. At $m \neq m^*$ we have tangential discontinuity of velocity in addition to shear: at $m > m^*$ (Fig. 1d) the flow in the mixing layer of the accompanying jets approaches wake flow, and at $m < m^*$ (Fig. 1c) it approaches the flow in a free mixing layer.

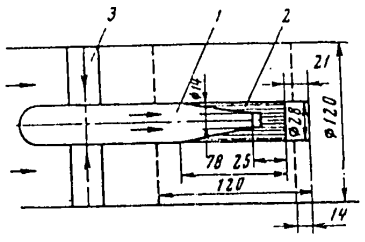

Fig. 2

A diagram of the working section of the facility is shown in Fig. 2. Central nozzle 1 with diameter d_0 = 28 mm and length of 260 mm is held in the

center of a tube 120 mm in diameter by two streamlined pylons 3. The working fluid was fed to the nozzle through the pylons. A thin metal jacket with taper of no more than 10° was placed over the outer surface of the nozzle with a gap of about 0.5 mm for thermal insulation of the flows. Fine screens with mesh of $M = 0.1$ mm and porosity $\psi = 0.35$ were placed in both flows to equalize the velocity profiles and quench turbulence. In jet experiments with stepwise change of velocity, a grid was placed on the nozzle tip over the cross section of both accompanying flows, and in experiments with velocity shear the last screen in the accompanying flow was placed at a distance of 14 mm from the nozzle tip. The turbulence intensity on such screens is less than 1%, and the coefficient of turbulent diffusion is only tiwce the molecular value at an air speed of 15 m/s. The thickness of the cylindrical edge of the nozzle on a length of 10 mm was 0.2 mm, and the thickness of the boundary layer on this edge was less than 1 mm.

The profile with velocity shear in the central jet was set up by honeycomb 2 assembled from tubes of various lengths with outside diameter of 1.2 mm and wall thickness of 0.1 mm. Tube length in the central part of the nozzle out to a radius of 7 mm was the same (25 mm), and then increased linearly to 78 mm on the inner wall of the nozzle. Tube packing in the honeycomb was mainly hexagonal, while on isolated places near the periphery it was close to square. For the given tube size, the porosity of the honeycomb with hexagonal packing was $\psi_1 = 0.65$, and with square packing--$\psi_1 = 0.55$. assuming absence of flow in the spaces between tubes. The equivalent size of bars of a square grating with the same mesh M and the same porosity, was 0.37 mm.

The working fluids sent through the central nozzle were helium and air, and the fluid in the accompanying flow was air.

The profiles of velocity heads and temperatures were measured in the experiments. The velocity heads were measured by a comb of 25 Pitot tubes with readings taken on an inclined manometer bank. To measure the temperature profile, the working fluid of the central jet was heated to 30-50°C. The temperature profiles were measured by a comb of 24 Chromel-Copel thermocouples. Their readings were recorded on the EPP-09 [strip-chart potentiometer].

The measured profiles were processed in relative units. The coordinates at which the relative excess temperature $T_* = (T - T_2)/(T_1 - T_2)$ was equal to 0.05 were taken as the outer boundary of the mixing zone.

In addition to the indicated measurements, the flows were photographed by the Töpler method at an exposure of 10^{-4} s, and by motion pictures at a speed of 1400 frames per second.

2. The transition to turbulent flow of a helium jet in an accompanying air stream in the case of a tangential velocity discontinuity in the initial cross section was studied for different thicknesses of the boundary layers on the edge, different velocity levels and variable ratio of the velocities of the accompanying jets. Fig. 3 shows photographs [not reproduced] of a helium jet with velocity of 16.5 m/s in an accompanying air flow of variable velocity. Velocities of the accompanying air flow: a) 3.3 m/s; b) 6.5 m/s; c) 9.8 m/s; d) 13.1 m/s; e) 16.5 m/s. The following conclusions can be drawn from an analysis of these photographs.

1. The length of the section of transition to turbulence increases with increasing velocity ratio m.

2. Flow typical of that in a wake arises at m close to unity.

3. Perturbations of single wavelength develop on the transition section. Flow on the transition section is three-dimensional.

4. An abrupt increase in amplitude of the perturbation accompanied by doubling of wavelength can be observed on the transition section.

5. In our experiments we failed to get any appreciable length of transition section at $m < 0.4$.

It can also be noted that the length of the transition section increases with a reduction in the initial nonuniformities of velocity, i. e. with a reduction in the boundary layers and the thickness of the edge, and decreases with an increase in the absolute velocity of the flows.

An investigation of transition to turbulent flow of jets with transverse velocity shear at the inlet was done with placement of a honeycomb in the central nozzle with variable tube length along the radius. To determine initial flow conditions the velocity profiles were measured at a distance of 5 mm from the nozzle tip. These measurements showed that the velocity profile set up by the honeycomb depends on the absolute level of velocities in the case of variation of the flow conditions in the tubes of the honeycomb. When the velocity is increased, the flow becomes turbulent earlier in the central tubes of the honeycomb, the drag in these tubes increases and the velocity profile becomes fuller.

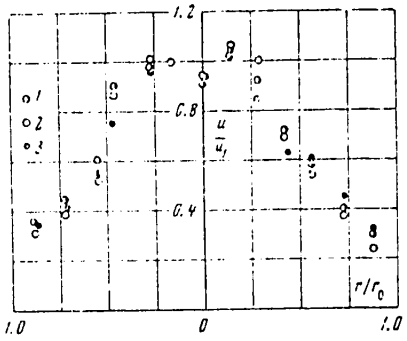

Fig. 4

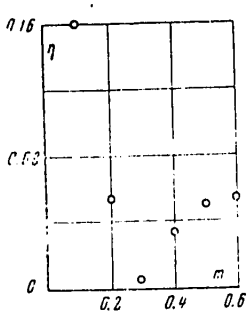

Fig. 5

For the case of air, the velocity ratio m* remained constant and equal to 0.28 with an increase in u_1 from 10 m/s to 15 m/s, and then rose to 0.65 with an increase in velocity to 30 m/s. Throughout the investigated range of helium jet velocities (10-50 m/s), flow in all tubes of the honeycomb was laminar, so that the velocity profile did not depend on the level of velocity, and ratio m* stayed constant and approximately equal to 0.28 (Fig. 4). Points 1, 2, 3 correspond to velocities $u_1 = 29$, 38, 58 m/s.

The localized nonuniformities of the velocity profile in the central part of the honeycomb can be attributed to irregularity in packing of the tubes.

Measurements of the temperature profile in the helium jet at the nozzle tip showed that the initial thickness of the temperature boundary layer on the outer wall of the nozzle did not exceed 2 mm. As pointed out above, the width b of the jet was determined from measurements of the temperature profile.

Fig. 5 shows the way that the dimensionless width of a helium jet $\eta = (b - d_0)/x$ depends on the velocity ratio m at constant velocity on the axis of the jet $u_1 = 17.6$ m/s at a distance x = 200 mm from the nozzle tip. The quantity η was used for convenience of comparison with data on mixing of turbulent jets. The results show that minimum mixing is observed at $m = m^*$, i. e. when the velocity on the boundary of the jet is equal to the velocity of the accompanying flow. Mixing intensity at $m = m^*$ is close to laminar.

Mixing intensity increases at $m \neq m^*$. Let us recall that when $m < m^*$, part of the velocity difference occurs in the tangential discontinuity (Fig. 1c). In this case, mixing increases rather abruptly with increasing m. When $m > m^*$, the velocity profile on the tip is close to that shown in Fig. 1d. The increase in mixing intensity in this case is small since the momentum loss takes place in a light gas.

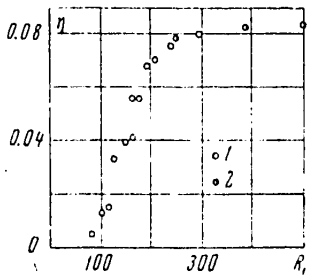

Fig. 6

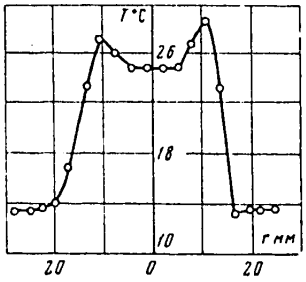

Fig. 7

Fig. 6 shows the way that the quantity η depends on the Reynolds number of flow around the output edges of the central tubes of the honeycomb at constant $m = m^* = 0.26$ at a distance of x = 200 mm from the nozzle tip. Points 1 and 2 correspond to jets of helium and air. The characteristic velocity used in the Reynolds number is the average velocity in a tube of the honeycomb, and the characteristic dimension is the diameter of a bar in an equivalent grating with mesh size equal to the tube diameter, and with porosity equal to that of the honeycomb. Thus the given Reynolds number is defined as

$$R_1 = \frac{u_1 M_1}{\nu_1} \frac{1 - \psi_1^{0,5}}{\psi_1}$$

For a given construction of the working section, this Reynolds number is proportional to the velocity on the axis of the jet. On Fig. 6 we can distinguish three characteristic regions of Reynolds number behavior. In the range $R_1 < 70$, mixing is close to laminar, and the width of the mixing zone increases as the

velocity decreases, which is what should be observed in laminar mixing. Experimental data in this region are not given since the measured width of the mixing zone is small, and we can only draw a qualitative conclusion on the behavior of the width of the jet. In the region $70 \leqslant R_1 \leqslant 200$ the width of the mixing zone increases with increasing Reynolds number, i. e. with increasing velocity. At $R_1 > 200$ the mixing intensity is already considerably greater than the molecular level, and it increases weakly with increasing Reynolds number. This same figure gives the results of measurement of the width of a jet of air in an accompanying flow of air. Thus the behavior of the Reynolds number was determined both by the change in velocity and by the change in type of gas. The data obtained in the two cases are in agreement. It can be assumed that a change of mixing intensity is due to the conditions of flow around the end face of the honeycomb. At $R_1 < 70$ the mode of flow around the end face is nearly laminar over the entire cross section, and when the number R_1 increases the turbulent flow around the edge, arising initially in the center, gradually spreads over the entire cross section, after which the mixing intensity increases weakly with a further increase in the number R_1. It should be noted that in measurements at other distances from the nozzle tip the curves shown in Fig. 5 and 6 may have another shape.

Fig. 7 shows the temperature profile in a helium jet in an accompanying flow of air at $m = m^*$ at a distance of 200 mm from the nozzle tip and at a velocity on the jet axis of $u_1 = 11$ m/s. A distinguishing feature of this profile is the presence of temperature peaks in the mixing zone: the maximum temperature in the mixing zone is three or four degress higher than the temperature on the axis of the jet. This may be due to a diffusion heat effect that is observed upon molecular mixing of helium with air [Ref. 6].

Fig. 8 and 9 show photographs [not reproduced] of a helium jet in an accompanying flow of air at a velocity on the jet axis of $u_1 = 11.1$ m/s, and at different values of m at distances from the nozzle tip of $0 \leqslant x \leqslant 180$ mm and $200 \leqslant x \leqslant 400$ mm. In photographing the jet at distances of $200 \leqslant x \leqslant 400$ mm, an extension was installed on the working section with length of 198 mm. Photographs a, b, c, d, e on Fig. 8 correspond to the values of the parameter $m = 0.1, 0.2, 0.3, 0.4, 0.6$. On Fig. 9, photographs a, b, c, d correspond to values of the parameter for $m = 0.2, 0.3, 0.4, 0.6$. Analysis of the photographs shows that at $m = m^*$ flow is close to laminar right up to 400 mm from the tip, although initially weak ordered perturbations are observed that damp out downstream. These perturbations are apparently from flow around the edge of the nozzle. At $m > m^*$, regular periodic perturbations arise that are typical of flow in a wake at low Reynolcs numbers R. These perturbations develop lengthwise, but do not lead to appreciable widening of the jet. At $m < m^*$ a transition can be seen to turbulence at distances $x > 300$ mm from the tip. Motion picture photography shows that the point of loss of stability fluctuates over a wide range.

Analysis of photographs made at high velocities shows that the transition to turbulence at $m < m^*$ takes place much faster. This can be attributed to an increase in the velocity break on the boundary with increasing velocity and at constant m. At $m = m^*$, the increase in velocity leads to irregular perturbations close to the nozzle, although the intensity of mixing still differs strongly from the intensity typical of turbulent jets.

The given experimental data show that the length of the section of transition to turbulent flow in jets with initial profile with velocity shear and at a low level

of initial perturbations increases as compared with jets with tangential velocity discontinuity. In this case, the mixing level is close to laminar. The results are rather unexpected since according to linear theory such flows are unstable, and in experiments one usually observes a rapid loss of stability and a transition to turbulent flow. In the given study the Reynolds number defined with respect to the diameter of the jet and velocity difference is about 5000. Probably the Reynolds number defined with respect to the width of the shear layer cannot characterize the stability of such a flow since turbulent flow sets in very rapidly in thin shear layers where the Reynolds number is low.

It can be assumed that elongation of the transition section is due either to small incremental increases in perturbations within the framework of the linear theory, or it can be attributed to stability of the secondary periodic flow that arises according to Landau [Ref. 7] after the amplitude of the primary perturbation reaches a final magnitude.

It can also be assumed that with conditions of laminar flow at the inlet, the ratio of the length of the transition section to the width of the shear layer does not depend on velocity at a constant ratio of flow velocities. In the given experiment the velocity at which transition to turbulent flow due to instability to long-wave perturbations is not distorted by initial turbulence is apparently determined by the conditions of flow around the end face of the honeycomb. A reduction in the diameter and wall thickness of the tubes in the honeycomb should increase the range of velocities at which there is an increase in the length of the section of transition to turbulence. In setting up the Reynolds number of flow around the end face of the honeycomb, consideration should be taken of the nonuniformity of velocity in the channel.

The authors thank V. M. Iyevlev for assistance and continued interest in the work.

REFERENCES

1. Monin, A. S. and Yaglom, A. M., "Statisticheskaya gidromekhanika" [Statistical Hydromechanics], Part 1, Moscow, "Nauka", 1966.

2. Esch, R. E., "The Instability of a Shear Layer Between Two Parallel Streams", JOURNAL OF FLUID MECHANICS, Vol 3, No 3, 1957.

3. Tatsumi, T. and Gotoh, K., "The Stability of Free Boundary Layers Between Two Uniform Streams", JOURNAL OF FLUID MECHANICS, Vol 7, No 3, 1960.

4. Schade, H., "Contribution to the Nonlinear Stability Theory of Inviscid Layers", PHYSICS OF FLUIDS, Vol 7, No 5, 1964.

5. Lin, C. C. and Benney, D. J., "On the Instability of Shear Flows", Proceedings of the Symposium of Applied Mathematics, 13, Hydrodynamics Instability, pp 1-24 [Russian translation: Lin Chia-Chiao and D. J. Benney, "O neustoychivosti techeniy s gradiyentom skorosti" in: "Gidrodinamicheskaya neustoychivost'" [Hydrodynamic Instability], Moscow, "Mir", 1964.]

6. Chapman, S., Cowling, T., "Matematicheskaya teoriya neodnorodnykh gazov" [Mathematical Theory of Heterogeneous Gases], Moscow, Foreign Literature Publishers, 1965.

7. Landau, L. D. and Lifshits, B. M., "Mekhanika sploshnykh sred" [Mechanics of Continuous Media], second edition, Moscow, Gostekhteoretizdat, 1953.

6610
CSO: 1862/139

TURBULENT FLOW OF A CONDUCTIVE FLUID IN A LONGITUDINAL MAGNETIC FIELD

Moscow IZVESTIYA AKADEMII NAUK SSSR: MEKHANIKA ZHIDKOSTI I GAZA in Russian No 1, 1970 pp 10-17

[Article by D. S. Kovner and V. G. Lushchik, Moscow]

[Text] The use of equations for the Reynolds stress tensor (equations of turbulence energy balance) that are closed by semi-empirical relations has been useful in the investigation of flows with transverse shear in conventional hydrodynamics [Ref. 1, 2, 7].

In magnetohydrodynamics the equations for the Reynolds stress tensor are supplemented by terms that account for the influence of the magnetic field on turbulence characteristics for which the semi-empirical representation is inconvenient because of the limited nature of the experimental material.

Nevertheless, attempts have been made [Ref. 3, 4] at constructing a semi-empirical theory of turbulence based on equations for the Reynolds stress tensor in the case of flow of a conductive fluid in a longitudinal magnetic field, where the effect of the field is accounted for by terms that describe the Joule dissipation of turbulence energy for which the corresponding representations are taken.

In this paper, following Ref. 3, 4, a hypothesis is formulated in its turn relative to the term that describes Joule dissipation of turbulence energy, which has a simple physical meaning and accounts for the change in structure of turbulence of the flow in a magnetic field. Using the assumed hypothesis together with the known Rotta relations [Ref. 2] for the other terms in the equation of the Reynolds stress tensor yields an expression for turbulent flow that is analogous to the well known Prandtl relation, differing only in the coefficient that accounts for the magnetic field.

1. In the Navier-Stokes equations[1]

$$\frac{\partial U_i}{\partial t}+U_k\frac{\partial U_i}{\partial x_k}=-\frac{1}{\rho}\frac{\partial P}{\partial x_i}+\nu\frac{\partial^2 U_i}{\partial x_k\partial x_k}+\frac{1}{\rho}X_i\quad(i=1,2,3). \tag{1.1}$$

the volumetric density of external forces X_i in the case of motion of an electrically conductive fluid in a magnetic field has the well known form

$$X_i=\varepsilon_{irs}J_rB_s \tag{1.2}$$

Here ε_{irs} is a completely antisymmetric tensor of third rank, while J_r and B_s are components of the vectors of induced electric current and magnetic field induction respectively.

Representing the individual values of the fields of the corresponding quantities appearing in the Navier-Stokes equations (1.1) as the sum of the average and pulsation values. e. g. $U_i=\overline{U}_i+u_i$, equations (1.1) with consideration of (1.2) and the equations of continuity for the average and pulsation values can be written as

$$\begin{aligned}&\frac{\partial\overline{U}_i}{\partial t}+\frac{\partial u_i}{\partial t}+\overline{U}_k\frac{\partial u_i}{\partial x_k}+u_k\frac{\partial\overline{U}_i}{\partial x_k}+\frac{\partial}{\partial x_k}(\overline{U}_i\overline{U}_k+u_iu_k)=\\&=-\frac{1}{\rho}\frac{\partial\overline{P}}{\partial x_i}-\frac{1}{\rho}\frac{\partial p}{\partial x_i}+\nu\frac{\partial^2\overline{U}_i}{\partial x_k\partial x_k}+\nu\frac{\partial^2 u_i}{\partial x_k\partial x_k}+\frac{1}{\rho}\varepsilon_{irs}(\overline{J}_r+j_r)(\overline{B}_s+b_s)\end{aligned} \tag{1.3}$$

Then by applying the operation of averaging to the terms of equation (1.3) and using the Reynolds condition [Ref. 1], we can get equations that are analogous to the Reynolds equations in ordinary hydrodynamics

$$\begin{aligned}&\frac{\partial\overline{U}_i}{\partial t}+\frac{\partial}{\partial x_k}(\overline{U}_i\overline{U}_k+\langle u_iu_k\rangle)=\\&=-\frac{1}{\rho}\frac{\partial\overline{P}}{\partial x_i}+\nu\frac{\partial^2\overline{U}_i}{\partial x_k\partial x_k}+\frac{1}{\rho}\varepsilon_{irs}(\overline{J}_r\overline{B}_s+\langle j_rb_s\rangle)\end{aligned} \tag{1.4}$$

From equations (1.3) and (1.4) by a conventional technique (see for example Ref. 1, 2) we get equations for the Reynolds stress tensor

$$\begin{aligned}&\frac{\partial}{\partial t}\langle u_iu_j\rangle+\overline{U}_k\frac{\partial}{\partial x_k}\langle u_iu_j\rangle+\langle u_ju_k\rangle\frac{\partial\overline{U}_i}{\partial x_k}+\langle u_iu_k\rangle\frac{\partial\overline{U}_j}{\partial x_k}=\\&=\frac{1}{\rho}\left\langle p\left(\frac{\partial u_i}{\partial x_j}+\frac{\partial u_j}{\partial x_i}\right)\right\rangle+\frac{\partial}{\partial x_k}\left[\nu\frac{\partial}{\partial x_k}\langle u_iu_j\rangle-\langle u_ku_iu_j\rangle-\right.\end{aligned}$$

[1]Here and below it is assumed that the index repeated twice refers to summation from one to three, e. g.

$$U_k\frac{\partial U_i}{\partial x_k}=\sum_{k=1}^{3}U_k\frac{\partial U_i}{\partial x_k}.$$

$$-\frac{1}{\rho}\langle p(\delta_{jk}u_i+\delta_{ik}u_j)\rangle\Big]-2\nu\left\langle\frac{\partial u_i}{\partial x_k}\frac{\partial u_j}{\partial x_k}\right\rangle+$$
$$+\varepsilon_{irs}\frac{1}{\rho}[\bar{J}_r\langle b_s u_j\rangle+\bar{B}_s\langle u_j j_r\rangle+\langle j_r b_s u_j\rangle]+ \qquad (1.5)$$
$$+\varepsilon_{jrs}\frac{1}{\rho}[\bar{J}_r\langle b_s u_i\rangle+\bar{B}_s\langle u_i j_r\rangle+\langle j_r b_s u_i\rangle]$$

Here δ_{ij} is the unit tensor ($\delta_{ij}=1$ when $i=j$, and $\delta_{ij}=0$ when $i\neq j$).

Setting $i=j$ in (1.5) we get the equation of balance of turbulence energy $E=\langle u_i^2\rangle/2$ that describes the time change of density of the energy of pulsation motion

$$\frac{\partial E}{\partial t}+\bar{U}_k\frac{\partial E}{\partial x_k}+\langle u_i u_k\rangle\frac{\partial \bar{U}_i}{\partial x_k}=\frac{\partial}{\partial x_k}\Big[\nu\frac{\partial E}{\partial x_k}-\frac{1}{2}\langle u_i^2 u_k\rangle-\frac{1}{\rho}\delta_{ik}\langle p u_i\rangle\Big]- \qquad (1.6)$$
$$-\nu\left\langle\left(\frac{\partial u_i}{\partial x_k}\right)^2\right\rangle+\frac{1}{\rho}\varepsilon_{irs}[\bar{J}_r\langle b_s u_i\rangle+\bar{B}_s\langle j_r u_i\rangle+\langle j_r b_s u_i\rangle] \qquad (1.6)$$

All terms of equation (1.6) have a clear physical meaning. In particular, the last term is the Joule dissipation of turbulence energy due to pulsation motion of the fluid in a magnetic field[1].

It is obvious that equations for the Reynolds stress tensor in form (1.5) cannot be resolved relative to $\langle u_i u_j\rangle$ in explicit form. However, this can be done in certain cases that permit considerable simplifications of equations (1.5).

2. Let us consider analogously to Ref. 3, 4 the steady-state flow of a conductive fluid in a longitudinal magnetic field in the case where there is equality between the production and dissipation of turbulence energy with consideration of its redistribution along the coordinate axes, i. e. we will disregard convective and diffusion terms in equations (1.5). As experience shows in the case of absence of a magnetic field, this takes place in the greater part of the flow in the tube [Ref. 5] and in the boundary layer on a flat plate in the absence of a pressure gradient in the external flow [Ref. 6]. It is further assumed that the Reynolds number defined with respect to the pulsation components of flow velocity is low so that the pulsation component of magnetic field induction can be disregarded as compared with the average induction of the field produced by external sources.

With respect to the terms that describe exchange of energy between pulsations along the different coordinate axes and viscous dissipation of the energy of pulsation motion in equations (1.5), we take the assumptions

$$\frac{1}{\rho}\left\langle p\left(\frac{\partial u_i}{\partial x_j}+\frac{\partial u_j}{\partial x_i}\right)\right\rangle=-k\frac{\sqrt{E}}{l}\left(\langle u_i u_j\rangle-\frac{2}{3}\delta_{ij}E\right). \qquad (2.1)$$

[1]See for example Ref. 1, 2 regarding the physical meaning of the other terms of equation (1.6).

$$2\nu\left\langle\frac{\partial u_i}{\partial x_k}\frac{\partial u_j}{\partial x_k}\right\rangle=\nu c_1\frac{\langle u_iu_j\rangle}{l^2}+\frac{2}{3}c\delta_{ij}\frac{\overline{E'^2}}{l} \tag{2.2}$$

proposed by Rotta[1].

Here k, c and c_1 are empirical constants, l is the scale of pulsation motion, which is taken as the Prandtl mixing path in the absence of a magnetic field.

With respect to the pulsation component of electric current due to turbulent motion of a conductive fluid in a magnetic field, we make the following assumption.

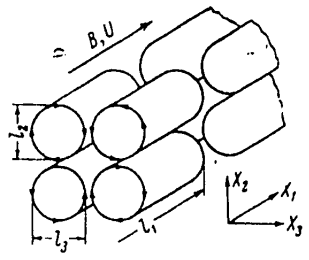

Fig. 1

Let the structure of turbulent flow be characterized by eddies that have different scales (mixing paths) along coordinate axes x_1, x_2, x_3 (Fig. 1), assuming at the same time that the ratios of the scales are equal to the respective pulsation velocities

$$\frac{l_1}{\sqrt{\langle u_1^2\rangle}}=\frac{l_2}{\sqrt{\langle u_2^2\rangle}}=\frac{l_3}{\sqrt{\langle u_3^2\rangle}} \tag{2.3}$$

implied by estimation of the order of magnitudes in the equation of continuity for the pulsation velocities.

The flow is considered in a longitudinal magnetic field (i. e. $B_2=B_3=0$, $B_1=B$), and therefore the emf of the induction arises as a consequence of interaction with the field of the transverse (relative to the magnetic field) components u_2 and u_3 of the pulsation velocity vector which are taken, as in the case of absence of a magnetic field, as approximately equal ($u_2\approx u_3$, and consequently $l_2\approx l_3$ as well according to (2.3)). The pulsation current that shows up in this way is closed in the longitudinal direction (along the magnetic field) so that the overall length of the current loop L_k is approximately equal in magnitude to the length of the vortex loop $2(l_1+l_2)$.

The overall emf $\Delta\phi$ that arises in a current loop of length L_k can be represented in the form

$$\Delta\varphi=2\alpha l_2u_2B \tag{2.4}$$

where α is a coefficient that accounts for the reduction in emf due to the induced pulsation electric field ($0<\alpha<1$).

The electric current caused by this emf in the direction of the magnetic field flows through a layer of fluid with cross section $l_2^2/4$, so that the overall resistance of the loop is equal to

$$\rho_k=L_k/(\sigma l_2^2/4)=8(l_1+l_2)/\sigma l_2^2,$$

and the total current in the loop is

$$J_k=\Delta\varphi/\rho_k=\alpha Bu_2l_2^3\sigma/4(l_1+l_2)$$

[1]It should be noted that equation (2.1), which is approximate even in conventional hydrodynamics [Ref. 1] additionally disregards in this case the magnetic field dependence of pressure pulsations.

Here σ is the specific conductance of the fluid. Consequently, the current density in the longitudinal direction with consideration of relations (2.3) takes the following form:

$$j_1 = \frac{J_k}{l_2^2/4} = \alpha \frac{\sigma B u_2}{l_1/l_2 + 1} = \alpha \frac{\sigma B u_2}{(\langle u_1^2\rangle/\langle u_2^2\rangle)^{1/2} + 1} \tag{2.5}$$

To determine the current density in the transverse direction, the overall current in the loop must be divided by the area of the cross section through which this current flows, i. e.

$$j_2 \approx j_3 = \frac{J_k}{l_1 l_2/4} = \alpha \frac{\sigma B u_2}{(l_1/l_2)^2 + l_1/l_2} = \alpha \frac{\sigma B u_2}{\langle u_1^2\rangle/\langle u_2^2\rangle + (\langle u_1^2\rangle/\langle u_2^2\rangle)^{1/2}} \tag{2.6}$$

Thus in the given case relations (2.1), (2.2), (2.5) and (2.6) close the equations for the Reynolds stress tensor (1.5) which, in the conventional notation

$$\overline{U}_1 = U, \quad u_1 = u, \quad u_2 = v, \quad x_1 = x, \quad x_2 = y$$

take the form

$$\langle uv\rangle \frac{dU}{dy} + \frac{k}{2}\frac{\sqrt{E}}{l}\left(\langle u^2\rangle - \frac{2}{3}E\right) + \nu\frac{c_1}{2}\frac{\langle u^2\rangle}{l^2} + \frac{c}{3}\frac{E^{3/2}}{l} = 0 \tag{2.7}$$

$$\frac{k}{2}\frac{\sqrt{E}}{l}\left(\langle v^2\rangle - \frac{2}{3}E\right) + \nu\frac{c_1}{2}\frac{\langle v^2\rangle}{l^2} + \frac{c}{3}\frac{E^{3/2}}{l} + \alpha\frac{\sigma B^2}{\rho}\frac{\langle v^2\rangle}{\langle u^2\rangle/\langle v^2\rangle + (\langle u^2\rangle/\langle v^2\rangle)^{1/2}} = 0 \tag{2.8}$$

$$\langle v^2\rangle \frac{dU}{dy} + k\frac{\sqrt{E}}{l}\langle uv\rangle + \nu c_1\frac{\langle uv\rangle}{l^2} + \alpha\frac{\sigma B^2}{\rho}\frac{\langle uv\rangle}{\langle u^2\rangle/\langle v^2\rangle + (\langle u^2\rangle/\langle v^2\rangle)^{1/2}} = 0 \tag{2.9}$$

The Reynolds equation (1.4) in the given case will take the well known form

$$\frac{d}{dy}\langle uv\rangle = -\frac{1}{\rho}\frac{dP}{dx} + \nu\frac{d^2U}{dy^2} \tag{2.10}$$

3. From equations (2.7)-(2.9) we can establish the relation between the Reynolds stress and the velocity gradient in flow outside of the viscous sublayer, i. e. disregarding the term that accounts for the direct influence of viscosity on large-scale pulsations in the Rotta relation for viscous dissipation (2.2).

Thus setting $c_1 = 0$ and introducing the coefficient of flow anisotropy $\xi = \langle u^2\rangle/\langle v^2\rangle$ in accordance with Ref. 3, we can get the following relation from (2.7)-(2.9):

$$\langle uv\rangle = -\psi l^2 \left|\frac{dU}{dy}\right| \frac{dU}{dy} \tag{3.1}$$

where

$$\psi = A_1^{3/4}\left[\sqrt{1+(A_2 S_l)^2} - A_2 S_l\right]$$

$$A_1 = \frac{12}{(\xi+2)\left[\xi(k/c-1)+5k/c-2\right]c^{1/4}}, \qquad A_2 = \frac{\alpha}{\xi+\xi^{1/4}}\left(\frac{\xi(k/c-1)+5k/c-2}{3(\xi+2)}\right)^{1/4} \tag{3.2}$$

The coefficient ψ is a function of the local Stewart number

$$S_l = \frac{\sigma B^2}{\rho}\frac{1}{dU/dy}$$

while ξ depends implicitly on the local Stewart number

$$S_l = \frac{\xi+\xi^{1/4}}{\alpha}\frac{\xi(k/c-1)-(k/c+2)}{\sqrt{3+2\left[\xi(k/c-1)-(k/c+2)\right]/(\xi+2)}} \tag{3.3}$$

In order for expression (3.1) for <uv> to become the familiar Prandtl formula in the case of absence of a magnetic field, we must require that $\psi = 1$ when $S_l = 0$. This imposes a certain constraint on the constants k and c, specifically ($\xi = \xi_0$ at B = 0)

$$\frac{12}{(\xi_0+2)\left[\xi_0(k/c-1)+5k/c-2\right]c^{1/4}} = 1 \tag{3.4}$$

On the other hand, from relation (3.3) for $\xi = \xi(S_l)$ in the case $S_l = 0$ we can get a second expression for the constants k and c:

$$\xi_0(k/c-1) - (k/c+2) = 0 \tag{3.5}$$

The coefficient of anisotropy ξ_0 in relations (3.4), (3.5) is a new empirical constant [Ref. 3] (instead of the former k and c) that has a clear physical meaning: the ratio of $\langle u^2\rangle$ to $\langle v^2\rangle$ in the absence of influence of viscosity and magnetic field, under conditions where the generation and dissipation of turbulence energy are in equilibrium.

Thus we can get the following expressions for k and c from (3.4) and (3.5):

$$\frac{k}{c} = \frac{\xi_0+2}{\xi_0-1}, \qquad k = \left[\frac{8}{(\xi_0+2)^2(\xi_0-1)}\right]^{1/4} \tag{3.6}$$

from which we see that for values of $\xi_0 = 1.5$-3 (corresponding to experimental data [Ref. 5, 6] in the given flow region), k/c = 2.5-7. Calculations done in Ref. 7 on the distribution of pulsation characteristics of flow in a tube based on equations (2.7)-(2.9) (at B = 0) in the range of k/c = 1.6-10 showed that the best agreement with experimental data is observed at $k/c \approx 7$.

With consideration of expressions (3.6) for k and c, relations (3.2) and (3.3) for ψ and $\xi(S_l)$ respectively can be transformed to

$$\psi = \left(\frac{2\vartheta}{1+\vartheta^{-1}}\right)^{3/2}\left[\sqrt{1+\left(\frac{\alpha}{\xi+\xi^{1/2}}\frac{1+\vartheta}{\xi_0-1}S_l\right)^2}-\frac{\alpha}{\xi+\xi^{1/2}}\frac{1+\vartheta}{\xi_0-1}S_l\right], \qquad \vartheta=\frac{\xi_0+2}{\xi+2} \tag{3.7}$$

$$S_l = \frac{\xi+\xi^{1/2}}{\alpha}\frac{\xi/\xi_0-1}{\sqrt{(\xi/\xi_0+4/\xi_0+1)(\xi+\xi/\xi_0-2/\xi_0)}} \tag{3.8}$$

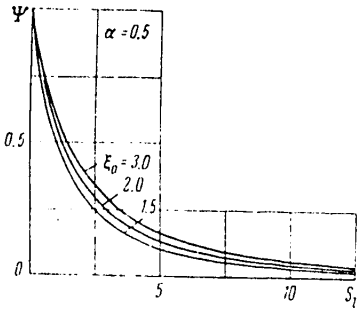

Fig. 2

Fig. 2 shows $\psi = \psi(S_l)$ for a number of values of the empirical constant ξ_0. It can be seen that a change in ξ_0 over a range from 1.5 to 3.0 has little effect on the form of the dependence of ψ on S_l, which allows us to take a constant value of 2 for ξ_0 in calculations.

With respect to the length of the mixing path that appears in expression (3.1) for the Reynolds stress, in the first approximation we take a hypothesis [Ref. 3] according to which the distribution of the transverse scale of turbulence l_2 (corresponding to mixing path l) is taken as independent of the action of the magnetic field, but dependent on flow geometry, i. e. $l_2 = l$ is taken just as in the case of absence of a magnetic field, assuming that the size of the energy-carrying eddies (along axis $x_2 = y$) is always proportional to the width of the flow (to the distance between the walls in the channel, and to the thickness of the boundary layer).

Thus with the magnetohydrodynamic analog of the Prandtl hypothesis (3.1) for the Reynolds stress, we can calculate the average flow.

4. As an example, let us consider steady-state flow of a conductive fluid in a circular tube of radius r in a longitudinal magnetic field at rather large Reynolds numbers.

Integrating the Reynolds equation (2.10) from 0 to y/r under condition $\tau|_{y=0} = \tau_w$, and setting $\sqrt{\tau_w/\rho} = u_*$, we get

$$-\langle uv\rangle + \nu\frac{dU}{dy} = u_*^2\left(1-\frac{y}{r}\right) \tag{4.1}$$

Using expression (3.1) for <uv> and converting to universal coordinates $\eta = yu_*/\nu$ and $\phi = U/u_*$, we rewrite equation (4.1) as

$$\psi l^2 R_*^2 \varphi'^2 + \varphi' = 1 - \eta/R_* \tag{4.2}$$

Here the prime denotes the derivative with respect to η, and $R_* = ru_*/\nu$ is the Reynolds number defined with respect to dynamic velocity and tube radius.

The local Stewart number (of which the coefficient ψ is a function) takes the following form in universal variables:

$$S_l = \left(\frac{H}{2R_*}\right)^2 \frac{1}{\varphi'}$$

The velocity profile $\phi = \phi(n)$ was calculated with the assumption of a two-layer flow model, i. e. for $\eta \leqslant 11.7$ it was assumed that[1] $\phi' = 1 - \eta/R_*$, and for $11.7 < n \leqslant R_*$ the value of ϕ' was found from simultaneous solution of equations (4.2), (3.7) and (3.8) by a method of successive approximations. In doing this, the Prandtl-Nikuradze formula is taken for the mixing path in equation (4.2)

$$\frac{l}{R_*} = 0.14 - 0.08\left(1 - \frac{\eta}{R_*}\right)^2 - 0.06\left(1 - \frac{\eta}{R_*}\right)^4 \qquad (4.3)$$

The coefficient of hydraulic drag for flow in a tube is equal to $\lambda = 8/\phi_0^2$, where

$$\varphi_0 = \frac{2}{R_*}\int_0^{R_*}\left(1 - \frac{\eta}{R_*}\right)\varphi\, d\eta$$

and R_* is related to the Reynolds number $R = 2rU_0/\nu$ by the expression

$$R = 2\varphi_0 R_*$$

Results of calculation of drag λ normalized to the drag λ_0 in the absence of a magnetic field as a function of the Hartmann number H are shown on Fig. 3, where the points also give experimental data from Ref. 8, 9. Points 1, 2, 3, 4, 5, 6, 7 correspond to Reynolds numbers $R \cdot 10^{-4} = 3.86$, 7.41, 7.51, 7.85, 8.82, 9.15, (1.9-2.1); the broken line corresponds to $R = 3.86 \cdot 10^4$, the solid line--to $R = 7.85 \cdot 10^4$, and the dot-and-dash-line corresponds to $R = 2 \cdot 10^4$.

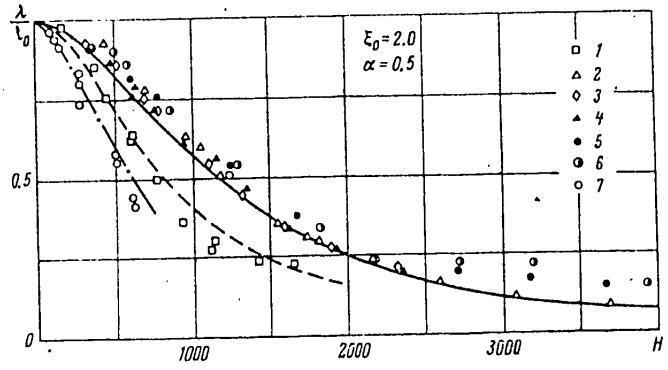

Fig. 4

Fig. 4 shows that the results of calculation are in completely satisfactory agreement with experiment in the given range of Reynolds numbers. However, at

[1] Obviously the assumption of constant thickness of the viscous sublayer does not take consideration of its growth in a longitudinal magnetic field (since $c_1 = 0$). This may lead to some overestimation of drag at large Hartmann numbers, but will not qualitatively change the results of calculation.

$R < 2 \cdot 10^4$, where the flow generally speaking does not have a well developed turbulence structure, comparison of calculation with experiment showed appreciable discrepancy (calculation gives overstated values of the drag). Some divergence is observed even at very low Hartmann numbers, where the flow is laminar, just as at very low Reynolds numbers. This means that accounting for the influence of a magnetic field on flow of a conductive fluid only via the mechanism of Joule dissipation of turbulence energy is apparently not sufficient for getting the passage in the limit to laminar flow, and it is necessary also to account for the influence of the field on the scale of turbulence. However, the lack of reliable results of experimental investigation of the turbulence structure in a magnetic field, and also the lack of a suitable physical model of the influence of the field on the scale of turbulence prevents us from doing this at present.

In conclusion the authors thank V. M. Iyevlev, I. G. Panevin and S. A. Regirer for discussing the work and for constructive advice, and also V. B. Levin for his kindness in furnishing tables of experimental results.

REFERENCES

1. Monin, A. S. and Yaglom, A. M., "Statisticheskaya gidromekhanika. Mekhanika turbulentnosti" [Statistical Hydromechanics. Mechanics of Turbulence], Part 1, Moscow, "Nauka", 1965.

2. Rotta, J., "Statistische Theorie nichthomogener Turbulenz, 1," Z. PHYSIK, Vol 129, No 6, 1951, pp 517-572.

3. Iyevlev, V. M., "Theoretical Investigation of the Influence of a Magnetic Field on Turbulence of a Flow of Electrically Conductive Fluid" in: "Simpozium po problemam turbulentnykh techeniy, vklyuchaya geofizicheskiye prilozheniya. Tezisy dokladov i soobshcheniy" [Symposium on Problems of Turbulent Flows, Including Geophysical Applications. Abstracts of Papers and Reports], Kiev, "Naukova dumka", 1967.

4. Kovner, D. S. and Levin, V. B., "On Turbulent Flow of an Electrically Conductive Fluid in a Longitudinal Magnetic Field," TEPLOFIZIKA VYSOKIKH TEMPERATUR, 1964, Vol 2, No 5.

5. Laufer, J., "The Structure of Turbulence in Fully Developed Tube Flow," NACA TECHN. REP., No 1174, 1954.

6. Klebanoff, P. S., "Characteristics of Turbulence in a Boundary Layer with Zero Pressure Gradient," NACA TECHN. NOTES, No 3178, 1954.

7. Levin, V. B., "On Calculating Major Characteristics of Turbulent Flows with Transverse Shear," TEPLOFIZIKA VYSOKIKH TEMPERATUR, Vol 2, No 4, 1964.

8. Genin, L. G., Zhilin, V. G. and Petukhov, B. S., "Experimental Investigation of Turbulent Flow of Mercury in a Circular Pipe in a Longitudinal Magnetic Field," TEPLOFIZIKA VYSOKIKH TEMPERATUR, Vol 5, No 2, 1967.

9. Levin, V. B. and Chinenkov, I. A., "Experimental Study of Turbulent Flow of an Electrically Conductive Fluid in a Pipe in a Longitudinal Magnetic Field," MAGNITNAYA GIDRODINAMIKA, No 4, 1966.

6610
CSO: 1862/140

UDC 532.517.3:532.525.2

TRANSITION TO TURBULENCE IN SUBMERGED AND ACCOMPANYING JETS

Moscow IZVESTIYA AKADEMII NAUK SSSR: MEKHANIKA ZHIDKOSTI I GAZA in Russian No 4, 1972 pp 148-154

[Article by O. I. Navoznov, A. A. Pavel'yev and A. V. Yatsenko, Moscow]

[Text] An experimental study was done on transition to turbulent flow in axisymmetric submerged and accompanying jets of helium in air for different velocity profiles in the initial cross section. The initial velocity profile in the submerged jets was determined by the boundary layer on the tip end of tubes of different lengths. In jets of helium and air in an accompanying air stream, the initial velocity profile was set up by a honeycomb with hydraulic drag varying along the radius.

Previous research on transition to turbulence in jets has shown that in the region of high Reynolds numbers the transition section is small, and the mixing level on considerable lengths was estimated from relations for the main section of the flow. However, as the results of Ref. 1 show, this is not always true. The length of the transition section may be considerably increased if a layer with smooth change of velocity and a low level of initial perturbations of a scale much less than the thickness of a layer with velocity shear is artificially set up on the boundary of accomapnying jets with considerably different velocities. In these experiments at Reynolds numbers of the order of 5000 (defined with respect to the diameter of the central jet and the difference in velocities of a jet of helium u_1 and accompanying air stream u_2), mixing was close to laminar out to distances of about 500 mm from the nozzle tip, which was about 20 jet diameters. The velocity ratio $m = u_1/u_2$ was 0.25, and the ratio of the thickness h of the velocity shear layer to the diameter d_0 of the central jet was 0.25. It was also noted in this paper that development of long-wave perturbations was not observed on the transition section.

The development of long-wave perturbations (as compared with the thickness of the shear layer) is at the present time the most extensively studied mechanism of transition to turbulence in free flows with a velocity gradient. This mechanism includes the initial stage of development of sinusoidal perturbations from the point where $Re \geqslant Re_{cr}$ (this stage is described by the linear theory), and also the nonlinear stage of development of secondary periodic motion with finite amplitude. A transition mechanism of this kind has been observed in a variety of research,

in particular Fig. 3a, b of Ref. 1 show photographs of a helium jet in an accompanying air flow on which all stages of the transition can be clearly seen. Several papers have dealt with theoretical analysis of the stability of free flows [Ref. 2, 3]; however, the currently existing theories do not permit determination of the length of the section of transition to turbulent flow, which is made up of linear and nonlinear stages of development of perturbations. There has been very little experimental research on the way that the length of the transition section depends on flow parameters. In particular, recent papers [Ref. 4, 5] have investigated the transition to turbulent flow of submerged jets discharged from long tubes and nozzles with a laminar or turbulent boundary layer produced on the walls. The authors of Ref. 4 determined the way that the ratio of the length x^* of the transition section to the thickness δ^{**} of loss of momentum in the boundary layer on the end face of the tube depends on the Reynolds number constructed with respect to pipe diameter. It is concluded from the resultant data that this ratio is independent of viscosity, and is determined only by the flow regime in the boundary layer. However, it would be more correct to define the Reynolds number with respect to the characteristic thickness of the layer with velocity shear, i. e. $Re^{**} = u\delta^{**}/\nu$. When processing the results of measurements in such coordinates, the dimensionless length of the transition section $x_j = x^*/\delta^{**}$ increases as Re^{**} decreases. It is noted in this same paper that the length of the transition section is maximum at equal densities of the ambient medium and the jet, and for accompanying jets it increases with an increase in velocity ratio m. In Ref. 5, where an investigation was made of the transition to turbulent flow of submerged jets discharged from a tube with length of about 100 diameters, no data are given on the initial velocity profile. The length of the transition section was determined from the abrupt increase in longitudinal velocity pulsations on the axis of the jet. It is stated on the basis of the resultant data that over a wide range of variation in the Reynolds number defined with respect to the flow parameters on the end face of the pipe, there is little change in the Reynolds number constructed with respect to the length of the transition section determined by the method indicated above, and with respect to the local velocity on the axis of the jet. This implies that the length of the transition section at constant velocity on the end face of the pipe does not depend on the initial form of the velocity profile or on pipe diameter.

Analysis of recent research shows that the available data are contradictory and inadequate for determining the way that the length of the transition section depends on such flow parameters as viscosity, the form of the initial velocity profile, the level of initial perturbations, the ratio of densities of the mixing jets and so on.

1. In this paper an experimental study was done on transition to turbulent flow of submerged and accompanying axisymmetric jets. A layer with velocity shear on the boundary of the central jet in the study of accompanying flows was set up by a honeycomb installed in the central nozzle, and in the case of submerged jets discharged from a pipe, velocity shear was created by a boundary layer increasing lengthwise in the tube. The system of controlling parameters for experiments with accompanying jets is given in Ref. 1. The experiments described below were done at equal velocities on the boundary of the central jet and in the accompanying flow, i. e. at $m^* = m = 0.25$. Certain parameters that characterize the form of the velocity profile must be added to those mentioned in Ref. 1. In the given experiments with accompanying jets, the form of the profile was not varied.

In the experiments with submerged jets discharged from a pipe, the following were the controlling parameters: M, ψ--mesh size and porosity of the screen; d_0, l--diameter and length of the pipe; ρ_1, ρ_2 and ν_1, ν_2--densities and kinematic viscosities of gases in the jet and in the ambient atmosphere respectively; u--mean velocity of the gas in the pipe. From these quantities and the length of the transition section we can make up six independent dimensionless parameters:

$$n = \frac{\rho_1}{\rho_2} \approx \frac{\nu_2}{\nu_1}, \quad \frac{l}{M}, \quad \psi, \quad \mathrm{Re}_l = \frac{ul}{\nu_1}$$

$$x_l = x^* \left(\frac{l\nu_1}{u}\right)^{-1/2} = \frac{x^*}{l}\mathrm{Re}_l^{-1/2}$$

$$\delta_0 = \frac{1}{d_0}\left(\frac{l\nu_1}{u}\right)^{1/2} = \frac{l}{d_0}\mathrm{Re}_l^{-1/2}$$

The second and third of these characterize the scale and level of the initial perturbations in the flow, and the others characterize respectively the thicknesses of the boundary layers and the ratios of the lengths of the transition section and tube diameter to the thicknesses of the boundary layers.

A detailed description of the working section for studying accompanying jets with velocity shear is given with a diagram in Ref. 1. The main parameters of the working section are as follows: diameter of the central nozzle $d_0 = 28$ mm, diameter of the accompanying flow is 120 mm. The central nozzle is held in the pipe on two pylons. A fine screen with mesh M = 0.1 mm is installed in the accompanying flow at a distance of 7 mm from the nozzle tip. The prosity of the screen is $\psi = 0.35$. A profile with velocity shear was set up in the central jet by a honeycomb made up of pipes of different lengths with outside diameter of 0.75 mm and wall thickness of 0.05 mm. The pipe length in the central part of the honeycomb out to a radius of 7 mm was a constant 19 mm, and from there increased linearly to 62 mm on the nozzle wall. Thus, just as in Ref. 1, the width of the shear layer h was 7 mm. Assuming absence of flow between tubes, the porosity of such a honeycomb is 0.67 with hexagonal packing. Fig. 1 [photo not reproduced] shows the outlet face of the honeycomb.

In the experiments with submerged jets, the gas was fed to an analogous working section only through a central nozzle 40 mm in diameter in which a fine screen was installed with mesh size M = 0.276 mm and porosity $\psi = 0.425$. Pipes of different lengths were fastened to the nozzle in such a way that the distance from the screen to the end of the pipe was 50, 150 and 500 mm. The wall thickness at the tip of the pipes with length of 150 and 500 mm was 2 mm, while that of the 50 mm pipe was 0.2 mm. The pipe was heat-insulated on the outside.

Profiles of velocities and temperatures were measured in the experiments. To measure the temperature profile, the working fluid of the jet was heated to 30-50°C. The temperature profiles were measured by a comb of 24 Chromel-Copel thermocouples. The profiles of velocity heads were measured by a comb of 25 Pitot tubes. The velocity profiles were measured by a sensor with heated tungsten wire 0.01 mm in diameter and about 4 mm long connected in a bridge circuit. The flows were also photographed by the IAB-451 schlieren camera with exposure of $\sim 10^{-4}$ s.

2. In experiments with submerged jets the critical Reynolds number of flow transition to turbulence in the boundary layer on the tip of the pipe was determined from the change in form of velocity profile in the boundary layer, and from the way that its thickness depends on velocity. Shown in Fig. 2 are dimensionless velocity profiles in the boundary layer on the tip of a tube 500 mm long at different Reynolds numbers Re_l defined with respect to the average air velocity in the pipe and with respect to pipe length: $Re_l = ul/\nu_1$. The symbols on Fig. 2

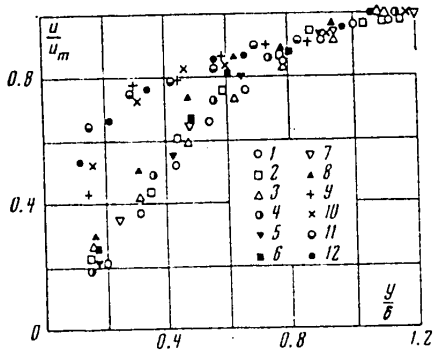

Fig. 2

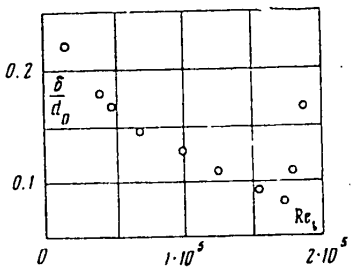

Fig. 3

correspond to the following values of Re_l: 1--16,680; 2--40,900; 3--48,500; 4--98,500; 5--124,800; 6--170,000; 7--179,000; 8--188,000; 9--212,000; 10--268,000; 11--306,000; 12-321,000. As can be seen from these data, at $Re_l = 1.88 \cdot 10^5$ there is a change in form of the velocity profile in the boundary layer: at lower Re_l the form of the profile is typical of a laminar boundary layer, while at higher Re_l it is typical of a turbulent boundary layer. The velocity profiles found in the laminar boundary layer agree within 10% with Nikuradze's data for the initial flow section in a pipe [Ref. 6]. Fig. 3 shows the relative thickness of the boundary layer $\delta_0 = \delta/d_0$ as a function of the Reynolds number Re_l plotted from the above-mentioned velocity profiles. The thickness of the boundary layer was determined with respect to the coordinate of the point in the boundary layer where the velocity differed by 3% from the maximum in the pipe. An abrupt increase in the boundary layer also occurs at $Re_l \cong 1.8 \cdot 10^5$. This was the figure taken in our experiments as the Reynolds number of transition to turbulent flow in the boundary layer.

In the course of the experiments, photographs were taken of submerged jets of helium and air discharged into quiet air with different velocities from pipes 50, 150 and 500 mm long. In all experiments, the average velocity u of the flow in the pipe was measured, and for the 500 mm tube the velocity profiles on the tip were also measured. Fig. 4 shows photographs [not reproduced] of jets of air (top row) and helium (bottom row) discharged from a pipe 500 mm long at the same Reynolds numbers Re_l. The numbers Re_l and average velocities of discharge u of air and helium in m/s are respectively equal to: a--$0.225 \cdot 10^5$, 0.75, 5.40; b--$0.455 \cdot 10^5$, 1.5, 11.0; c--$0.76 \cdot 10^5$, 2.5, 17.6; d--$0.45 \cdot 10^5$, 8.0, 57.6. The length of the transition section was taken as the distance from the tip of the pipe to the cross section (indicated by the dot at the left of the photos) where the jet was maximally constricted after the first vortex ring. As can be seen from these photos, the length of the section of transition to turbulence for jets of helium and air decreases with increasing discharge velocity. Turbulent pulsations for

Jets of air and helium from the very tip of the pipe are observed at approximately the same Reynolds number Re_ζ equal to $1.8 \cdot 10^5$, which corresponds to a change in flow conditions in the boundary layer. At the same Reynolds numbers, the length of the transition section for jets of air is several times longer than for jets of helium. The spread in lengths of transition sections determined from seven photographs of air jets discharged from a pipe 500 mm long at velocity $u = 2.5$ m/s was about 10%.

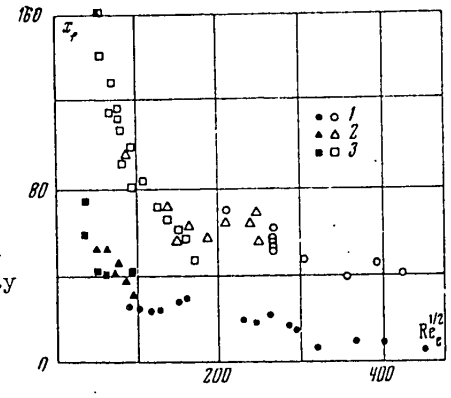

Fig. 5

Fig. 5 shows the dimensionless length of the transition section for submerged jets of air (white symbols) and helium (black symbols) as a function of $\sqrt{Re_\zeta}$. Points 1, 2, 3 refer to the lengths of transition sections found on pipes of lengths 50, 150 and 500 mm resepctively. The data show how the ratio of the length of the transition section to the characteristic dimension of the zone with velocity gradient depends on the Reynolds number constructed with respect to this same dimension. The greatest imprecision in determining the length of the transition section could have occurred at jet velocities of less than 1 m/s and at short lengths of the transition section itself. Nevertheless, Fig. 5 gives the data of all experiments that were done. The use of pipes of different lengths enabled determination of the dimensionless length of the transition section at identical Reynolds numbers Re_ζ, with respect to different parameters δ_0 characterizing the ratio of the thickness δ of the boundary layer to pipe diameter d_0. The coincidence of x_j at different δ_0 shows that in the given experiments the length of the transition section does not depend on δ_0 at $\delta_0 \leqslant 0.25$. Besides, the coincidence of x_j at the same numbers Re_ζ and at different distances from the screen to the tip of the tube shows that initial perturbations on the screen did not affect the length of the transition section since these perturbations decrease with increasing distance from the screen. The results shown in Fig. 5 imply that the dimensionless length x_j of the transition section increases with decreasing Reynolds number Re_ζ, a strong increase being observed both for air and helium jets, beginning with the same value of $\sqrt{Re_\zeta} \approx 150$.

All the data presented above were obtained for laminar flow of the boundary layer on the tip of the pipe. In the case of a turbulent boundary layer on the tip, long-wave perturbations are observed in the jet against a background of small-scale turbulence (see Fig. 4d), even to considerable distances from the tip. It can be noted that such a jet flares much more slowly than in the case of well developed turbulence in the jet after the transition section (see Fig. 4e).

3. In studying the transition to turbulent flow in accompanying jets, the above-described honeycomb was placed in the central nozzle. The working section was set up vertically, and flow was from the top downwards. Fig. 6 shows dimensionless velocity profiles in a central jet of helium measured at a distance of 5 mm from the nozzle tip. Points 1, 2, 3 correspond to velocities in the central part of the honeycomb of $u_1 = 28.0$, 39.7, 56.1 m/s. Throughout the investigated range of velocities u_1, the flow in tubes of the honeycomb remained laminar with the discharge of helium [Ref. 1], and as a result the dimensionless velocity profiles are similar for different velocities u_1. The velocity ratio m^* on the boundary

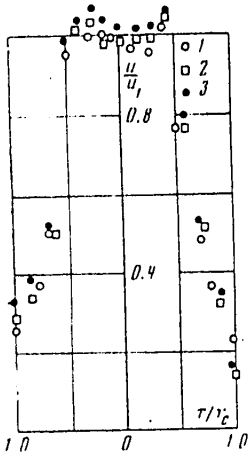

Fig. 6

of the jet (u_1^*) and in the central part of the homeycomb (u_1) remained constant at approximately 0.2-0.25. In all the experiments described below, unless specifically stipulated, the ratio of velocities of the accompanying flow (u_2) and of the central jet is taken as constant at $m = m^* = 0.25$.

Shown in Fig. 7a, b, c, d, e [photos not reproduced] are photographs of a helium jet at different velocities u_1 of the accompanying flow of air at a constant velocity ratio of $m = m^* = 0.25$. The velocities u_1 on the axis of the helium jet are equal to 7.0, 9.0, 10.0, 12.2 and 18.2 m/s. The dots to the left indicate the cross sections of the jet where disordered perturbations arise on its surface. The distances to these points were subsequently taken as the length of the transition section. The scale on the jet axis is laid off to the right of the photos. The photographs were taken at the tip of extension sections with diameter equal to that of the accompanying flow in the initial cross section. In photographing the jets up to a velocity of $u_1 = 10$ m/s, extension sections were used with length of 100 and 200 mm, while only the 200 mm extensions were used at higher velocities.

It is clear from these photographs that as the velocity of the central jet u_1 increases from 7.0 to 10 m/s, there is an increase in the length of the transition section, and then a reduction as the velocity is increased further. At a velocity of $u_1 = 50$ m/s turbulent flow is observed from the very tip of the nozzle. At such a velocity, flow around the edges of the outlet face of the honeycomb is turbulent over the entire stream. At velocities $u_1 > 10$ m/s, periodic perturbations appear on the surface of the jet close to the nozzle that are apparently due to flow around the edge of the nozzle. At lower velocities, these perturbations are quenched, and at higher velocities they can be seen right up to the appearance of disordered perturbations. Analysis of the photographs shows a considerable difference in the nature of the transition at velocities higher or lower than 10 m/s. At velocities higher than 10 m/s, disordered three-dimensional perturbations suddenly appear on the surface of the jet at a certain distance from the tip. The scale of these disturbances is less than the width of the velocity shear layer, and at velocities lower than 10 m/s, long-wave bends are observed on the surface of the jet with an abrupt rise at a distance of one wavelength.

This same figure shows photographs of a jet of air (f) in an accompanying flow of air at a velocity on the axis of the jet of $u_1 = 5$ m/s and $m = 0.25$. There are no periodic perturbations behind the edge in this case since the velocity of the accompanying air flow is low. With a further reduction in the velocity u_1 of the air jet to 3 m/s, there is an increase in the length of the transition section.

Fig. 8 shows a curve obtained from photographic data for the dimensionless length of the transition section $x_c = x_c^*/h$ as a function of the Reynolds number constructed with respect to the velocity and viscosity of the central jet and the thickness of the layer with velocity gradient. Points 1 and 2 refer to jets of helium in an accompanying air flow at m equal to 0.25 and 0.15 respectively, and points 3 refer to air jets in an accompanying flow of air at $m = 0.25$. The curve has a sharp maximum. The maximum dimensionless length of the transition section equal to ~80 is observed at $Re_h \cong 800$.

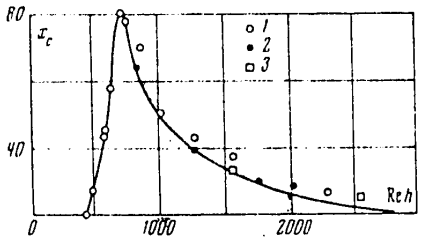

Fig. 8

4. Before going on to discuss the results, let us consider the definitions of length of the transition section used in this paper and by other researchers. In different papers, this length is defined with respect to different flow characteristics, and accordingly by different methods: with respect to downstream pulsations of velocity or distributions of average values, or with respect to changes in the flow structure observed with visualization of the stream. For example, in Ref. 8 measurements were made of the longitudinal velocity pulsations along the jet, and the section of exponential increase in these pulsations was taken as the length of the transition section: the end of this section coincided with the beginning of an abrupt increase in the size of the jet b determined from the point of the velocity profile at which the velocity was equal to half the velocity on the axis of the jet. In Ref. 9 the length of the transition section determined only from photographs of the jet was taken as the distance from the nozzle tip to the point at which long-wave bends of the surface begin to twist, forming vortex rings. In Ref. 4 this length was determined from the length of the section of exponential increase in the maximum of pulsations in the mixing boundary layer of the jet. Thus in all these papers the length of the transition section was taken as only that part characterized by an exponential growth of initial perturbations in the flow and corresponding to the approximate beginning of formation of vortex rings. In the authors' experiments with submerged jets, the length of the transition section x^* was taken as the distance from the nozzle tip to the minimum cross section of the jet beyond the first vortex ring (indicated by the dots to the left of the photographs). This distance is approximately 30% greater than the distance at which abrupt flaring of the jet is observed as determined from measurements of the temperature profiles. In experiments with accompanying jets the length of the transition section was taken as the distance x_c^* from the nozzle tip to the point of appearance of disordered three-dimentional perturbations on the surface of the jet.

Comparison of the relations for relative lengths of transition sections in submerged and accompanying jets of helium given on Fig. 5 and Fig. 8 shows a considerable difference in the form of these relations: in the case of submerged jets the length of the transition section decreases monotonically with increasing Reynolds number, whereas in the case of accompanying jets there is a sharp maximum at a certain value of the Reynolds number Re_h.

In comparing these data, the characteristic thickness of the layer with velocity gradient in the submerged jets was taken as the part of the thickness of the boundary layer on the tip of the pipe δ with high gradients of the average velocity approximately equal to $3.5\sqrt{l\nu_1/u}$. Assuming likewise that in accompanying jets the length of the transition section increases with increasing m in proportion to $(1+m)/(1-m)$, we find that in the given experiments the maximum length of the transition section in accompanying jets is approximately an order greater than in submerged jets. For a given construction of the honeycomb, the maximum length of the transition section in accompanying jets was realized at $Re_{hm} \cong 800$. In submerged jets this corresponds approximately to $\sqrt{Re_l} = 230$. At $Re_h < Re_{hm}$ the difference in lengths of the transition section in submerged and accompanying jets decreases, and at low Re_h we see quantities of the same order of magnitude. When

$Re_h > Re_{hm}$ this difference also decreases, but nevertheless remains appreciable over the investigated range of Re_h. In accompanying jets with a honeycomb, the flow structure upon transition to turbulent flow when $Re_h > Re_{hm}$ differs considerably from the the transition structures in these jets at $Re_h < Re_{hm}$ and in submerged jets. In the first case the transition is not preceded by the development of long-wave perturbations, and at different distances from the nozzle tip, disordered perturbations appear on the surface of the jets with a scale less than the thickness of the layer with velocity shear. In the second case the transition is realized by the development of long-wave perturbations. If we consider in addition that the length of the transition section in accompanying jets at $Re_h > Re_{hm}$ depends weakly on the velocity ratio m when $m < m^*$ (data are not given in the paper) and on the density ratio (see Fig. 8), then it can be assumed that in this case the transition to turbulent flow is due to development in the central jet of small-scale initial turbulence that arises with flow around the outlet face of the honeycomb. The weak development of long-wave perturbations is apparently determined by an increase in the effective viscosity of the flow due to the presence of small-scale turbulence. The appearance of the maximum on Fig. 8 is determined by the interaction of these two transition mechanisms pointed out above. The influence of initial turbulence on wave motion in turbulent shear flows of different types was accounted for by Reynolds through the introduction of effective viscosity in calculations of the stability of these flows in the linear approximation [Ref. 7].

A comparison of the results found in this paper for submerged jets of air in the case of a laminar boundary layer on the tip of the pipe with the data of Ref. 1 and 5 shows that the quantitative difference in lengths of transition sections does not exceed 30-40%. Such agreement can be considered satisfactory considering the differences in the techniques used for determining the lengths of the transition sections. However, on the basis of the data given in Fig. 5 it is clear that the conclusion of Ref. 4 that the dimensionless length of the transition section is independent of Reynolds number in the case of a laminar boundary layer on the tip of the pipe is not confirmed. The same can be said of the conclusion of Ref. 5 that there is a critical transition Reynolds number defined with respect to the length of the transition section and the local velocity on the axis of the jet.

The authors thank V. M. Iyevlev for assistance and for discussing the results.

REFERENCES

1. Navoznov, O. I. and Pavel'yev, A. A., "Transition to Turbulence in Accompanying Jets," IZVESTIYA AKADEMII NAUK SSSR: MEKHANIKA ZHIDKOSTI I GAZA, No 6, 1969.

2. Monin, A. S. and Yaglom, A. M., "Statisticheskaya gidromekhanika" [Statistical Hydromechanics], Part 1, Moscow, "Nauka", 1966.

3. Stuart, L. T., "On Finite Amplitude Oscillation in Laminar Mixing Layers," JOURNAL OF FLUID MECHANICS, Vol 29, No 3, 1967.

4. Sokundov, A. N. and Yakovlenskiy, O. V., "Some Problems of the Transition of Channel Flow to Jet Flow," IZVESTIYA AKADEMII NAUK SSSR: MEKHANIKA ZHIDKOSTI I GAZA, No 3, 1967.

5. Vulis, L. A., Zhivov, V. G. and Yarin, L. P., "Transition Flow Region in a Free Jet," INZHENERNO-FIZICHESKIY ZHURNAL, Vol 18, No 2, 1969.

6. Schlichting, G., "Teoriya pogranichnogo sloya" [Boundary Layer Theory], Moscow, Izdatel'stvo inostrannoy literatury, 1969.

7. Flowes, W. J. E., Rosenblat, S. and Stuart, I. T., "Transition from Laminar to Turbulent Flow," JOURNAL OF FLUID MECHANICS, Vol 39, No 3, 1969.

8. Sato, H., "The Stability and Transition of a Two-Dimensional Jet," JOURNAL OF FLUID MECHANICS, Vol 7, No 1, 1960.

9. Becker, H. O. and Massaro, T. A., "Vortex Condition in a Round Jet," JOURNAL OF FLUID MECHANICS, Vol 31, No 3, 1968.

6610
CSO: 1862/141

UDC 532.517.4:538.4

MIXING OF ACCOMPANYING JETS IN A LONGITUDINAL MAGNETIC FIELD

Moscow IZVESTIYA AKADEMII NAUK SSSR: MEKHANIKA ZHIDKOSTI I GAZA in Russian No 5, 1972 pp 33-44

[Article by B. N. Baushev, Ye. Yu. Krasil'nikov, V. G. Lushchik and I. G. Panevin, Moscow]

[Text] The paper gives the results of measurement of the velocity profiles on the initial mixing section of accompanying turbulent jets of electrically conductive fluid in a longitudinal magnetic field. It is shown that the magnetic field has a considerable effect on jet flow: it constricts the width of the mixing zone and increases the length of the initial section as compared with the case of absence of a magnetic field. The results show that the velocity profiles in the mixing layer with flow in a longitudinal magnetic field are self-similar.

On the basis of the experimental data the authors determine the function Ψ that accounts for the influence of the magnetic field in the expression for turbulent friction stress. The width of the mixing zone in flow on the initial section of accompanying jets in a longitudinal magnetic field is calculated using the relation derived for Ψ. The results of the calculation are compared with experimental data.

1. In the case of turbulent flow in a longitudinal (relative to the direction of average motion) magnetic field, the equation of motion lacks a term that describes the interaction of the average motion with the magnetic field (the so-called Hartmann effect), which is much greater than the term that accounts for turbulent friction, even in the case of a weak magnetic field. In this connection it is important to take appropriate consideration of the influence that the field has on the characteristics of pulsation motion, and especially on the turbulent friction stress τ, for correct qualitative and quantitative description of flow in a longitudinal magnetic field.

In the general case of turbulent flow with shear in a magnetic field, the quantity τ, being a function of the local characteristics of the flow and the magnetic

field, can be represented as a product of two functions. One of these is the turbulent friction (τ_0) in accordance with some hypothesis of turbulence in the absence of a magnetic field, and the other (Ψ) accounts for the influence of the magnetic field.

Dimensional considerations imply that upon flow of an electrically conductive fluid (with coefficient of electrical conductivity σ) with transverse velocity gradient ($\partial U/\partial y$) in a magnetic field (with induction B) in the case of local equilibrium between the production and dissipation of turbulence energy without the direct influence of viscosity on turbulent pulsations, the function Ψ may depend only on a single dimensionless parameter--the criterion of local interaction (the local Stewart number) S_l [Ref. 1].

Thus

$$\tau = \Psi(S_l)\tau_0 \qquad \left(S_l = \frac{\sigma B^2}{\rho}\left(\frac{\partial U}{\partial y}\right)^{-1}\right) \tag{1.1}$$

It is obvious in this case that the form of the function $\Psi(S_l)$ will be different for magnetic fields with different orientations.

The theoretical investigation of turbulent flow of an electrically conductive fluid in a longitudinal magnetic field has been fairly well covered [see for example Ref. 2]. Most of this research has dealt with a wall boundary layer with generalization to flow in pipes and channels, and only a few papers have studied the jet boundary layer directly. To determine the form of the function $\Psi(S_l)$, studies dealing with flow near the wall are of interest in addition to direct investigations of the jet flows since it is always possible in the wall boundary layer to distinguish a flow region far from the solid surface where the turbulent friction, just as in the free boundary layer, is much higher than molecular friction.

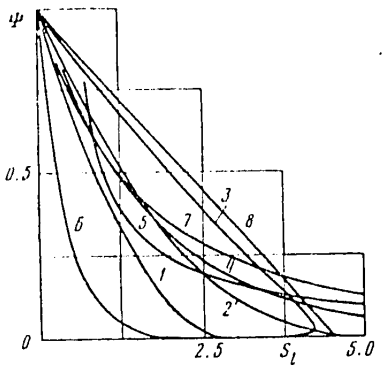

Fig. 1

Fig. 1 shows curves for the function $\Psi(S_l)$ plotted (or taken intact) from the following papers: 1--curve 1 corresponds to the function $\Psi(S_l)$ from Ref. 3, 4; 2--from Ref. 3, 6; 3--from Ref. 7; 4--from Ref. 8; 5--from Ref. 9; 6--from Ref. 10; 7--from Ref. 11; 8--from Ref. 12.

As can be seen from Fig. 1, most of these curves for $\Psi(S_l)$ do not agree, although we can notice that the results of Ref. 8 and 11 (curves 4 and 7) in which consideration is taken of the change in turbulence structure with flow in a magnetic field are close to each other. The model used in these papers of turbulence anisotropy with preferred orientation of vortices along the magnetic field, as will be shown below, enables a satisfactory explanation of the experimental data on flow in the initial section of mixing of accompanying jets.

Considerable research has been devoted to the experimental study of jet flows in ordinary hydrodynamics (for example an extensive bibliography is given in

Ref. 13, 14). Much less study has been done on jet flows in a magnetic field. There have been studies [see Ref. 2] of the averaged characteristics of jet flow of a conductive fluid in a confined space in a transverse magnetic field. However, it is difficult to extract information from these papers on the influence of the magnetic field on turbulence since the field has an appreciable effect on the average flow. Therefore an investigation of mixing of axisymmetric jets in a longitudinal magnetic field can apparently yield much more information on the influence that the field has on free turbulence.

There have been only three papers dealing with the experimental investigation of mixing of accompanying jets of conductive fluid in a longitudinal magnetic field [Ref. 15-17], where studies were done on flow in the main section of mixing of a submerged jet and a jet in an accompanying flow. The results obtained in Ref. 16 and 17 on measurement of velocity profiles show slower expansion of the jet than in the case of absence of a magnetic field, which is a consequence of a reduction of turbulence intensity with flow in a magnetic field[1]. The latter has been directly confirmed by data of heat-loss anemometer experiments [Ref. 16].

Our paper is devoted to the study of flow of an electrically conductive fluid in a mixing layer on the initial section of accompanying jets in a longitudinal magnetic field which, as far as we know, has not been done previously.

2. The Working Section and Method of Conducting the Experiments. Mixing of accompanying jets was studied on a facility with a liquid metal loop described in Ref 18. The conductive fluid was an alloy consisting of 67% gallium, 20.5% indium and 12.5% tin by weight with melting point of 10.6°C.

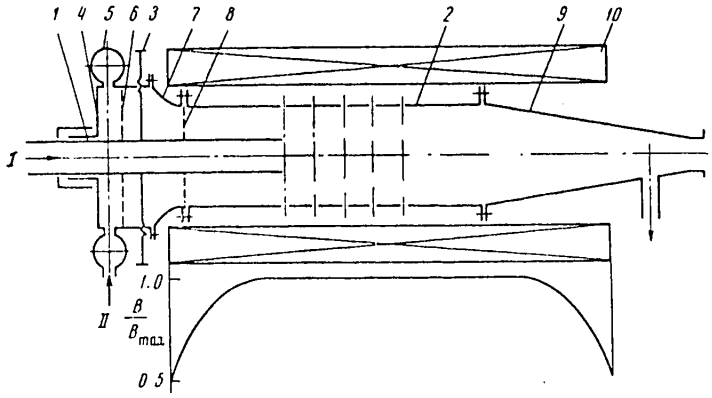

Fig. 2

The accompanying jets were formed and their mixing was studied on the working section diagrammed in Fig. 2. The central jet I was discharged from nozzle 1, 700 mm long and 40 mm in diameter with edge thickness of no more than 0.1 mm. The outer surface of the nozzle at a distance of 110 mm from the tip was made in the form of a cone with half-angle of 2°30'. The nozzle was centered relative to

[1]The results of Ref. 15 were obtained at very low values of the interaction parameter (Stewart number $S \approx 10^{-2}$-10^{-3})and consequently, as was to be expected, no appreciable effect of the longitudinal field was observed on jet flow.

experimental section 2, 1100 mm long and 100 mm in diameter, by means of screws 3 on the inlet section 4 of the accompanying flow.

The liquid metal was fed into the cavity of accompanying flow II through a distribution header 5 and a perforated plate 6, which were conducive to equalizing the flow velocity over the cross section of the cavity. The liquid metal then passed through Vitoshinskiy nozzle 7 pressed against [experimental section] 2, and through honeycomb 8 with porosity of 0.234 in the form of a disk 6 mm thick drilled with holes 3 mm in diameter at the intersections of a rectangular grid with spacing of 5.5 mm, and entered the experimental section of the working part. The experimental section in which mixing of the accompanying jets took place had five static pressure hoops situated 100 mm apart (6 orifices 0.5 mm in diameter in each hoop). In the outlet section 9 of the working part, 870 mm in length in the form of a cone with taper of 2° was either a coordinate spacer with a probe, or a unit for longitudinal displacement of a comb of 20 Pitot tubes. The working section was placed in the cavity of a solenoid 10, 1700 mm long, the flanges of the section serving as supports to maintain the working section coaxial with the solenoid. As we can see from the behavior of magnetic field induction shown along the working section in Fig. 2, mixing of the accompanying jets took place in a magnetic field that was homogeneous within ±1.5%.

The following major parameters were measured in the course of the experiment:

1) volumetric flowrates of liquid metal in the lines of the central jet and the accompanying flow;

2) static pressure on the wall and its distribution over the diameter of the experimental section at different distances from the nozzle tip;

3) the distribution of total pressure over the diameter of the experimental section at different distances from the nozzle tip;

4) the current flowing through the solenoid winding;

5) the temperature of the liquid metal in the working section.

Venturi flowmeters were used to measure the volumetric flowrate of the liquid metal in the main lines of the central jet and accompanying flow.

To measure the distribution of static pressure over the cross section of the experimental part, a probe was used with a Prandtl tip 1.4 mm in diameter. The distance from the spherical head of the Prandtl tip to a static pressure hoop with four orifices 0.3 mm in diameter, which is usually taken in a range of 3-8 tip diameters in the absence of a magnetic field, was increased to 14 diameters in accordance with results of Ref. 10 for the Stewart number calculated with respect to tip diameter, $S \lesssim 1$, due to slower equalization of pressure along the surface of the tip in a longitudinal magnetic field. A special coordinate spacer was used to shift the probe over the cross section and along the experimental section. Displacement of the probe along the diameter of the experimental section was in the vertical plane. Before doing the experiments, a special gage was used to calibrate probe displacement in three cross sections chosen for the measurements. The probe and the static pressure hoop on the wall of the experimental section were connected by tubes to two-fluid piezometers on a pressure board.

An isolated probe was likewise used to measure the total pressure distribution with a Pitot tube with diameter of 2 x 0.25 mm. The outside of the tube, on a length of 10 mm from the end, was made in the form of a cone (by the method of electrohydraulic polishing).

In addition, to measure the distribution of total pressure lengthwise of the experimental section, a comb was used that was made up of 20 Pitot tubes with diameter of 1.3 x 0.25 mm. The end of each tube to a length of 15 mm was machined and polished by the electrohydraulic method, taking the shape of a cone, and the edge thickness at the tip did not exceed 0.02 mm. All the Pitot tubes were 40 mm long and were set with a predetermined spacing (varied from 4 to 7 mm) on the two arms of a cross spider (along the diameter of the experimental section) that was moved along the experimental section (the clearance between the arms of the spider and the inside of the experimental section was no more than 0.3 mm). The distances between the ends of the Pitot tubes were checked before placing the comb in the working section and after completion of the experiments by a special gage.

Flow blockages caused by all Pitot tubes, by the spider, and by the connecting tubing of the Pitot tubes were 0.004, 0.094 and 0.063 respectively. The connecting tubing was led out to the pressure panel carrying the two-fluid piezometers with direct feed of liquid metal, the light fluid being alcohol or water with amplification factor of 6.51 and 5.25 respectively.

The temperature of the liquid metal was measured by a Chromel-Copel thermocouple placed directly at the outlet from the working section. The induction of the longitudinal magnetic field was determined from the current flowing through the solenoid winding, which was determined in turn from the voltage drop across a shunt.

The experiments were done in the following way. An electromagnetic pump and choke valves were used to set up the necessary flowrate of liquid metal in the main lines of the central jet and accompanying flows corresponding to a given velocity ratio $m = U_2/U_1$ (where U_1 is the velocity of the central jet and U_2 is the velocity of the accompanying flow). Then in the steady state, using a probe with Pitot tube, measurements were made of the distribution of total pressure both with and without a magnetic field in several cross sections lengthwise of the experimental part. In each cross section the measurements were taken first at $B = 0$ and then at $B \neq 0$.

It should be noted that special experiments were done beforehand to eliminate deviations from coaxiality of the accomapnying flows. Static pressure hoops were used to measure the static pressure on the wall of the experimental section simultaneously with measurement of the total pressure. Analogous experiments were done with a Prandtl-tip probe measuring the distribution of static pressure over the cross section of the experimental part, all these experiments being done at the same flow parameters and in the same cross sections.

The technique used in doing experiments in which the total pressure distribution was measured by a comb of Pitot tubes was no different from that described above. The coaxiality of the accompanying flows could be judged by comparing the results of measurements made in mutually perpendicular planes in one cross section.

According to estimates, the relative maximum errors of measurement of velocity, volumetric flowrate and magnetic field induction are 3.4, 3 and 4.2% respectively.

In addition, a check was made on the validity of the results of measurement of the distribution of velocity over the cross section of the experimental part by comparing the overall volumetric flowrate measured by two Venturi flowmeters with the volumetric flowrate determined by integrating the resultant velocity profiles. The divergence of volumetric flowrates determined in this way is less than 5%.

3. Results of the Experiment. Three series of measurements were made for a velocity ratio of m = 0.18 and magnetic field inductions of B = 0.34 and 0.5 T and also in the absence of a magnetic field. In series I, a probe with Prandtl and Pitot tips was used to measure the distributions of static and total pressure on the diameter of the experimental section in cross sections x/d = 2, 5 and 10 (x is the distance from the nozzle tip, d is the diameter of the nozzle). In series II and III, a comb of 20 Pitot tubes was used to measure the distributions of total pressure in cross sections x/d = 1-10 with a step of x/d = 2 (series II) and x/d = 1 (control series III).

In all three series of measurements the velocities of the accompanying jets at fixed m varied slightly from experiment to experiment, being U_1 = 67, 75 and 73 cm/s and U_2 = 12, 13.5 and 13 cm/s at x = 0 on the axis of the central jet and in the accompanying flow for series I, II and III respectively. The Reynolds numbers defined with respect to the hydraulic diameters and average flowrates are respectively $R_1 \approx 5.5 \cdot 10^4$, $R_2 \approx 1.5 \cdot 10^4$, and the Hartmann numbers defined with respect to the diameter of the nozzle are H = 455 and H = 670 for B = 0.34 and 0.5 T respectively. In the results of experimental research given below, points 1, 2 and 3, and the broken, dot-dash and solid curves drawn through them refer to magnetic field inductions B = 0, 0.34 and 0.5 T respectively.

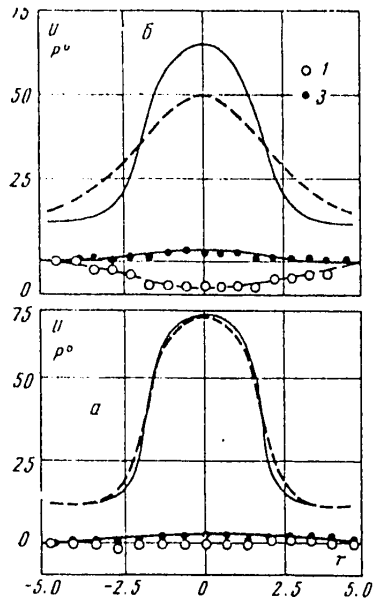

Fig. 3

Fig. 3 shows the results of measurements of the distribution of relative static pressure p° (points) and velocity in cm/s (lines) with respect to the radius r (in cm) of the experimental section in cross sections x/d = 2 (Fig. 3a) and x/d = 10 (Fig. 3b) obtained at B = 0, 0.5 T in measurement series I. The quantity p° expressed in percent was defined as the difference between the static pressure P in the flow and the pressure P_w on the wall normalized to the excess velocity head $\rho(U_m - U_2)^2/2g$ (where U_m is velocity on the axis of the central jet).

Fig. 4 shows typical results of measurement of the profiles of velocity U (in cm/s) with respect to radius r (in cm) of the experimental section found in the experiments of series I. It should be noted that in determining the velocity from the difference in values of the total and static pressure at a given point, the static pressure was taken as constant and equal to the value of the pressure at the wall over the cross section of the experimental part.

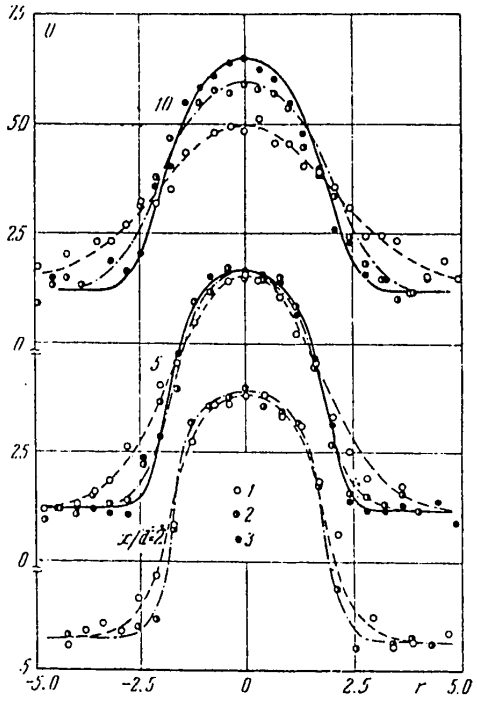

Fig. 4

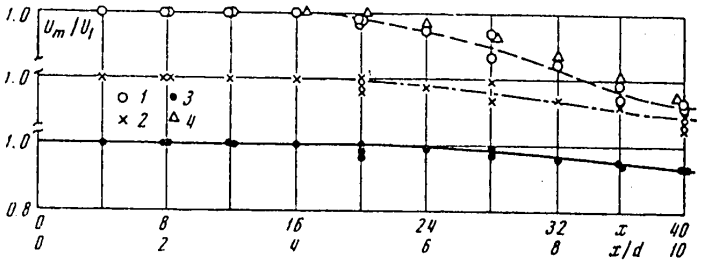

Fig. 5

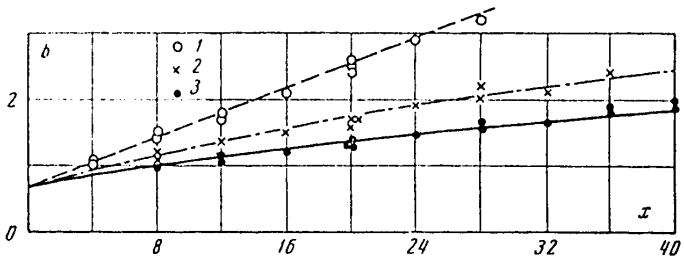

Fig. 6

Of interest from the standpoint of analyzing the results are curves that characterize the change in velocity on the axis of the central jet and the width of of the zone of mixing of accompanying jets as functions of the longitudinal coordinate and induction of the magnetic field.

Fig. 5 shows the behavior with respect to length x (in cm) of the experimental section on the part of the velocity U_m on the axis of the central jet normalized to the corresponding velocity on the nozzle tip U_1 (at $x=0$) for all three series of measurements.

Fig. 6 shows the results of measurements of the 10% width of the mixing zone b (in cm) with respect to the length of the experimental section x (in cm). The quantity b was defined as the difference of coordinates of points $r_{0.1} - r_{0.9}$ at which the dimensionless excess velocity $u^o = (U - U_2)/(U_1 - U_2)$ is 0.1 and 0.9 respectively. Fig. 7a shows the relations for the boundaries of the mixing zone y_1 and y_2 (in cm) ($y_1 - y_2 = b$) reckoned respectively toward the central jet and the accompanying flow from the x' axis that is the continuation of the edge of the nozzle in the direction of the x axis ($x' \equiv x$), and Fig. 7b shows the ratio of the boundaries of the mixing zone $\theta = -y_2/y_1$.

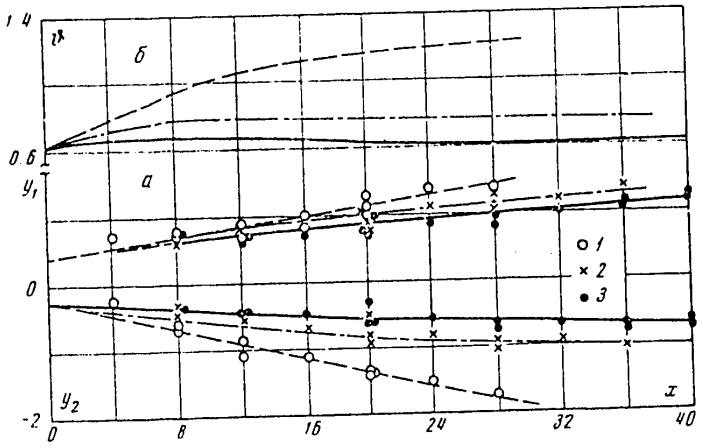

Fig. 7

Before going on to analysis of the results, let us consider the conditions in the accompanying flows on the inlet to the experimental section (on the nozzle tip). In the central jet on the nozzle tip according to estimates for pipe flow in a longitudinal magnetic field, the flow was obviously turbulent. Actually, in order for the flow in a nozzle at $R_1 = 5.5 \cdot 10^4$ to be laminar, the Hartmann number according to Ref. 20 must be $1.8 \cdot 10^3$, whereas in the experiment it did not exceed 670. Therefore on the nozzle tip for a length of 700 mm ($x/d = 17.5$, see Fig. 2) the velocity profile must be close to developed turbulence. This is also confirmed by the ratio of the velocity U_m on the axis of the jet to the average flowrate $\langle U \rangle$ which was ≈ 1.15 in the experiments, and this is close to the value $U_m/\langle U \rangle = 1.25$ corresponding to flow in the absence of a magnetic field at $R = 5.5 \cdot 10^4$ [Ref. 21]. The level of turbulence in the accompanying flow at $R_2 = 1.5 \cdot 10^4$ is obviously much lower than in the central jet. However, considering the fact that the magnetic field drops off beyond the limits of the

experimental section (see Fig. 2) and the Hartmann number decreases upstream from the experimental section, we can assume that turbulence in the accompanying flow was not completely suppressed. In this connection, the ratio $U_m/\langle U\rangle \approx 1.08$, showing the homogeneity of the velocity profile, which does not have time to develop on the 300 mm length from the honeycomb to the nozzle tip (see Fig. 2).

The thicknesses of the boundary layers estimated on the assumption of turbulent flow were $\Delta_1 \approx 1.5$ cm, $\Delta_2 \approx 1$ cm in the central jet and in the accompanying flow respectively, i. e. the boundary layer on the outside of the nozzle was thinner than on the inside ($\Delta_2/\Delta_1 \approx 0.67$).

The choice of velocity ratio $m = 0.18$ is dictated by the following considerations. At low m, the boundedness of the space in which jet mixing occurs may have an effect, which may lead to the formation of vortex zones due to jet ejection, considerably distorting the flow pattern and having an effect on measurement results (which was observed for example in Ref. 16, 17 at $m \approx 0$). However, as the velocity ratio increases, there will be an increase in the effect of the initial boundary layers. According to experimental data of Ref. 22, the result of this will be that the width of the mixing zone will cease to depend on the velocity ratio beginning with $m \approx 0.5$.

4. Analysis of the Experimental Results. The results of measurements of the distribution of static pressure (Fig. 3) show that in the absence of a magnetic field the pressure on the cross section in the initial part of the jet (at x/d=2, Fig. 3a) is practically constant, and equal to the pressure on the wall ($p^\circ = 0$). At $x/d = 10$ (Fig. 3b) a "dip" of static pressure is observed in the paraxial region of about 8% on the axis of the jet, which agrees with experimental results of Bar (7.5%), and Miller and Cummings (7.2%) [Ref. 23] obtained for free jets (circular and flat respectively) also in the corss section $x/d = 10$.

With flow in a magnetic field, as can be seen from Fig. 3, there is an increase of static pressure in the paraxial region and in the zone of mixing of accompanying jets that reaches 3% of the pressure on the wall (at $x/d = 10$, Fig. 3b) on the axis of the jet, or 11% of the static pressure on the axis of the jet in the absence of a magnetic field. The observed effect of pressure increase with flow in a magnetic field can be qualitatively explained on the basis of analysis of the equation of motion in the projection on the transverse axis. Actually, if we assume that during flow in a magnetic field the pressure gradient is balanced by the Lorentz force [Ref. 1]

$$\partial P / \partial y = -\sigma B^2 V$$

then we can see that a positive (due to jet expansion) transverse velocity V corresponds to a negative pressure gradient, i. e. the pressure decreases in the direction toward the wall. In other words the Lorentz force due to the radial rate of spreading of the fluid will set up a drag. To overcome this drag, an excess pressure must arise in the core of the jet, and this is what was observed in the experiments. However, the change in static pressure is slight ($P - P_w$ is of the order of $0.03\rho(U_m - U_2)^2/2g$ or less). This gives a basis in determining the velocity of flow in a magnetic field (with more right than at $B = 0$) to consider the static pressure constant over the cross section and equal to the pressure on the wall.

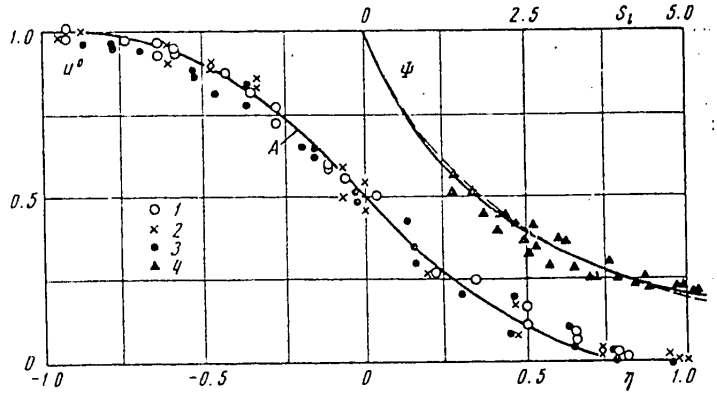

Fig. 8

The results of velocity profile measurements (Fig. 4) show that upon application of a magnetic field the blurring of the velocity profile decreases, and the range of the jet increases. Actually, the velocity U_m on the jet axis (see Fig. 5) damps out less intensively with increasing magnetic field induction, and the length of the initial section within the limits of which U_m remains constant ($U_m = U_1$) increases by a factor of about 1.7 at B = 0.5 T as compared with the case of absence of any magnetic field (from $x/d \approx 4$ to $x/d \approx 7$). It should be noted that when B = 0 the results of the measurements agree with the data of A. S. Ginevskiy et al. [Ref. 14] (points 4 on Fig. 5) obtained at m = 0 for a jet in an unbounded space. This shows that the flow characteristics on the transitional and main sections are influenced by the boundedness of the space in which the mixing occurs. Thus the results of measurements beyond the limits of the initial section (both at B = 0, and apparently when $B \neq 0$ as well), should be taken as qualitative rather than quantitative.

Analysis of experimental data on the width of the mixing zone (Fig. 6) shows that in the absence of a magnetic field the experimental points fit nicely on a straight line $b = \delta + kx$, where $\delta = 0.65$ cm is the conditional initial width of the mixing layer, k = 0.095 is an empirical constant (the coefficient of expansion of the mixing layer). The resultant value of k agrees with the value (k = 0.107) determined from the experiment of Lipmann and Laufer (see Ref. 14) for submerged jet with consideration of a correction for m = 0.18 in accordance with the relation proposed by G. M. Abramovich [Ref. 13]. With an increase in magnetic field induction the function b(x) departs further and further from that corresponding to the case of absence of a magnetic field.

Analysis of the results that characterize the change in position of the boundaries of the mixing zone y_1 and y_2 shows the following. It can be seen from Fig. 7a that in the absence of a magnetic field the experimental points fit on straight lines $y_1 = \delta_1 + k_1 x$, $-y_2 = \delta_2 + k_2 x$ with the following values of conditional thicknesses δ of initial boundary layers and empirical constants k: $\delta_1 = 0.4$ cm, $\delta_2 = 0.25$ cm, $k_1 = 0.038$, $k_2 = 0.057$. In this case the ratio $\delta_2/\delta_1 = 0.625$ was close to the above-mentioned quantity $\Delta_2/\Delta_1 \approx 0.67$ characterizing the ratio of the estimated thicknesses of real boundary layers in accompanying flows on the nozzle tip.

The behavior of $\theta = -y_2/y_1$ shown in Fig. 7b with increasing x approaches the value $\theta = 1.5$ implied by the relation k_2/k_1 that is true as $x \to \infty$, when we can disregard the initial boundary layers, the quantity $\theta = 1.5$ being close to the calculated value $\theta = 1.65$ [Ref. 1].

Upon application of a magnetic field, the boundaries of the mixing zone deviate from the linear relations corresponding to the case of absence of a magnetic field, the deviation for $y_2(x)$ being greater than that for $y_1(x)$. There may be several causes for such an appreciably different influence of a longitudinal magnetic field on the change in position of the boundaries of the mixing zone. In particular, it can be assumed that large-scale vortices on the outer boundary (y_2) that cause expansion of the jet (so-called volumetric convection of large votices [Ref. 23]) are more intensively suppressed by the magnetic field than the small-scale vortex structure inside the jet. In addition, the magnetic field is apparently conducive to reduced "suction" from the accompanying flow into the central jet, which according to Ref. 1 may lead to a reduction in the value of θ that characterizes the degree of symmetry of the mixing zone relative to the edge of the nozzle. We may take as confirmation of the latter the fact that the measured value of the static pressure gradient (see Fig. 3) in the mixing zone was quite unappreciable. In one way or another the results show that the magnetic field tends to maintain the initial inhomogeneity existing in the flow as boundary layers on the nozzle tip in the direction of the magnetic field induction vector. This is confirmed by the fact that when flow takes place in a magnetic field the function $\theta(x)$ goes out to an asymptote that approaches the initial value of θ (at $x = 0$) as the magnetic field increases.

It is of interest to study the self-similarity of velocity profiles in the zone of mixing of accompanying jets in a longitudinal magnetic field. To do this, the velocity profiles were replotted in the following way. The excess velocity u° was taken as the dimensionless velocity, and the dimensionless coordinate was taken as $\eta = (r - r_{0.5})/b$, where $r_{0.5}$ corresponds to the value of $u^\circ = 0.5$, and $b = r_{0.1} - r_{0.9}$. The velocity profiles of measurements of series I (at $x/d = 2.5$ for $B = 0$, 0.34 T and at $x/d = 5$, 10 for $B = 0.5$ T) are shown as plotted in these coordinates on Fig. 8. Curve A on this figure corresponds to the results of measurements by G. N. Abramovich, as well as Albertson et al. [Ref. 13] for a free jet in the absence of a magnetic field.

The results presented on Fig. 8 show that the velocity profiles in the mixing layer with flow in a longitudinal magnetic field are actually self-similar and agree well with known experimental data that correspond to the case of absence of a magnetic field. However, upon application of a longitudinal magnetic field the self-similarity begins at great distances from the edge of the nozzle, which is probably due to the presence of initial boundary layers whose influence on mixing in the magnetic field, as indicated above, is more appreciable than in the absence of such a field.

Let us note that the following experiment was done to study the possible effect that emergence from the working section in the inhomogeneous magnetic field of the solenoid might have on measurement results. Flow with a homogeneous velocity profile ($U = 20$ cm/s, $m \approx 1$) was organized at the inlet to the experimental section and a longitudinal magnetic field with induction $B = 0.5$ T was then applied to this flow. Measurements of velocity profiles in a number of cross sections

lengthwise of the experimental part revealed no appreciable difference of the experimental results with flow in a magnetic field or when no field was present (out to x/d = 12). From this we can conclude that upstream propagation of perturbations [Ref. 19] due to crossing of magnetic lines of force by the electrically conductive fluid at the outlet from the working section up to values of the interaction parameter defined with respect to the diameter of the experimental section (D = 100 mm), S = 65, does not reach the part of the experimental section where the measurements were made.

Thus the experimental data show that a longitudinal magnetic field has a considerable effect on turbulence in a free boundary layer, and may serve as a basis for checking various semi-empirical theories of free turbulent magnetohydrodynamic flows and selection of empirical constants.

5. Relation for $\Psi(S_l)$. The experimental results found above with respect to flow on the initial section of mixing of accompanying jets enable us to construct the empirical function $\Psi(S_l)$ that accounts for the influence of the magnetic field in the expression for turbulent friction stress (1.1). To do this, the value of Ψ was found for each experimental value of the width b of the mixing zone in accordance with Ref. 1, 11 to give the best agreement between the results of the calculation and experimental data at a known value of the local Stewart number (1.1) (see below for a more detailed discussion of calculating the width of the mixing zone). The local Stewart number in the case of the mixing layer can be approximated as [Ref. 1]

$$S_l \approx S_b = \frac{\sigma B^2}{\rho} \frac{b}{\Delta U} \tag{5.1}$$

where ΔU is the velocity difference on the boundaries of the mixing zone b.

The results of such processing of experimental data are shown by points 4 on Fig. 8. This figure also shows the calculated curve for Ψ from Ref. 11 at a value of $\alpha = 0.34$ for the empirical constant in the expression for Joule dissipation of turbulence energy, and a coefficient of initial turbulence anisotropy $k_0 = 2.0$. It should be noted that the expression for Ψ derived in Ref. 11 is rather cumbersome, and therefore it is more convenient to use the approximate relation of Ref. 1

$$\Psi' = (1 + \beta S_l)^{-1} \tag{5.2}$$

which is fairly close to the exact solution for $\Psi(S_l)$ [Ref. 11] over the entire range of Stewart numbers. The curve corresponding to relation (5.2) at a value of $\beta = 0.14$ is also shown on Fig. 8 (the broken curve).

Thus, having at our disposal relation (5.2) for Ψ, confirmed by experiment (Fig. 8), we can get the solution of specific problems of a jet turbulent boundary layer in a longitudinal magnetic field.

For approximate solution we can use the assumption of constancy $S_l \approx S_b$ (5.1) and consequently $\Psi = \Psi(S_l)$ as well across the zone of mixing of accompanying jets, and introduce the new variables proposed by V. M. Iyevlev [Ref. 8]:

$$x_1 = \int_0^x \Psi' \, dx', \quad V_1 = V/\Psi' \tag{5.3}$$

Then the equation of motion for a plane boundary layer with consideration of relation (1.1) can be transformed to

$$U\frac{\partial U}{\partial x_1}+V_1\frac{\partial U}{\partial y}=\frac{1}{\rho}\frac{\partial \tau_0}{\partial y}$$

The resultant equation in variables (x_1, y) coincides completely with the equation of motion in a free turbulent boundary layer in the case of absence of a magnetic field, an equation that has been solved for many cases of practical importance, so that it remains only to make the transition from the deformed plane (x_1, y) to the physical plane (x, y).

In the case of flow on the initial section of a flat or axisymmetric jet, the dependence of width b of the mixing zone on x_1 (in the general case of non-zero initial width $\delta=\delta_1+\delta_2$) has the known form [Ref. 13]

$$b=\delta+k(m)x_1 \qquad (m=U_2/U_1) \tag{5.4}$$

where k is the same empirical constant as in the case of absence of a field [Ref. 13]. Using relations (5.1), (5.3) and (5.4), we can get the relation between variables x_1 and x

$$\frac{x_1}{x}=\frac{[(1+\beta S_0)+4k\beta S_x]^{1/2}-(1+\beta S_0)}{k\beta S_x} \qquad \left(S_0=\frac{\sigma B^2}{\rho}\frac{\delta}{\Delta U},\ S_x=\frac{\sigma B^2}{\rho}\frac{x}{\Delta U}\right) \tag{5.5}$$

The values of $\delta=0.65$ cm and $k=0.095$ determined on the basis of the experiment in the case of absence of a magnetic field ($B=0$, $x_1\equiv x$) were then used to calculate the width of the mixing zone in the case of flow in a magnetic field in accordance with (5.4), (5.5) at the value of $\beta=0.14$ defined above. The results of the calculation are shown in Fig. 6, where the broken, dot-dash and solid curves refer to magnetic field inductions $B=0$, 0.34 and 0.5 T, and points 1, 2, 3 are experimental data corresponding to the same values of induction B. As can be seen, the calculation is in completely satisfactory agreement with experiment.

In conclusion it should be noted that the expression found in this paper for turbulent friction stress can apparently be used not only for calculating jet flows, but also for flow in the wall boundary layer and for other shear flows.

The authors thank B. P. Borisov, V. M. Derevyago, Ye. D. Zamotina and V. S. Nikolayenko for assistance with the experiments, and also G. M. Abramovich for constructive discussion.

REFERENCES

1. Bushchik, V. G. and Regirer, S. A., "Mixing Layer of Turbulent Flows in a Homogeneous Nonconductive and Conductive Fluid," IZVESTIYA AKADEMII NAUK SSSR: MEKHANIKA ZHIDKOSTI I GAZA, No 1, 1971.

2. Branover, G. G. and Tsinober, A. B., "Magnitnaya gidrodinamika neszhimayemykh sred" [Magnetohydrodynamics of Incompressible Media," Moscow, "Nauka", 1970.

3. Kovner, D. S., "Turbulent Flow of an Electrically Conductive Fluid in a Longitudinal Magnetic Field," IZVESTIYA VUZOV: SERIYA AVIATSIONNOY TEKHNIKI, No 1, 1964.

4. Gurfink, M. M., "The Influence of a Longitudinal Magnetic Field on Pipe Flow," IZVESTIYA AKADEMII NAUK SSSR: MEKHANIKA ZHIDKOSTI I GAZA, No 3, 1967.

5. Kovner, D. S. and Levin, V. B., "Turbulent Flow of an Electrically Conductive Fluid in a Pipe in a Longitudinal Magnetic Field," TEPLOFIZIKA VYSOKIKH TEMPERATUR, Vol 2, No 5, 1964.

6. Dzhaugashtin, K. Ye., "Turbulent Jets of Conductive Fluid, I: Formulation of the Problem; II: Results of Calculation," MAGNITNAYA GIDRODINAMIKA, No 2, 3, 1970.

7. Levin, V. B., "Stabilizing Influence of a Longitudinal Magnetic Field on Nonhomogeneous Turbulent Flows of Electrically Conductive Fluid," MAGNITNAYA GIDRODINAMIKA, No 2, 1965.

8. Lyevlev, V. M., "Theoretical Study of the Influence of a Magnetic Field on Turbulence of a Flow of Electrically Conductive Fluid" in: "Simpozium po problemam turbulentnykh techeniy, vklyuchaya geofizicheskiye prilozheniya. Tezisy dokladov i soobshcheniy" [Symposium on Problems of Turbulent Flows, Including Geophysical Applications. Abstracts of the Papers and Reports], Kiev, Naukova dumka, 1967.

9. Lushchik, V. G., "A Turbulent Submerged Jet of Electrically Conductive Fluid in a Longitudinal Magnetic Field," MAGNITNAYA GIDRODINAMIKA, No 2, 1968.

10. Dzhaugashtin, K. Ye., "Propagation of an Axisymmetric Turbulent Jet of Electrically Conductive Fluid in a Longitudinal Magnetic Field," MAGNITNAYA GIDRODINAMIKA, No 4, 1969.

11. Kovner, D. S. and Lushchik, V. G., "Turbulent Flow of a Conductive Fluid in a Longitudinal Magnetic Field," IZVESTIYA AKADEMII NAUK SSSR: MEKHANIKA ZHIDKOSTI I GAZA, No 1, 1970.

12. Abramovich, G. N., Kovner, D. S. and Lushchik, V. G., "Effect of a Magnetic Field on Turbulence in Shear Flow," DOKLADY AKADEMII NAUK SSSR, Vol 202, No 4, 1972.

13. Abramovich, G. N., "Teoriya turbulentnykh struy" [Theory of Turbulent Jets], Moscow, Fizmatgiz, 1960.

14. Ginevskiy, A. S., "Teoriya turbulentnykh struy i sledov" [Theory of Turbulent Jets and Wakes], Moscow, Mashinostroyeniye, 1969.

15. Hoult, D. P., "Turbulent Mercury Jet," PHYSICS OF FLUIDS, Vol 10, No 11, 1967, p 2345.

16. Sajben, M. and Fay, J. A., "Measurement of the Growth of a Turbulent Mercury Jet in a Coaxial Magnetic Field," JOURNAL OF FLUID MECHANICS, Vol 27, part 1, 1967, p 81

17. Preobrazhenskiy, S. S. and Chinenkov, S. S., "An Experimental Study of the Influence of a Longitudinal Magnetic Field on Turbulent Jets of Conductive Fluid," MAGNITNAYA GIDRODINAMIKA, No 2, 1970.

18. Baushev, B. N., Borisov, B. P., Krasil'nikov, Ye. Yu., Lushchik, V. G., Nikolayenko, V. S. and Panevin, I. G., "A Liquid Metal Loop for Studying Flows and Heat Exchange in a Longitudinal Magnetic Field," MAGNITNAYA GIDRODINAMIKA, No 4, 1972.

19. Parbhakar, K. J. and Uberoi, M. B., "Magnetohydrodynamic Flow Past Axisymmetric Bodies with Aligned Magnetic Field," PHYSICS OF FLUIDS, Vol 12, No 10, 1969, p 2083.

20. Fraim, F. W. and Heiser, W. H., "The Effect of a Strong Longitudinal Magnetic Field on the Flow of Mercury in a Circular Tube," JOURNAL OF FLUID MECHANICS, Vol 33, part 2, 1968, p 397.

21. Schlichting, G., "Teoriya pogranichnogo sloya" [Boundary Layer Theory], Moscow, Nauka, 1969.

22. Navoznov, O. I. and Pavel'yev, A. A., "On Mixing of Accompanying Gas Jets," IZVESTIYA AKADEMII NAUK SSSR: ENERGETIKA I TRANSPORT, No 2, 1968.

23. Khintse, I. O., "Turbulentnost'. Yeye mekhanizm i teoriya" [Turbulence. Its Mechanism and Theory], Moscow, Fizmatgiz, 1963.

6610
CSO: 1862/142

UDC 532.517.4

DEVELOPMENT OF GRID TURBULENCE IN A FLOW WITH CONSTANT VELOCITY GRADIENT

Moscow IZVESTIYA AKADEMII NAUK SSSR: MEKHANIKA ZHIDKOSTI I GAZA in Russian No 1, 1974 pp 38-47

[Article by A. A. Pavel'yev, Moscow]

[Text] On the basis of equations for Reynolds stresses and the equation for the scale of turbulence, an analysis is made of the development of grid turbulence in a flow with fixed velocity gradient. The constants in the equations are determined from the assumption that far from the grid at high Reynolds numbers the turbulence structure tends toward a limiting state with constant values of the correlation coefficient, the degree of anisotropy and the dimensionless velocity gradient. The constants in terms with viscosity are determined from consideration of flow behind a grid without a velocity gradient on the final stage of turbulence degeneracy. The resultant equations are solved on a computer. The calculation agrees satisfactorily with available experimental data.

It is proposed that the equation for frequency of turbulent pulsations derived in this paper be used instead of the equation of scale to calculate flows with a variable velocity gradient.

The computer calculations were done by S. I. Bekritskaya.

1. Model representations of the effect of a velocity gradient on turbulence structure are used in developing methods for calculating flows in a boundary layer, pipe, mixing layer and other turbulent flows with shear. However, the way that the velocity gradient influences the turbulence structure is usually difficult to isolate because of flow nonuniformity due to the boundary effect. A study of homogeneous turbulence in a flow with constant velocity gradient eliminates the boundary effect, which considerably simplifies theoretical analysis.

In recent years, several papers have appeared in which a study was done on the development of grid turbulence in a flow with constant velocity gradient [Ref. 1, 2]. In these papers, heat-loss anemometry was used to measure such turbulence characteristics as the intensity of pulsations with respect to three axes, the Reynolds stress and the scales of turbulence. The experimental results show that the structure of turbulence in a flow with velocity gradient far from the grid

tends toward a limiting state, and the scale of turbulence, whose initial value is determined by the cell size of the grid, increases.

Data were found in Ref. 4, 5 on development of initial small-scale perturbations in a flow with velocity gradient during mixing of jets, and it was shown that the influence of these perturbations on the transition to turbulence and on mixing on the initial section may be quite appreciable.

2. From the Navier-Stokes equations we can get equations for $\langle u_i u_j \rangle$

$$\frac{\partial \langle u_i u_j \rangle}{\partial t} + \sum_{k=1}^{3} U_k \frac{\partial \langle u_i u_j \rangle}{\partial x_k} + \sum_{k=1}^{3} \langle u_k u_j \rangle \frac{\partial U_i}{\partial x_k} +$$
$$+ \sum_{k=1}^{3} \langle u_k u_i \rangle \frac{\partial U_j}{\partial x_k} - \frac{1}{\rho} \left\langle p' \left(\frac{\partial u_i}{\partial x_j} + \frac{\partial u_j}{\partial x_i} \right) \right\rangle +$$
$$+ \sum_{k=1}^{3} \frac{\partial}{\partial x_k} \left[-\nu \frac{\partial \langle u_i u_j \rangle}{\partial x_k} + \langle u_k u_i u_j \rangle + \left\langle (\delta_{jk} u_i + \delta_{ik} u_j) \frac{p'}{\rho} \right\rangle \right] + \tag{2.1}$$
$$+ 2\nu \sum_{k=1}^{3} \left\langle \frac{\partial u_i}{\partial x_k} \frac{\partial u_j}{\partial x} \right\rangle = 0$$

Here the U_i are the components of the average velocity, u_i are the components of pulsation velocity, p' is pressure pulsation, ν is kinematic viscosity, ρ is density, δ_{ij} is the Kronecker delta, $\langle\rangle$ are averaged quantities.

We will assume that

$$\partial \langle u_i u_j \rangle / \partial t = 0, \quad U_1 \neq 0, \quad U_2 = U_3 = 0, \quad \partial U_1 / \partial x_2 = \text{const}$$
$$\partial U_i / \partial x_1 = \partial U_i / \partial x_3 = 0, \quad \rho = \text{const}$$
$$\sum_{k=1}^{3} \frac{\partial}{\partial x_k} \left[-\nu \frac{\partial \langle u_i u_j \rangle}{\partial x_k} + \langle u_k u_i u_j \rangle + \left\langle (\delta_{jk} u_i + \delta_{ik} u_j) \frac{p'}{\rho} \right\rangle \right] = 0 \tag{2.2}$$

With consideration of (2.2), equations (2.1) take the form

$$U_1 \frac{\partial \langle u_i u_j \rangle}{\partial x_1} = -\langle u_2 u_j \rangle \frac{\partial U_i}{\partial x_2} - \langle u_2 u_i \rangle \frac{\partial U_j}{\partial x_2} +$$
$$+ \frac{1}{\rho} \left\langle p' \left(\frac{\partial u_i}{\partial x_j} + \frac{\partial u_j}{\partial x_i} \right) \right\rangle - 2\nu \sum_{k=1}^{3} \left\langle \frac{\partial u_i}{\partial x_k} \frac{\partial u_j}{\partial x_k} \right\rangle \tag{2.3}$$

From (2.3) we can get an equation for the turbulence energy

$$E = \frac{\langle u_1^2 \rangle + \langle u_2^2 \rangle + \langle u_3^2 \rangle}{2}, \quad U_1 \frac{\partial E}{\partial x_1} = -\langle u_2 u_1 \rangle \frac{\partial U_1}{\partial x_2} -$$
$$- \nu \sum_{\alpha, \beta = 1}^{3} \left\langle \left(\frac{\partial u_\alpha}{\partial x_\beta} \right)^2 \right\rangle$$

Expressions for the individual terms of (2.3) are proposed in Ref. 6. The interpolation formula

$$S_{ij}=\nu\sum_{k=1}^{3}\left\langle\left(\frac{\partial u_i}{\partial x_k}\right)\left(\frac{\partial u_j}{\partial x_k}\right)\right\rangle=\frac{c}{3}\frac{E^{3/2}}{L}\delta_{ij}+\frac{\nu}{2}c_1\left\langle\frac{u_iu_j}{L^2}\right\rangle$$

is proposed for the term that describes dissipation.

If we consider that energy-containing vortices in a flow with gradient velocity are anisotropic, then for the dissipative term we can write

$$S_{ij}=\nu\sum_{k=1}^{3}\left\langle\left(\frac{\partial u_i}{\partial x_k}\right)\left(\frac{\partial u_j}{\partial x_k}\right)\right\rangle=\frac{1}{2}\frac{\langle u_iu_j\rangle}{L^2}(c_1\nu+cE^{1/2}L) \tag{2.4}$$

Henceforth we will use expression (2.4) for the dissipative term.

The term

$$K_{ij}=1/\rho\langle p'(\partial u_i/\partial x_j+\partial u_j/\partial x_i)\rangle$$

in (2.3) describes the exchange of energy between the components of velocity pulsation along the different axes, and therefore does not appear in the equation for E. It is shown in Ref. 6 that the quantity K_{ij} is the sum of two terms, one of which depends on the mean velocity profile, while the other depends only on the turbulence characteristic. Therefore the approximating expression for K_{ij} in Ref. 6 should also be broken down into two parts. The following expressions for the exchange term K_{ij} are proposed in Ref. 6 on the basis of solutions for isotropic turbulence for flow with a constant velocity gradient:

$$\begin{aligned}
\frac{1}{\rho}\left\langle p'\frac{\partial u_1}{\partial x_1}\right\rangle&=-(\alpha+\beta)\langle u_1u_2\rangle\frac{\partial U_1}{\partial x_2}-\frac{\gamma}{2}\frac{E^{1/2}}{L}\left(\langle u_1^2\rangle-\frac{2}{3}E\right)\\
\frac{1}{\rho}\left\langle p'\frac{\partial u_2}{\partial x_2}\right\rangle&=\alpha\langle u_1u_2\rangle\frac{\partial U_1}{\partial x_2}-\frac{\gamma}{2}\frac{E^{1/2}}{L}\left(\langle u_2^2\rangle-\frac{2}{3}E\right)\\
\frac{1}{\rho}\left\langle p'\frac{\partial u_3}{\partial x_3}\right\rangle&=\beta\langle u_1u_2\rangle\frac{\partial U_1}{\partial x_2}-\frac{\gamma}{2}\frac{E^{1/2}}{L}\left(\langle u_3^2\rangle-\frac{2}{3}E\right)\\
\frac{1}{\rho}\left\langle p'\left(\frac{\partial u_1}{\partial x_2}+\frac{\partial u_2}{\partial x_1}\right)\right\rangle&=(0.6\langle u_2^2\rangle-0.2\langle u_1^2\rangle+0.2\langle u_3^2\rangle)\frac{\partial U_1}{\partial x_2}-\gamma\frac{E^{1/2}}{L}\langle u_1u_2\rangle
\end{aligned} \tag{2.5}$$

Thus the system of equations for $\langle u_1^2\rangle$, $\langle u_2^2\rangle$, $\langle u_3^2\rangle$ and $\langle u_1u_2\rangle$ takes the form

$$\begin{aligned}
U_1\frac{\partial\langle u_1u_2\rangle}{\partial x_1}&=-0.2[\langle u_2^2\rangle+2(E-\langle u_3^2\rangle)]\frac{\partial U_1}{\partial x_2}-\\
&-\gamma\frac{E^{1/2}}{L}\langle u_1u_2\rangle-c_1\nu\frac{\langle u_1u_2\rangle}{L^2}
\end{aligned} \tag{2.6}$$

$$\begin{aligned}
U_1\frac{\partial\langle u_1^2\rangle}{\partial x_1}&=-2\langle u_1u_2\rangle\frac{\partial U_1}{\partial x_2}-2(\alpha+\beta)\langle u_1u_2\rangle\frac{\partial U_1}{\partial x_2}-\\
&-\gamma\frac{E^{1/2}}{L}\left(\langle u_1^2\rangle-\frac{2}{3}E\right)-c\frac{\langle u_1^2\rangle E^{1/2}}{L}-c_1\nu\frac{\langle u_1^2\rangle}{L^2}
\end{aligned} \tag{2.7}$$

$$\begin{aligned}
U_1\frac{\partial\langle u_2^2\rangle}{\partial x_1}&=2\alpha\langle u_1u_2\rangle\frac{\partial U_1}{\partial x_2}-\gamma\frac{E^{1/2}}{L}\left(\langle u_2^2\rangle-\frac{2}{3}E\right)-\\
&-c\frac{\langle u_2^2\rangle E^{1/2}}{L}-c_1\nu\frac{\langle u_2^2\rangle}{L^2}
\end{aligned} \tag{2.8}$$

$$U_1\frac{\partial\langle u_3^2\rangle}{\partial x_1}=2\beta\langle u_1u_2\rangle\frac{\partial U_1}{\partial x_2}-\gamma\frac{E^{3/2}}{L}\left(\langle u_3^2\rangle-\frac{2}{3}E\right)-$$
$$-c\frac{\langle u_3^2\rangle E^{3/2}}{L}-c_1\nu\frac{\langle u_3^2\rangle}{L^2} \qquad (2.9)$$

One of the equations (2.9)-(2.11) [sic] can be replaced by the equation for turbulence energy

$$U_1\frac{\partial E}{\partial x_1}=-\langle u_1u_2\rangle\frac{\partial U_1}{\partial x_2}-c\frac{E^{3/2}}{L}-\nu c_1\frac{E}{L^2} \qquad (2.10)$$

Henceforth we shall use equations (2.6), (2.8), (2.9), (2.10), which are a closed system if we define in addition the scale of turbulence L and the value of the constants c, c_1, γ, α and β.

Let us note that (2.6) contains two constants whose values were obtained in Ref. 6.

The quantities $-\langle u_1u_2\rangle$ and L appear in the equation for turbulence energy.

To get a closed system of equations, we can derive an expression for $-\langle u_1u_2\rangle$ by using the assumption that at the given point of the flow the quantity $-\langle u_1u_2\rangle$ depends on E, L, $\partial U_1/\partial x_2$ and ν. From dimensional analysis

$$-\langle u_1u_2\rangle/E=\psi(E^{-3/2}L\partial U_1/\partial x_2,\ E^{1/2}L/\nu) \qquad (2.11)$$

Expanding (2.11) in a Taylor series with respect to powers of $z=E^{-1/2}L\partial U_1/\partial x_2$ at constant $Re^\circ=E^{1/2}L/\nu$, and limiting ourselves to the first two terms of the expansion, we get

$$-\langle u_1u_2\rangle=\psi(0,\ Re^\circ)E+\psi'(0,\ Re^\circ)E^{-3/2}L\partial U_1/\partial x_2+\ldots \qquad (2.12)$$

Since at zero velocity gradient $\langle u_1u_2\rangle=0$, we have $\psi(0,\ Re^\circ)=0$.

Then

$$-\langle u_1u_2\rangle=\psi'(0,\ Re^\circ)E^{-3/2}L\partial U_1/\partial x_2$$

which is analogous to the known formula

$$-\langle u_1u_2\rangle=\psi'(0,\ Re^\circ)E^{1/2}L\partial U_1/\partial x_2 \qquad (2.13)$$

At large Re° the quantity $\psi'(0,\ Re^\circ)=c_5$ can apparently be taken as constant. Let us note that if we set $\psi'(0,\ Re^\circ)=0$ and take the next term of expansion (2.12), we likewise get the known expression for $-\langle u_1u_2\rangle$

$$-\langle u_1u_2\rangle=c_5'L^2(\partial U_1/\partial x_2)^2$$

We cannot exclude the possibility that at large values of $z=E^{-1/2}L\partial U_1/\partial x_2$ that may be observed in flows with low Reynolds numbers, it is necessary to account for both terms in expansion (2.12).

Since there are no grounds for assuming $\psi'(0,\ Re^\circ)=0$, henceforth we will use expression (2.13).

Thus the second version of the closed system of equations includes equation (2.10) and relation (2.13) as well as a certain relation for the scale of turbulence. In this case it is necessary to determine constants c, c_1 and c_5 as well.

3. If we assume that a change in turbulence scale at a given point is determined by quantities E, L, $\partial U_1/\partial x_2$ and ν, then we can write

$$U_1 \partial L/\partial x_1 = f_1(E, \nu, \partial U_1/\partial x_2, L)$$

As before, the turbulence characteristics are assumed to be constant along axis x_2. The inclusion of E, L, $\partial U_1/\partial x_2$ and ν alone among the quantities that determine the change in scale presupposes that the other turbulence characteristics are determined by these four quantities.

Let us assume further that

$$f(E, \nu, \partial U_1/\partial x_2, L) = f_1(E, L) + f_2(\nu, L) + f_3(\partial U_1/\partial x_2, L)$$

This assumption means that the changes in the scale of turbulence due to the action of viscosity, turbulence energy and average velocity gradient are independent.

Then we find from dimensional analysis

$$U_1 \partial L/\partial x_1 = c_2 E^{1/2} + c_3 \nu L^{-1} + c_4 L \partial U_1/\partial x_2 \qquad (3.1)$$

In the case of flow behind a grid without velocity gradient on the initial section at large Reynolds numbers, the second member of equation (3.1) retains only the first term, and the equation coincides with the known equation for the scale of turbulence in this case.

For flow behind a grid without velocity gradient on the final section of degeneracy, where the turbulence Reynolds number is small, (3.1) retains only the second term, and for the lengthwise change of scale we get the well known formula that has been obtained both theoretically and experimentally. The third term in (3.1) describes the change in turbulence scale with deformation of the field of turbulent pulsations by a constant velocity gradient.

Thus (3.1), together with (2.6), (2.8-2.10) forms a closed system of equations that contains constants c, c_1, γ, α, β, c_2, c_3, c_4 that must be additionally determined. The second version of the closed system of equations contains equations (2.10), (2.13) and (3.1) with experimental constants c_5, c, c_1, c_2, c_3 and c_4. In this case, c_5 is a function of the turbulence Reynolds number and z. If the problem is being solved for fairly large numbers Re°, then terms with viscosity can be disregarded, and it is necessary to determine six constants in the case of system (2.6), (2.8)-(2.10) and (3.1), or four constants in the case of system (2.10), (2.13) and (3.1).

Another approach to derivation of the equation for turbulence scale was considered in Ref. 7, developed in application to a boundary layer in Ref. 8.

Using (2.10) and (3.1) we can get an equation for the lengthwise change in the quantity $\omega = E^{1/2}/L$, which is the frequency of turbulent pulsations or the intensity of turbulent vortices

$$U_1\frac{\partial\omega}{\partial x_1}=-c\omega^2-\left(c_1+\frac{1}{2}\frac{\langle u_1u_2\rangle}{E}\right)\omega\frac{\partial U_1}{\partial x_2}-0.7c_1\nu\frac{\omega^3}{E} \tag{3.2}$$

In the case of flow with constant velocity gradient, (3.2) can be used instead of (3.1). However, the use of (3.2) in heterogeneous flows gives greater justification for writing the expression for the diffusion term.

An equation for ω was considered in Ref 9, where it was first proposed that the equation of turbulence energy balance be used in analysis of turbulent flows.

4. The values of the constants in the equations depend on the choice of characteristic scale of turbulence. Let us take the transverse integral scale of turbulence

$$L=\int_0^\infty\frac{\langle u_1(x_1,x_2,x_3)u_1(x_1,x_2+r,x_3)\rangle}{(\langle u_1^2(x_1,x_2,x_3)\rangle)^{1/2}(\langle u_1^2(x_1,x_2+r,x_3)\rangle)^{1/2}}dr$$

as such a scale.

In the case of a zero velocity gradient and a large turbulence Reynolds number, the system of equations is reduced to the form

$$U_1\partial E/\partial x_1=cE^{3/2}/L,\quad U_1\partial L/\partial x_1=c_2E^{1/2} \tag{4.1}$$

It is noted in Ref. 10, 11 that on the initial section of degeneracy at large Reynolds numbers $E\sim(x_1-x_1^0)^{-1}$. Then from (4.1) $c_2=c/2$.

At low Reynolds numbers in flows with zero velocity gradient the change of energy and turbulence scale is described by the eauations

$$U_1\partial E/\partial x_1=-\nu c_1E/L^2,\quad U_1\partial L/\partial x_1=c_3\nu L^{-1} \tag{4.2}$$

It is shown in Ref. 12 that on the final stage of degeneracy of grid turbulence $E\sim(x_1-x_1^0)^{-1/2}$. This and (4.2) imply that $c_3=0.2c_1$.

It is shown in Ref. 12 that for grid turbulence on the final stage of degeneracy $c_1=5/4\pi$.

According to experimental data on degeneracy of turbulence behind a grid given in Ref. 11, 12, the constant c can be taken as equal to 0.4.

Thus from the experimental data for grid turbulence on the initial and final stages of degeneracy we get the following values of the constants:

$$c=0.4,\ c_2=0.2,\ c_1=3.927,\ c_3=0.785$$

For closure of the system of equations it is necessary to determine the values of four more constants (γ, α, β and c_4). Let us assume that in the development of grid turbulence at large Reynolds numbers in a flow with constant velocity gradient far from the grid, a turbulence structure is set up such that the quantities

$$c^*=E^{1/2}\left(L\frac{\partial U_1}{\partial x_2}\right)^{-1},\quad c^{**}=-\frac{\langle u_1u_2\rangle}{E},\quad c_*=\frac{\langle u_2^2\rangle}{E},\quad c_{**}=\frac{\langle u_3^2\rangle}{E}$$

are constant and do not depend on distance. Since system of equations (2.6), (2.8)-(2.10) and (3.1) is to describe this state of turbulence, by taking the derivatives with respect to x_1 and setting them equal to zero, we can use (2.8), (2.10)-(2.12) and (3.1) to get four relations between constants γ, α, β, c_4 and c^*, c^{**}, c_*, c_{**}. For the sake of illustration, let us obtain one of these relations:

$$U_1\frac{\partial\langle u_1u_2\rangle/E}{\partial x_1}=U_1\left(-\frac{\langle u_1u_2\rangle}{E^2}\right)\frac{\partial E}{\partial x_1}+\frac{1}{E}U_1\frac{\partial\langle u_1u_2\rangle}{\partial x_1}=0$$

Substituting the second members of equations (2.10) and (2.6) in place of $U_1\partial E/\partial x_1$ and $U_1\partial\langle u_1u_2\rangle/\partial x_1$ in (4.3) and setting $U_1\partial\langle u_1u_2\rangle E^{-1}/\partial x_1=0$, we get

$$\left(\frac{\langle u_1u_2\rangle}{E}\right)^2+(c-\gamma)E^{1/2}\left(L\frac{\partial U_1}{\partial x_2}\right)^{-1}\frac{\langle u_1u_2\rangle}{E}-0.2\left[\frac{\langle u_2^2\rangle}{E}+2\left(1-\frac{\langle u_3^2\rangle}{E}\right)\right]=0$$

From this we get

$$c^{**2}-(c-\gamma)c^*c^{**}-0.2[c_*+2(1-c_{**})]=0 \tag{4.4}$$

In an analogous way we get the three other relations

$$2\alpha+\gamma c^*(c_*-{}^2/_3)c^{**-1}+c_*=0 \tag{4.5}$$

$$2\beta+\gamma c^*(c_{**}-{}^2/_3)c^{**-1}+c_{**}=0 \tag{4.6}$$

$$cc^*+c_4-{}^1/_2c^{**}=0 \tag{4.7}$$

In deriving these relations, it was assumed that $c_2={}^1/_2c$. Thus to determine α, β, γ, c_4, it is necessary to know the values of c^{**}, c^*, c_*, c_{**} far from the grid.

For system (2.10), (2.13) and (3.1) the relations for determining the constants take the form $c_5=c^{**}c^*$ and (4.7).

The equation for turbulence scale (3.1) at $Re^\circ\to\infty$ and $c_2={}^1/_2c$ can be given in the form

$$U_1\frac{\partial L}{\partial x_1}=\left[\frac{c}{2}E^{1/2}\left(L\frac{\partial U_1}{\partial x_2}\right)^{-1}+c_4\right]L\frac{\partial U_1}{\partial x_2}$$

The solution of this equation at a constant value of $E^{1/2}(L\partial U_1/\partial x_2)^{-1}$ takes the form

$$L=L_0\exp\left[\Lambda(\partial\ln U_1/\partial x_2)(x_1-x_1^\circ)\right]\quad\Lambda={}^1/_2(c^{**}-cc^*)$$

5. In Ref. 2, measurements were made of the turbulence structure far from the grid in a turbulent flow with constant velocity gradient. If the constants c^*, c^{**}, c_*, c_{**} are calculated from the data of Ref. 2 at the maximum distance from the grid, we get

$$c^*=0.72,\quad c^{**}=0.34,\quad c_*=0.48,\quad c_{**}=0.57. \tag{5.1}$$

Substituting (5.1) in (4.7)-(4.10) and assuming $c=0.4$, we find

$$c_4=-0.118,\quad \gamma=1.013,\quad 2\alpha=-0.09,\quad 2\beta=0.374,\quad c_5=0.245 \tag{5.2}$$

According to the estimate of Ref. 6, $2\alpha+2\beta=-0.8$. In the case being considered here $2\alpha+2\beta=-0.464$.

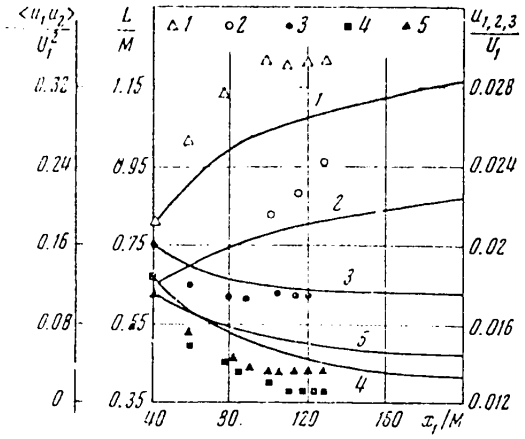

Fig. 1

The values of the constants found above enable us to do calculations by the above-described system of five equations at any Reynolds numbers, and by the system of two equations at large values of the Reynolds number. All the calculations were done on the Nairi computer using a standard program.

The flow that was experimentally investigated in Ref. 2 was calculated. Since the quantity L was not measured in the initial cross section in Ref. 2, its value in that section was determined from relation (2.13) in which all quantities except L were known.

Fig. 1 gives a comparison of calculation by the system of five equations with constants (5.2) and the results of the experiment of Ref. 2. Behavior with respect to length is shown for the quantities $-\langle u_1u_2\rangle/E-1$, $L/M-2$, u_1/U_1-3, u_2/U_1-4, u_3/U_1-5.

We should note the good qualitative and satisfactory quantitative agreement of the results of calcualtion and experiment. Let us note that the calculated value of $-\langle u_1u_2\rangle/E$ far from the grid tends toward a constant value equal to that taken as the limiting value in determining the constants in the equations. However, the approach to the limiting value is slower than in the experiment. This may be due to the fact that the limiting state was not reached in the experiment. If we assume that the limiting state has not been reached, and that the quantities $-\langle u_1u_2\rangle/E$, $E^{1/2}(L\partial U_1/\partial x_2)^{-1}$, $\langle u_2^2\rangle/E$, $\langle u_3^2\rangle/E$ at the maximum distance from the grid differ from the limiting values by as many times as in the calculation, then the corresponding recalculation of the quantities c*, c**, c_*, c_{**} yields $c_*=0.43$, $c_{**}=0.53$, $c^*=0.6$, $c^{**}=0.385$.

At these values of c*, c**, c_*, c_{**}, the constants in the equations are

$$c_4=-0.0475,\ \gamma=0.945,\ 2\alpha=-0.08,\ 2\beta=-0.33,\ c_5=0.231 \qquad (5.3)$$

Fig. 2 shows the values of $-\langle u_1u_2\rangle/E^{-1}$, $L/M-2$, E/U_1^2-3 calculated by the system of five (solid curves) and two (broken curves) equations with constants (5.3).

At low numbers Re°, the quantity $-\langle u_1u_2\rangle/E$ goes through a maximum in approaching the limiting state.

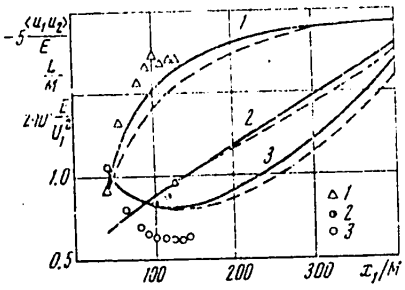

Fig. 2

Calculations show that in the case of flow behind a grid with velocity gradient, the energy first decreases, and then increases, the limiting state being reached on the section of increasing turbulence energy. At the present time the results of measurements of turbulence characteristics have not been published for a sufficient distance from the grid, and the increase in turbulence energy has not been registered. While Ref. 4, 5 do indicate an increase in turbulence energy in a flow with velocity gradient, the data are qualitative in nature.

For calculations by the system of two equations at low Reynolds numbers, it is necessary to find the dependence of c_5 on the Reynolds number and z. This dependence can be found from calculation of the flow behind the grid by the system of five equations at a large initial value of Re° and a low initial value of $E^{-1/2}L\partial U_1/\partial x_2$. It was assumed in the calculations that $U_1^{-1}M\partial U_1/\partial x_2 = 10^{-4}$, and the quantity $Re = MU_1/\nu$ was taken as variable. Here M is the mesh size of the turbulizer. The maximum value of Re was 10^4. At $x_1/M = 20$ it was assumed that $L/M = 0.2$, and $E/U_1^2 = 0.0005$, which corresponds to the conditions of Ref. 11, 12. Turbulence in the initial section was taken as isotropic, and the value of $-\langle u_1u_2\rangle$ was calculated by (2.13). The resultant dependence of c_5 on Re° and z is shown on Fig. 3. The ratio of the instantaneous value of c_5 to the value at high Re° and low z is laid off along the axis of ordinates and denoted by F. At low z and large Re°, $c_5 = 0.28$.

Measurements far from the grid at various Reynolds numbers give more exact values of the limiting state, and enable more detailed analysis of properties of the system of equations under consideration.

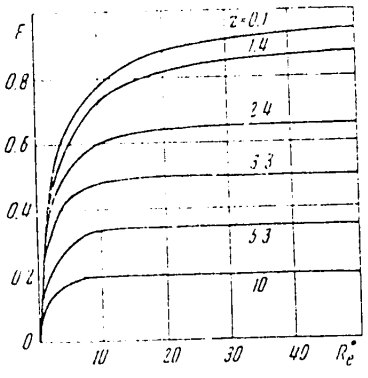

Fig. 3

Calculations show that factor $-0.2[\langle u_2^2\rangle - 2(E - \langle u_3^2\rangle)]$ in (2.6) can be replaced by the expression $-\delta E$. In the calculations, δ was varied over a range of 0.26-0.28. In this case the equations for components of pulsations along the different axes can be eliminated from the system of equations.

6. Using these equations to calculate flows with variable velocity gradient requires the introduction of terms that describe diffusion of the turbulence characteristics. In this case, it is advisable to use the equation for ω rather than the equation for scale. The diffusion term in the equation for ω can be written in the same way as for turbulence energy in gradient form.

If we use the equations for E and ω together with the dependences of c_5 on Re° and $E^{-1/2}L\partial U_1/\partial x_2$ given in Fig. 3, then for flow in a flat channel the system of equations takes the form

$$-c\omega^2 - c_4\omega\frac{\partial U_1}{\partial x_2} + c_5\left(\frac{\partial U_1}{\partial x_2}\right)^2 - 0.7\frac{c_1}{\mathrm{Re}_*}\frac{\omega^3}{E} + \frac{\partial}{\partial x_2}\left\{\left(c_5\frac{E}{\omega}+\frac{1}{\mathrm{Re}^*}\right)\frac{\partial\omega}{\partial x_2}\right\} = 0 \qquad (6.1)$$

$$c_5\frac{E}{\omega}\left(\frac{\partial U_1}{\partial x_2}\right)^2 - cE\omega - c_1\frac{\omega^2}{\mathrm{Re}_*} + \frac{\partial}{\partial x_2}\left\{\left(c_5\frac{E}{\omega}+\frac{1}{\mathrm{Re}^*}\right)\frac{\partial E}{\partial x_2}\right\} = 0 \qquad (6.2)$$

$$\frac{\partial}{\partial x_2}\left\{\left(c_5\frac{E}{\omega}+\frac{1}{\mathrm{Re}^*}\right)\frac{\partial U_1}{\partial x_2}\right\} = -1, \quad \mathrm{Re}^* = \frac{u^* h}{\nu} \qquad (6.3)$$

Here all quantities are reduced to dimensionless form by using the quantities h (the half-width of the channel) and $u^* = (\tau_*/\rho)^{1/2}$, where τ_* is the friction on the wall.

The boundary conditions of these equations are as follows:

$$\begin{aligned} &U_1 = 0,\ E = 0,\ E^{1/2}\omega^{-1} = 0 \text{ at } x_2 = 0 \\ &\partial E/\partial x_2 = \partial\omega/\partial x_2 = \partial U_1/\partial x_2 = 0 \quad \text{at} \quad x_2 = 1 \end{aligned} \qquad (6.4)$$

In writing these equations it was assumed that the transport coefficients in the equations for E, ω and U_1 are the same.

Calculations by system of equations (6.1)-(6.3) with boundary conditions (6.4) can be used to check the feasibility of extending the methods proposed in this paper to flows with a variable velocity gradient. However, it should be noted that in formulating this problem two additional assumptions were made: on the gradient nature of transport, and on equality of the transport coefficients in the equations for E, ω and U_1.

The author thanks V. M. Iyevlev for discussing and supporting this work, and S. I. Beritskaya for doing all the calculations.

REFERENCES

1. Rose, W. G., "Results of an Attempt to Generate a Homogeneous Turbulent Shear Flow," JOURNAL OF FLUID MECHANICS, Vol 26, Part 1, 1966, pp 97-120.

2. Champagne, F. H., Harris, V. G. and Corrsin, S., "Experiments on Nearly Homogeneous Turbulent Shear Flow," JOURNAL OF FLUID MECHANICS, Vol 41, Part 1, 1970, pp 81-139.

3. Rose, W. G., "Interaction of Grid Turbulence with a Uniform Mean Shear," JOURNAL OF FLUID MECHANICS, Vol 44, Part 4, 1970 pp 767-779.

4. Navoznov, O. I. and Pavel'yev, A. A., "Transition to Turbulence in Accompanying Jets," IZVESTIYA AKADEMII NAUK SSSR: MEKHANIKA ZHIDKOSTI I GAZA, No 6, 1969.

5. Navoznov, O. I., Pavel'yev, A. A. and Yatsenko, A. V., "Transition to Turbulence in Submerged and Accompanying Jets," IZVESTIYA AKADEMII NAUK SSSR: MEKHANIKA ZHIDKOSTI I GAZA, No 4, 1972.

6. Rotta, J. "Statistische Theorie nichthomogener Turbulenz," part 1, Z. PHYS., Vol 129, No 5, 1951, pp 547-572.

7. Rotta, J., "Statistische Theorie nichthomogener Turbulenz," part 2, Z. PHYS., Vol 131, No 1, 1951, pp 51-77.

8. Glushko, G. S., "Differential Equation for Turbulence Scale, and Calculation of the Turbulent Boundary Layer on a Flat Plate" in: "Turbulentnyye techeniya" [Turbulent Flows], Moscow, Nauka, 1970.

9. Kolmogorov, A. N., "Equations of Turbulent Motion of an Incompressible Fluid," IZVESTIYA AKADEMII NAUK SSSR: SERIYA FIZICHESKAYA, Vol 6, No 1, 2, 1942.

10. Batchelor, G. K., "Teoriya odnorodnoy turbulentnosti" [Theory of Uniform Turbulence], Moscow, Izdatel'stvo inostrannoy literatury, 1955.

11. Batchelor, G. K. and Townsend, A. A., "Decay of Isotropic Turbulence in the Initial Period," PROCEEDINGS OF THE ROYAL SOCIETY, A193, No 1035, 1948, pp 539-558.

12. Batchelor, G. K. and Townsend, A. A., "Decay of Turbulence in the Final Period," PROCEEDINGS OF THE ROYAL SOCIETY, Series A, Vol 194, No 1039, 1948.

6610
CSO: 1862/143

UDC 532.5.013.4:536.2

NONLINEAR STABILIZATION OF UNSTABLE ACOUSTIC OSCILLATIONS IN A BOUNDED HEAT-RELEASING MEDIUM

Moscow IZVESTIYA AKADEMII NAUK SSSR: MEKHANIKA ZHIDKOSTI I GAZA in Russian No 6, 1978 pp 34-41

[Article by K. I. Artamonov and A. P. Vorob'yev]

[Text] In many power installations the working process that takes place with release of energy is acoustically unstable in the linear approximation under certain conditions. Of practical interest is the problem of determining the amplitudes of unstable waves that are set up as a consequence of energy transfer from an unstable mode to damped modes upon nonlinear interaction. In this paper, equations are derived for the steady-state amplitudes of plane acoustic oscillations in the three-wave approximation with consideration of boundary impedances that disrupt the "internal" resonance of stimulated acoustic overtones. The analysis applies to a high-temperature heat-releasing gas for which the general conditions of stability were formulated in Ref. 1, and were also considered in Ref. 2, 3.

1. Equations of thermal gas dynamics with satisfaction of conditions of local thermodynamic equilibrium and in the diffusion description of radiant thermal fluxes take the form [Ref. 4]

$$\frac{\partial \rho}{\partial t}+\operatorname{div}\rho\mathbf{V}=0,\quad \rho T\left(\frac{\partial S}{\partial t}+\mathbf{V}\nabla S\right)=\rho\varepsilon-Q$$

$$\frac{\partial \mathbf{V}}{\partial t}+(\mathbf{V},\nabla)\mathbf{V}=-\frac{1}{\rho}\nabla p,\quad p=\rho RT,\quad S=c_v\ln p\rho^{-\gamma}$$

Here $\rho\varepsilon$ and Q are heat release and heat removal per unit of volume. The influence of viscosity is disregarded since the viscous dissipation of acoustic oscillations is small compared with dissipation by radiant heat conduction.

We will consider thermoacoustic instability of a heat-releasing medium in which the heat release is proportional to its density ($\varepsilon = \text{const}$). The steady state at $\vec{V}=0$ is reached when the heat supply determined by volumetric heat release is equal to the heat transfer through the side wall of the channel in the direction perpendicular to its axis $\rho\varepsilon = F(T,\rho)$, where $F(T,\rho)$ is a function that describes the heat runoff in the transverse direction.

In analyzing oscillations, we write the heat transfer as

$$Q=F(T,\rho)-\lambda\frac{\partial^2 T}{\partial z^2},\quad F=\alpha(T-T_0),\quad \alpha=\text{const}$$

where z is the coordinate along the axis of the channel, λ is the coefficient of radiant heat conduction. Such a representation of heat transfer for a large ratio of channel length to diameter enables us to reduce the stability problem to the one-dimensional formulation and account for dissipation of oscillations by heat conduction.

We note that the analysis of other mechanisms of heat drainage that were discussed in Ref. 3 does not present any fundamental difficulties, and can be done analogously.

Let us set $V=0+V^{(1)}$, $p=p^{(0)}+p^{(1)}$ and so on, where quantities with the index 1 refer to deviations of the corresponding parameters from their steady-state values, while those with index 0 are the steady-state values. Henceforth we will dispense with the index 0.

Let us introduce the following dimensionless parameters:

$$\eta=\frac{p^{(1)}}{\rho a^2},\ \delta=\frac{\rho^{(1)}}{\rho},\ u=\frac{V^{(1)}}{a},\ \theta=\frac{T^{(1)}}{T},\ \xi=\frac{z}{L},\ \tau=\frac{at}{L}$$

where a is the speed of sound in the medium, L is the length of the channel.

The system of equations written in dimensionless form for oscillations with the retention of nonlinear terms takes the form

$$\frac{\partial\delta}{\partial\tau}+\frac{\partial}{\partial\xi}[(1+\delta)u]=0,\quad \frac{\partial u}{\partial\tau}+u\frac{\partial u}{\partial\xi}=-\frac{1}{1+\delta}\frac{\partial\eta}{\partial\xi} \tag{1.1}$$

$$\frac{\partial\eta}{\partial\tau}+u\frac{\partial\eta}{\partial\xi}+(1+\gamma\eta)\frac{\partial u}{\partial\xi}=\Gamma_1(\delta-\theta)+\frac{1}{\mathrm{Pe}}\frac{\partial^2\theta}{\partial\xi^2} \tag{1.2}$$

$$\gamma\eta=\delta+\theta+\delta\theta \tag{1.3}$$

$$\Gamma_1=\frac{\varepsilon L}{c_p T a},\quad \mathrm{Pe}=\frac{aL}{\varkappa}\qquad\left(\varkappa=\frac{\lambda}{c_p\rho}\right)$$

In deriving equation (1.2), it was assumed that the ambient temperature T_0 is considerably lower than the temperature T of the heat-releasing gas.

Let us restrict ourselves to the quadratic approximation, i. e. we will retain only linear and quadratic terms in the equations for oscillations. The dimensionless parameters Γ_1 and Pe characterize the supply of energy to the oscillations and its dissipation by heat conduction, i. e. they describe the nonconservative nature of the oscillations. For many problems the values of these parameters satisfy the conditions $\Gamma_1,\ 1/\mathrm{Pe}\ll 1$.

When these conditions are met, the dimensionless amplitudes of pressure oscillations are much greater than the amplitude of entropy oscillations, and we can use the so-called quasiadiabatic approximation [Ref. 1] in calculating the second member of equation (1.2).

With these assumptions, system of equations (1.1)-(1.3) is reduced to the form

$$\frac{\partial \delta}{\partial \tau}+\frac{\partial u}{\partial \xi}=\frac{1}{2}\frac{\partial}{\partial \tau}(\eta^2+u^2), \quad \frac{\partial u}{\partial \tau}+\frac{\partial \eta}{\partial \xi}=\frac{1}{2}\frac{\partial}{\partial \xi}(\eta^2-u^2)$$
$$\frac{\partial \eta}{\partial \tau}+\frac{\partial u}{\partial \xi}=-\frac{1}{2}\frac{\partial}{\partial \tau}(\gamma\eta^2+u^2)+\Gamma\left(1+\frac{\gamma-1}{\mathrm{Pe}\,\Gamma}\frac{\partial^2}{\partial \xi^2}\right)\eta$$
$$\Gamma=(2-\gamma)\Gamma_1=(2-\gamma)\frac{\varepsilon}{c_p T}\frac{L}{a}$$

from which we get a nonlinear wave equation for pressure oscillations

$$\frac{\partial^2 \eta}{\partial \tau^2}-\frac{\partial^2 \eta}{\partial \xi^2}=\frac{1}{2}\frac{\partial^2}{\partial \xi^2}(u^2-\eta^2)+\frac{1}{2}\frac{\partial^2}{\partial \tau^2}(u^2+\gamma\eta^2)+\Gamma\left(1+\frac{\gamma-1}{\mathrm{Pe}\,\Gamma}\frac{\partial^2}{\partial \xi^2}\right)\frac{\partial \eta}{\partial \tau} \qquad (1.4)$$

In this equation, the first two terms in the second member characterize the nonlinearity of the hydrodynamic system, while the third term shows the nonconservative nature of the oscillations.

2. For a linear conservative system, instead of (1.4) we have the ordinary wave equation

$$\frac{\partial^2 \eta}{\partial \tau^2}-\frac{\partial^2 \eta}{\partial \xi^2}=0$$

The solution of this equation in a channel of finite length can be represented as a sum of standing waves

$$\eta=\frac{1}{2}\sum \eta_n+K=\frac{1}{2}\sum A_n e^{i\omega_n \tau}\cos(k_n \xi+\varphi_n)+K, \quad \omega_n^2=k_n^2 \qquad (2.1)$$

where A_n is arbitrary amplitude, ω_n is the natural frequency of the mode of oscillations with number n, ϕ_n is phase, and K denotes the complex conjugate part.

The values of k_n and ϕ_n are determined from the boundary conditions of the linear problem. If the ends of the channel are acoustically closed (conditions $u=0$ at $\xi=0$ and $\xi=1$), then $k_n=n\pi$, $\phi_n=0$ ($n=1, 2,\ldots$), and the value $n=1$ corresponds to the fundamental mode of oscillations, $n=2$ corresponds to the second mode and so on, the frequencies of these waveforms making a harmonic series.

Let us consider more general boundary conditions expressed in terms of the acoustic impedances of oscillations on the ends [Ref. 5]. The boundary conditions will be kept conservative (introducing no buildup or dissipation into the system), i. e. we will take the impedances to be purely imaginary quantities. Then the boundary conditions for each natural oscillation ($n=1, 2,\ldots$) take the form

$$\left.\frac{\eta_n}{u_n}\right|_{\xi=0}=-iZ_{0n}, \quad \left.\frac{\eta_n}{u_n}\right|_{\xi=1}=iZ_{1n} \qquad (2.2)$$

From this we get

$$k_n=n\pi+\operatorname{arc\,tg}\frac{1}{Z_{0n}}+\operatorname{arc\,tg}\frac{1}{Z_{1n}} \qquad (2.3)$$

(the case of acoustically closed boundaries corresponds to $Z_{0n}, Z_{1n}\to\infty$).

Let us restrict ourselves to consideration of the case where the influence of finite conductivity of the ends does not lead to low-frequency natural vibration with $n = 0$, and we will henceforth assume that natural oscillations with values $n = 1, 2, \ldots$ may be present in the channel.

3. Let us examine the linear part of equation (1.4) with consideration of the nonconservative term. Substituting a solution in the form (2.1) in this equation, we get a relation

$$\omega_n^2 + i\omega_n\Gamma\left(1 - \frac{\gamma - 1}{\mathrm{Pe}\,\Gamma}k_n^2\right) - k_n^2 = 0 \qquad (3.1)$$

for each mode of oscillations, where the value of the wave number k_n is defined in (2.3). From relation (3.1) when the conditions Γ, $1/\mathrm{Pe} \ll 1$ are met, we get

$$\omega_n \approx \pm k_n - \frac{i\Gamma}{2}\left(1 - \frac{\gamma - 1}{\mathrm{Pe}\,\Gamma}k_n^2\right)$$

from which we get the condition of thermoacoustic stability

$$k_n^2 > k_*^2 = \frac{\mathrm{Pe}\,\Gamma}{\gamma - 1} \qquad (3.2)$$

Oscillations with wave numbers $k_n^2 > k_*^2$ will damp out due to dissipation by heat conduction, while those with wave numbers $k_n^2 < k_*^2$ will be unstable. The value of the critical wave number (3.2) coincides with the value obtained in Ref. 3.

4. Nonlinear terms in equation (1.4) lead to interaction between different modes of oscillations, which limits the amplitudes of unsteady oscillations.

We will seek the solution of equation (1.4) in the form

$$\eta = \frac{1}{2}\sum_n A_n e^{i\omega_n\tau}\cos\chi_n + K, \quad u = -\frac{i}{2}\sum_n A_n e^{i\omega_n\tau}\sin\chi_n + K, \quad \omega_n^2 = k_n^2, \quad \chi_n = k_n\xi + \varphi_n \qquad (4.1)$$

k_n and φ_n being determined from boundary conditions (2.2). However, we will assume that complex amplitudes A_n are slowly varying functions of time τ and coordinate ξ

$$\left|\frac{\partial A_n}{\partial \tau}\right| \ll \omega_n |A_n|, \quad \left|\frac{\partial A_n}{\partial \xi}\right| \ll k_n |A_n|$$

The idea of solution of nonlinear wave equation (1.4) is to substitute expressions (4.1) in this equation, and then equate the terms of the first and second members that have the same space and time dependences, the so-called resonant terms.

Using (4.1) we can show that the resonant terms for η^2 and u^2 are identically expressed, and take the form

$$\eta_0^2 = u_0^2 = \frac{1}{2}\sum_{m,n}\left[A_m A_n e^{i(\omega_m+\omega_n)\tau}\cos(\chi_m+\chi_n) + A_m A_n^* e^{i(\omega_m-\omega_n)\tau}\cos(\chi_m-\chi_n)\right] + K \qquad (4.2)$$

where * is the sign of complex conjugation. This enables us to write equation (1.4) in the simplified form

$$\frac{\partial^2\eta}{\partial\tau^2}-\frac{\partial^2\eta}{\partial\xi^2}=\frac{\gamma+1}{2}\frac{\partial^2}{\partial\tau^2}(\eta_0^2)+\Gamma\left(1+\frac{1}{k_*^2}\frac{\partial^2}{\partial\xi^2}\right)\frac{\partial\eta}{\partial\tau}+H \tag{4.3}$$

where H denotes nonresonant terms.

Substituting the equation for η (4.1) in equation (4.3), and using (4.2), we get

$$\begin{aligned}&\sum_n\left[i\omega_n\left(\frac{\partial A_n}{\partial\tau}-\alpha_nA_n\right)e^{i\omega_n\tau}\cos\chi_n+k_n\frac{\partial A_n}{\partial\xi}e^{i\omega_n\tau}\sin\chi_n\right]+K=\\&=-\frac{\gamma+1}{16}\sum_{m,n}[(\omega_m+\omega_n)^2A_mA_ne^{i(\omega_m+\omega_n)\tau}\cos(\chi_m+\chi_n)+\\&+(\omega_m-\omega_n)^2A_mA_n^*e^{i(\omega_m-\omega_n)\tau}\cos(\chi_m-\chi_n)]+K+H\\&\alpha_n=\frac{1}{2}\Gamma\left(1-\frac{k_n^2}{k_*^2}\right).\end{aligned} \tag{4.4}$$

In the case of acoustically closed ends $\omega_n = k_n = n\pi$, $\chi_n = n\pi\xi$ and without further transformations we can equate the resonant terms in (4.4). We note that in doing this, $\partial A_n/\partial\xi = 0$.

We will take up the case where the ends are close to closed. Let us set $\omega_n = k_n = n\pi + \delta_n$ $(n = 1, 2, \ldots)$, then $\chi_n = n\pi\xi + \psi_n$, where $\psi_n = \psi_n\xi + \phi_n$, where δ_n and ϕ_n are determined from conditions (2.2).

Consideration of the linear stability problem shows that the magnitude of the attenuation factor of the oscillations for damped modes increases with mode number. Therefore in accounting for the nonlinear interaction we limit ourselves to interaction of three modes of oscillations. Equating the resonant terms of equation (4.4) that are proportional to $\exp(in\pi\tau)\cos n\pi\xi$, or $\exp(in\pi\tau)\sin n\pi\xi$, we get the following system of equations:

$$\begin{aligned}i\omega_1\left[\frac{\partial B_1}{\partial\tau}-(\alpha_1+i\delta_1)B_1\right]&=-2b_{21}B_1^*B_2\cos(\psi_2-2\psi_1)\ -2b_{32}B_2^*B_3\cos(\psi_1+\psi_2-\psi_3)\\i\omega_2\left[\frac{\partial B_2}{\partial\tau}-(\alpha_2+i\delta_2)B_2\right]&=-a_{11}B_1^2\cos(\psi_2-2\psi_1)\ -2b_{31}B_1^*B_3\cos(\psi_1+\psi_2-\psi_3)\\i\omega_3\left[\frac{\partial B_3}{\partial\tau}-(\alpha_3+i\delta_3)B_3\right]&=-2a_{12}B_1B_2\cos(\psi_3-\psi_1-\psi_2)\\k_1\frac{\partial B_1}{\partial\xi}&=2b_{21}B_1^*B_2\sin(\psi_2-2\psi_1)+2b_{32}B_2^*B_3\sin(\psi_3-\psi_2-\psi_1)\\k_2\frac{\partial B_2}{\partial\xi}&=a_{11}B_1^2\sin(2\psi_1-\psi_2)+2b_{31}B_1^*B_3\sin(\psi_3-\psi_2-\psi_1)\\k_3\frac{\partial B_3}{\partial\xi}&=2a_{12}B_1B_2\sin(\psi_1+\psi_2-\psi_3)\end{aligned} \tag{4.5, 4.6}$$

$$B_n = A_n e^{i\delta_n \tau}, \quad a_{mn} = \frac{\gamma+1}{16}(\omega_m+\omega_n)^2,$$

$$b_{mn} = \frac{\gamma+1}{16}(\omega_m-\omega_n)^2 \quad (m, n=1, 2, 3)$$

Considering that the spatial distribution of each of the three modes of oscillations differs weakly from that of the corresponding harmonic (ends close to acoustically closed), we can disregard the dependence of B_n on ξ, since in this case the second members in equations (4.6) will have a higher order of smallness than in equations (4.5). Therefore, instead of system (4.6), we will study a system of three equations

$$\begin{aligned} &\frac{\partial B_1}{\partial \tau} - (\alpha_1+i\delta_1)B_1 = i\beta B_1^* B_2 + i\beta B_2^* B_3, \quad \beta = \frac{(\gamma+1)\pi}{8} \\ &\frac{\partial B_2}{\partial \tau} - (\alpha_2+i\delta_2)B_2 = i\beta B_1^2 + 2i\beta B_1^* B_3, \quad \alpha_n \simeq \frac{1}{2}\Gamma\left(1-\frac{n^2\pi^2}{k_*^2}\right) \\ &\frac{\partial B_3}{\partial \tau} - (\alpha_3+i\delta_3)B_3 = 3i\beta B_1 B_2 \quad (n=1, 2, 3) \end{aligned} \tag{4.7}$$

where β is a coefficient close to unity.

Let us introduce into consideration real amplitudes and phases, i. e. we will set $B_n = p_n e^{i\theta_n}$ $(n = 1, 2, 3)$, where p_n is amplitude, θ_n is phase.

Separating the real and imaginary parts in equations (4.7), and using the notation $\Delta_1 = \theta_2 - 2\theta_1$, $\Delta_2 = \theta_3 - \theta_2 - \theta_1$, we get a system of equations that describes the model of nonlinear three-frequency interaction in the quadratic approximation

$$\begin{aligned} &\frac{\partial p_1}{\partial \tau} = \alpha_1 p_1 - \beta p_1 p_2 \sin\Delta_1 - \beta p_2 p_3 \sin\Delta_2 \\ &\frac{\partial p_2}{\partial \tau} = \alpha_2 p_2 + \beta p_1^2 \sin\Delta_1 - 2\beta p_1 p_2 \sin\Delta_2, \quad \frac{\partial p_3}{\partial \tau} = \alpha_3 p_3 + 3\beta p_1 p_2 \sin\Delta_2 \end{aligned} \tag{4.8}$$

$$\begin{aligned} &\frac{\partial \Delta_1}{\partial \tau} = \gamma_1 + \beta\left(\frac{p_1^2}{p_2} - 2p_2\right)\cos\Delta_1 + 2\beta\left(\frac{p_1 p_3}{p_2} - \frac{p_2 p_3}{p_1}\right)\cos\Delta_2 \\ &\frac{\partial \Delta_2}{\partial \tau} = \gamma_2 - \beta\left(\frac{p_1^2}{p_2} + p_2\right)\cos\Delta_1 + \beta\left(\frac{3p_1 p_2}{p_3} - \frac{2p_1 p_3}{p_2} - \frac{p_2 p_3}{p_1}\right)\cos\Delta_2 \end{aligned} \tag{4.9}$$

where $\gamma_1 = \delta_2 - 2\delta_1 = k_2 - 2k_1$; $\gamma_2 = \delta_3 - \delta_2 - \delta_1 = k_3 - k_2 - k_1$, and the value of δ_n $(n = 1, 2, 3)$ is determined from the boundary conditions.

If equations (4.8) are added after each has been multiplied by p_1, p_2, p_3 respectively, we get the relation

$$\frac{1}{2}\frac{\partial}{\partial \tau}(p_1^2 + p_2^2 + p_3^2) = \alpha_1 p_1^2 + \alpha_2 p_2^2 + \alpha_3 p_3^2$$

which implies that a necessary condition of existence of non-zero steady-state amplitudes of oscillations is the presence of at least one mode that is unstable

with respect to the linear approximation, and at least one mode that is damped in the linear approximation, i. e. at least one pair of α_n ($n=1, 2, 3$) must have opposite signs. If all $\alpha_n<0$, the amplitudes $p_n\to 0$ as $\tau\to\infty$. If all $\alpha_n>0$, the oscillations increase with time, and the quadratic approximation is insufficient for finding steady-state amplitudes.

5. Let us consider two-wave interaction in the case where the fundamental mode is unstable with respect to the linear approximation ($\alpha_1>0$), and the second mode is damped due to dissipation by heat conduction ($\alpha_2<0$). The interaction of the modes of the waveforms is described by the system

$$\frac{\partial p_1}{\partial\tau}=\alpha_1 p_1-\beta p_1 p_2\sin\Delta_1,\quad \frac{\partial p_2}{\partial\tau}=-|\alpha_2|p_2+\beta p_1^2\sin\Delta_1$$
$$\frac{\partial\Delta_1}{\partial\tau}=\gamma_1+\beta\left(\frac{p_1^2}{p_2}-2p_2\right)\cos\Delta_1 \qquad (5.1)$$

This system is analogous to that given in Ref. 6.

The values of the steady-state amplitudes are found from this system if the derivatives with respect to time are set equal to zero. The values of the steady-state amplitudes of the oscillations are written as

$$p_1=\frac{\sqrt{\alpha_1|\alpha_2|}}{\beta\sin\Delta_1},\quad p_2=\frac{\alpha_1}{\beta\sin\Delta_1},\quad \Delta_1=\operatorname{arctg}\left|\frac{2\alpha_1-|\alpha_2|}{\gamma_1}\right| \qquad (5.2)$$

At $\gamma_1=0$, i. e. when the second mode is a harmonic of the fundamental tone ($\omega_2=2\omega_1$), the values of the steady-state amplitudes are minimum ($\Delta_1=\pi/2$).

Let us write (5.2) as

$$p_1=\frac{\sqrt{(1-x)(1x-1)}}{2\beta}\sqrt{\Gamma^2+\left(\frac{2}{3}\frac{\gamma_1}{2x-1}\right)^2}$$
$$p_2=\frac{1-x}{2\beta}\sqrt{\Gamma^2+\left(\frac{2}{3}\frac{\gamma_1}{2x-1}\right)^2},\quad x=\frac{\pi^2}{k_*^2}=\frac{(\gamma-1)\pi^2}{\Gamma\,\mathrm{Pe}}.$$

The resultant steady-state amplitudes were studied for stability with respect to the linear approximation by perturbation of system (5.1). Based on the stability condition, we get the constraint $\frac{1}{2}<x<1$.

Fig. 1 shows the behavior of amplitudes p_1 and p_2 as a function of distance from the stability boundary in the case $\gamma_1=0$ ($f_n=\beta p_n/\Gamma$, $x=\pi^2/k_*^2$).

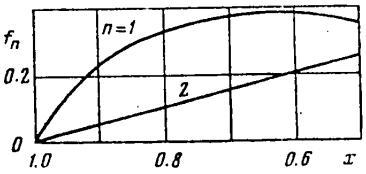

Fig. 1

From a comparison of amplitudes in the cases where the ends have finite conductivity ($\gamma_1\neq 0$) and are acoustically closed ($\gamma_1=0$) we find

$$\frac{p_n}{p_{n0}}=\sqrt{1+y^2},\quad y=\mu\frac{x}{2x-1},\quad \mu=\frac{2}{3}\frac{\gamma_1\mathrm{Pe}}{(\gamma-1)\pi^2}$$

where p_n is the amplitude of the n-th mode at $\gamma_1\neq 0$, p_{n0} is the amplitude of the n-th mode at $\gamma_1=0$.

Since $Pe \gg 1$, the coefficient μ may be considerably greater than unity even at a low value of γ_1. At large μ, amplitude p_n may considerably exceed the amplitude for acoustically closed ends. The behavior of p_n/p_{n0} ($n = 1, 2$) as a function of distance from the stability boundary at different values of μ is shown on Fig. 2 ($\kappa_n = p_n/p_{n0}$, $x = (\pi/k_*)^2$).

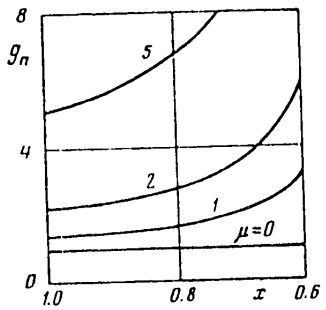

Fig. 2

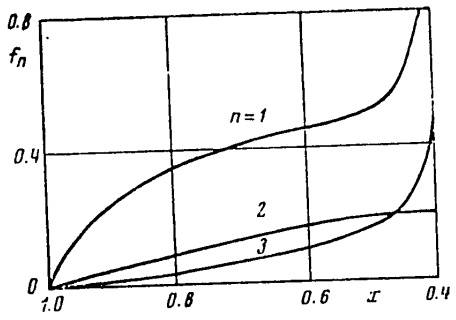

Fig. 3

Our analysis shows that the existence of steady-state amplitudes of acoustic waveforms is a consequence of nonlinear hydrodynamic interaction of a fundamental mode that is unstable with respect to the linear approximation, with a second damped mode. The steady-state amplitude has a minimum value in the case of acoustically closed boundaries, i. e. when the interaction between waveforms is maximum.

6. Let us consider three-wave interaction of oscillations in the case where the fundamental mode is unstable with respect to the linear approximation ($\alpha_1 > 0$), while the other two modes are damped due to dissipation by thermal conductivity ($\alpha_2, \alpha_3 < 0$). We will compare the results with the case of two-wave interaction. Let us restrict ourselves to consideration of acoustically closed boundaries. In this case, we must study system (4.8), (4.9), setting $\gamma_1 = \gamma_2 = 0$.

The steady-state amplitudes of the oscillations are determined from the expressions

$$p_2 = \frac{|\alpha_3|}{6\beta}\left(\sqrt{1+12\frac{\alpha_1}{|\alpha_3|}}-1\right), \quad p_1^2 = \frac{|\alpha_2|p_2}{\beta(1-6\beta p_2/|\alpha_3|)}, \quad p_3 = \frac{3\beta p_1 p_2}{|\alpha_3|} \tag{6.1}$$

where the phase shifts $\Delta_1 = \Delta_2 = \pi/2$.

As the stability boundary is approached in the linear approximation, i. e. when $x \to 1$, (6.1) implies that the amplitudes approach values (5.2) obtained in the case of two-wave interaction with acoustically closed ends.

The steady-state amplitudes determined by using (6.1) were studied for stability with respect to the linear approximation by perturbation of system (4.8), (4.9) at $\Delta_1 = \Delta_2 = \pi/2$. The result was the range of admissible values $5/13 < x < 1$ in which the resultant steady-state amplitudes are stable. From a comparison of the ranges of admissible values of x we see that with consideration of three-wave interaction the expressions for steady-state amplitudes are valid at a greater distance from the stability boundary than in the case of two-wave interaction.

The behavior of amplitudes p_n (n = 1, 2, 3) determined by expressions (6.1) as a function of distance from the stability boundary is shown in Fig. 3 ($f_n = \beta p_n/\Gamma$, $x = \pi^2/k_*^2$).

From an examination of relations $p_n(x)$ (n = 1, 2) shown in Fig. 1 and 3 we see that the values of the steady-state amplitudes of waveforms in both cases near the stability boundary (x close to unity) differ weakly from one another. This gives ground for restriction to the fairly simple case of two-wave interaction in estimating the steady-state amplitudes of oscillations close to the stability boundary.

REFERENCES

1. Artamonov, K. I., "Thermoacoustic Stability of a High-Temperature Heat-Releasing Gas," DOKLADY AKADEMII NAUK SSSR, Vol 231, No 3, 1976.

2. McNeil, B., Becker, M., "Acoustic Instabilities in a Constant Flux Gas Core Nuclear Rocket," AIAA JOURNAL, Vol 8, No 2, 1979. (Russian translation: "Akusticheskaya neustoychivost' gazovogo reaktora yadernogo raketnogo dvigatelya s postoyannym neytronnym potokom," RAKETNAYA TEKHNIKA I KOSMONAVTIKA, Vol 8, No 2, 1970.)

3. Novikov, V. M., "O gidrodinamike delyashchikhsya veshchestv. 2. Nelineynyye resheniya tipa prostoy volny" [Hydrodynamics of Fissionables. 2. Nonlinear Solutions of the Simple Wave Type], Moscow, Prerpint No 2380, Institute of Atomic Energy, 1974.

4. Landau, L. D., Lifshits, Ye. M., "Mekhanika sploshnykh sred" [Mechanics of Continuous Media], Moscow, Gostekhizdat, 1953.

5. Isakovich, M. A., "Obshchaya akustika" [General Acoustics], Moscow, Nauka, 1973.

6. Rudenko, O. V., Soluyan, S. I., "Teoreticheskiye osnovy nelineynoy akustiki" [Theoretical Principles of Nonlinear Acoustics], Moscow, Nauka, 1975.

6610
CSO: 1862/144

UDC 533.6.011.6:538.6:534

INFLUENCE OF A MAGNETIC FIELD ON THERMOACOUSTIC STABILITY OF A HIGH-TEMPERATURE HEAT-RELEASING GAS

Moscow IZVESTIYA AKADEMII NAUK SSSR: MEKHANIKA ZHIDKOSTI I GAZA in Russian No 4, 1979 pp 102-107

[Article by K. I. Artamonov, A. P. Vorob'yev and M. M. Lomonosov, Moscow]

[Text] In this paper, conditions are found for thermoacoustic stability of a high-temperature electrically conductive gas with internal heat release located in a fixed magnetic field that transforms acoustic waves to fast and slow magnetoacoustic oscillations, and also introduces Joule dissipation. The analysis is done by the energy balance method, and also by direct solution of equations for small perturbations in the special case of wavelengths of acoustic oscillations that are small compared with the dimensions of inhomogeneities in the zone of heat release. The stability boundaries are found as compared with fast and slow magnetoacoustic oscillations.

The conditions of thermoacoustic stability of a high-temperature dense gas with volumetric heat release were found by the energy method in Ref. 1. It was shown that a stabilizing factor at sufficiently short wavelengths of acoustic oscillations is the dissipation due to radiant heat conduction.

The results of investigations of the thermoacoustic stability of a plane layer of heat-releasing gas are given in Ref. 2, while Ref. 3 gives the analogous results with consideration of the electrical conductivity of the gas and the effect of an applied weak transverse magnetic field, showing expansion of the stability region with application of a magnetic field. An analogous effect is also noted in Ref. 4.

In the following, we study the influence of a magnetic field on thermoacoustic stability of a high-temperature gas in which heat release is proportional to its density. It is assumed that conditions of local thermodynamic equilibrium are satisfied for the gas, and radiant thermal fluxes are described in the diffusion approximation. The principal effect of a magnetic field when it is of small magnitude is seen in dissipation of acoustic waveforms that have a component of vibrational velocity directed across the magnetic field.

1. The steady state of the investigated system is defined by the equations

$$\mathbf{V}=0,\ p=\text{const},\ \mathbf{H}=\text{const}$$
$$\rho\varepsilon+\operatorname{div}(\lambda\nabla T)=0,\ \lambda=\lambda(p,T)$$
$$\rho=\rho(p,S),\ T=T(p,S)$$

Here ε is the constant heat release per unit of mass of the gas, λ is the coefficient of radiant heat conduction.

The system of equations of magnetic thermal gasdynamics for oscillations of small amplitude (the corresponding quantities are indicated by subscript 1) in the linear approximation takes the form

$$\rho\frac{\partial \mathbf{V}_1}{\partial t}=-\nabla p_1+\frac{1}{4\pi}\operatorname{rot}\mathbf{H}_1\times\mathbf{H},\quad \frac{\partial\rho_1}{\partial t}+\operatorname{div}\rho\mathbf{V}_1=0$$
$$\rho T\left(\frac{\partial S_1}{\partial t}+\mathbf{V}_1\nabla S\right)=\rho_1\varepsilon-\operatorname{div}\mathbf{q}_1,\quad \mathbf{q}_1=-\lambda\nabla T_1-\lambda_1\nabla T$$
$$\frac{\partial\mathbf{H}_1}{\partial t}=\operatorname{rot}[\mathbf{V}_1\times\mathbf{H}]-\operatorname{rot}(\nu_m\operatorname{rot}\mathbf{H}_1),\quad \operatorname{div}\mathbf{H}_1=0 \qquad (1.1)$$
$$\frac{\rho_1}{\rho}=\frac{p_1}{\rho a^2}-\beta T\frac{S_1}{c_p},\quad \frac{T_1}{T}=(\gamma-1)\frac{p_1}{\rho a^2}+\frac{S_1}{c_p}$$
$$\frac{\lambda_1}{\lambda}=m\frac{T_1}{T}+n\frac{p_1}{p},\quad m=\left(\frac{\partial\ln\lambda}{\partial\ln T}\right)_p,\quad n=\left(\frac{\partial\ln\lambda}{\partial\ln p}\right)_T$$
$$a^2=(\partial p/\partial\rho)_S,\ \beta=-\rho^{-1}(\partial\rho/\partial T)_p,\ c_p=T^{-1}(\partial S/\partial T)_p$$

Here a^2, β, c_p are respectively the square of the speed of sound, the coefficient of thermal expansion and the specific heat at constant pressure, $\gamma-1=\beta a^2/c_p$.

The effect of viscosity on acoustic oscillations is disregarded since viscous dissipation is small compared with Joule dissipation and the dissipation by radiant heat conduction.

From the equation of energy we can estimate the relation between amplitudes of S_1/c_p and $p_1/\rho a^2$. When the conditions

$$\frac{\varepsilon}{c_pT}\frac{l}{a}\ll 1,\quad \frac{\varkappa}{al}\ll 1\quad\left(\varkappa=\frac{\lambda}{c_p\rho}\right),\quad \frac{l|\nabla T|}{T}\ll 1 \qquad (1.2)$$

are met (l is the wavelength of acoustic oscillations), we can use the quasi-adiabatic approximation, i. e. we can assume that $S_1/c_p\ll p_1/\rho a^2$.

The first two conditions in (1.2) denote that heat exchange of the gas by radiant conduction and heat transfer to the gas during the period of acoustic oscillations are much less than its enthalpy, while the last condition denotes insignificance of the change in steady-state temperature of the medium on the wavelength of the acoustic oscillations.

2. Let us derive the conditions of thermoacoustic stability in a magnetic field by the energy method [Ref. 1]. The equation of energy balance of acoustic oscillations takes the form

$$\frac{\partial e}{\partial t}=N+N_H+N_F+N_{FH}$$

$$e=\int\left(\frac{\rho V_1^2}{2}+\frac{p_1^2}{2\rho a^2}+\frac{H_1^2}{8\pi}\right)dv, \quad N=\int p_1\frac{(\rho\varepsilon-\operatorname{div}q)_1}{c_p\rho T}dv$$

$$N_F=-\int p_1 V_1\,d\Gamma, \quad N_{FH}=-\frac{c}{4\pi}\int[\mathbf{E}_1\times\mathbf{H}_1]d\mathbf{F}$$

$$N_H=-\frac{1}{4\pi}\int\nu_m(\operatorname{rot}\mathbf{H}_1)^2\,dv$$

$$\mathbf{E}_1=(\nu_m\operatorname{rot}\mathbf{H}_1-[\mathbf{V}_1\times\mathbf{H}])/c$$

Here E_1 is the perturbation of the electric field (c is the speed of light), e is the energy of acoustic oscillations in the volume of the heat-releasing gas, N and N_H are volumetric integrals that define the work of thermal expansion of the gas and the Joule losses in the gas respectively; N_F and N_{FH} are surface integrals, the first corresponding to the mechanical work of the gas, and the second corresponding to the flux of electromagnetic energy through the surface that bounds the given volume of gas.

Physically, the amplification of acoustic oscillations in the heat-releasing medium is due to irreversible work of thermal expansion of the gas if at the instant of compression of an element of gas in the acoustic wave, heat is supplied to the gas in virtue of the specific dependence of the rate of heat release and the magnitude of the radiant heat flux on pressure and temperature.

If the boundaries of the investigated region are "conservative," i. e. they do not introduce buildup or dissipation into the system, then the surface integrals vanish. In this case, a sufficient condition of thermoacoustic stability in a magnetic field is

$$\int\frac{p_1(\rho\varepsilon-\operatorname{div}q)_1}{c_p\rho T}dv<\frac{1}{4\pi}\int\nu_m(\operatorname{rot}\mathbf{H}_1)^2\,dv \qquad (2.1)$$

To obtain the specific conditions of stability, a relation must be established between oscillations of the electric current and of pressure. Assuming weak influence of the magnetic field on the form of acoustic oscillations, which corresponds to the condition $H^2/4\pi\rho a^2\ll 1$, and at sufficiently high electrical conductivity of the medium ($al/\nu_m\gg 1$), the electric currents that arise during oscillations are determined by inductive reactance and we have the following estimate:

$$\operatorname{rot}H_1\sim\frac{H}{l}\frac{V_*}{a}\sim\frac{H}{l_*}\frac{p_1}{\rho a^2}$$

Here V_* is the component of vibrational velocity perpendicular to the direction of the magnetic field, l_* is the characteristic length of the acoustic wave in the direction across the magnetic field.

Disregarding the dissipation of acoustic oscillations due to radiant heat conduction, and considering Joule dissipation in the magnetic field as the only mechanism of dissipation, we get a sufficient condition of thermoacoustic stability from (2.1):

$$\frac{H^2}{4\pi\rho a^2} > (1-A)\frac{\varepsilon}{c_pT}\frac{l_*^2}{\nu_m}, \quad A=(\gamma-1)(m+1)+\gamma n \quad \left(\frac{al}{\nu_m} \gg 1\right)$$

The magnetic field stabilizes the acoustic oscillations that are unstable in the absence of such a field, if $A<1$. The ratio of magnetic pressure to gas pressure at which acoustic oscillations damp out is proportional to the rate of heat release ε/c_pT, the square of the wavelength in the direction across the magnetic field, and the electrical conductivity of the gas.

3. Let us study the influence of a magnetic field on thermoacoustic stability of an electrically conductive heat-releasing gas by solving equations for small oscillations. We will limit ourselves to consideration of wavelengths of acoustic oscillations that are short compared with the dimensions of inhomogeneities in the zone of heat release.

Taking the dependence of oscillations on time and coordinates in the form $\sim \exp i(\omega t + k_1 x + k_2 y + k_3 z)$, we get the dispersion equation

$$\left(\alpha^2 - \frac{i\alpha}{\mathrm{Re}_m} - b\right)(\alpha^2 - 1 + i\alpha\Gamma) = b\mu, \quad \Gamma = (1-A)\frac{\varepsilon}{c_pT}\frac{1}{ka} - (\gamma-1)\frac{\varkappa k}{a} \tag{3.1}$$

$$\alpha=\omega/ka,\ k=\sqrt{k_*^2+k_3^2},\ k_*^2=k_1^2+k_2^2,\ b=H^2/4\pi\rho a^2$$

from system of equations (1.1) in the case of a constant magnetic field directed along the z-axis ($H = H_z = \text{const}$), and with satisfaction of conditions (1.2). Here b is a parameter that characterizes the ratio of magnetic pressure to gas pressure, k_*, k_3 are the transverse and longitudinal components of the wave number with respect to the magnetic field, $\mathrm{Re}_m = a/k\nu_m$ is the magnetic Reynolds number, $\mu = k_*^2/k^2$ is a parameter that characterizes the deviation of oscillations from planar as compared with the applied magnetic field.

In the given formulation of the problem the wave numbers are considered as predetermined real parameters, whereas they must be determined from the boundary conditions in solving the complete problem of thermoacoustic stability.

Let us note that equation (3.1) does not contain an entropy mode, which is a consequence of the previously assumed quasiadiabatic approximation.

For waves that propagate along the magnetic field ($\mu = 0$), equation (3.1) breaks down into two equations, one of which takes the form

$$\alpha^2 - 1 + i\alpha\Gamma = 0$$

and establishes the condition of thermoacoustic stability for pressure waves that do not interact with the magnetic field, in the form of the inequality

$$\Gamma < 0 \tag{3.2}$$

Inequality (3.2) defines the range of wave numbers of acoustic oscillations that are unstable in the heat-releasing medium, if dissipation by radiant heat conduction is taken into consideration:

$$k^2 < \frac{1-A}{\gamma-1}\frac{\rho\varepsilon}{\lambda T}$$

At $\lambda = \text{const}$ ($m = n = 0$, $A = \gamma - 1$), the latter condition coincides with that given in Ref. 2.

The second equation coincides with the dispersion equation for Alfven waves propagating along the magnetic field with damping in a medium with finite electrical conductivity:

$$\alpha^2 - i\alpha/\mathrm{Re}_m - b = 0$$

Let us construct the stability boundary of acoustic oscillations at $\mu \neq 0$, disregarding dissipation by radiant heat conduction, i. e. setting $\Gamma = (1 - A)\varepsilon/c_p T k a$.

On the stability boundary $\mathrm{Im}\,\alpha = 0$, and therefore, taking α as a real number and separating the real and imaginary parts in equation (3.1), we get a system of two equations from which to determine the frequencies of neutral oscillations and the stability boundary

$$\alpha^4 - \left(1 + b - \frac{\Gamma}{\mathrm{Re}_m}\right)\alpha^2 + b(1-\mu) = 0 \qquad (3.3)$$

$$\alpha^2\left(\Gamma - \frac{1}{\mathrm{Re}_m}\right) + \frac{1}{\mathrm{Re}_m} - b\Gamma = 0 \qquad (3.4)$$

Let us find the solution of this equation on the assumption that $\Gamma/\mathrm{Re}_m \ll 1 + b$. This condition is met for high-temperature media that are sufficiently good electrical conductors regardless of the wavelength of the oscillations, and is not a strong constraint. In this case, equation (3.3) becomes independent of (3.4) and determines the frequencies of neutral oscillations on the stability boundary that do not depend on the parameter of heat release Γ:

$$\alpha^2_{1,2} = {}^1/_2(1+b) \pm \sqrt{{}^1/_4(1+b)^2 - b(1-\mu)}$$

The values of α_1^2 and α_2^2 coincide with known expressions for the squares of dimensionless phase velocities of fast and slow magnetoacoustic oscillations in a medium with infinite electrical conductivity [Ref. 5]. The dependences of these parameters on b are shown in Fig. 1 for $\mu = {}^1/_4$ (curves 1 and 2 respectively).

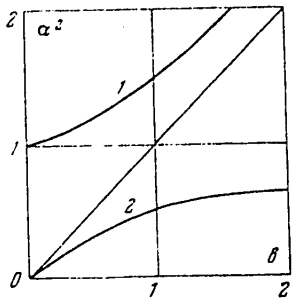

Fig. 1

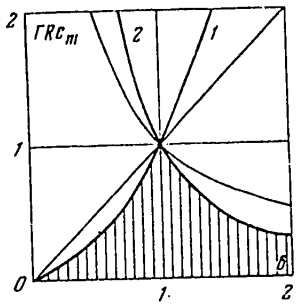

Fig. 2

From (3.4) we get the expression for the stability boundary

$$\Gamma\mathrm{Re}_m = (\alpha^2 - 1)/(\alpha^2 - b)$$

Substituting here the values found above for $\alpha_{1,2}^2$, we get the stability boundaries relative to fast and slow magnetoacoustic oscillations plotted on Fig. 2.

The region of thermoacoustic stability is a region in which both types of oscillations are stable (shaded region in the figure). The stability boundary for oscillations that propagate across the magnetic field ($\mu = 1$) is determined at $0 \leqslant b \leqslant 1$ by the straight line $\Gamma \mathrm{Re}_m = b$, and at $b \geqslant 1$, by the hyperbola $\Gamma \mathrm{Re}_m = 1/b$.

The asymptotic expressions for stability boundaries and frequencies of neutral oscillations in cases of weak and strong magnetic fields for fast and slow magnetoacoustic oscillations have the respective forms

$$\Gamma \mathrm{Re}_m \to \begin{cases} b\mu, & b \to 0 \\ b/\mu, & b \to \infty \end{cases}, \quad \alpha_1^2 \to \begin{cases} 1+b\mu, & b \to 0 \\ b, & b \to \infty \end{cases}$$
$$\Gamma \mathrm{Re}_m \to \begin{cases} 1/b\mu, & b \to 0 \\ \mu/b, & b \to \infty \end{cases}, \quad \alpha_2^2 \to \begin{cases} b(1-\mu), & b \to 0 \\ 1-\mu, & b \to \infty \end{cases} \qquad (3.5)$$

Let us note that the condition of thermoacoustic stability for fast magnetoacoustic oscillations in the case of a weak magnetic field ($b \ll 1$) coincides with condition (2.2) obtained by the energy balance method, if $l_* = 1/k_*$ is taken as the characteristic acoustic wavelength in the direction across the magnetic field.

As implied by our examination of the stability region, an increase in the amplitude of magnetoacoustic oscillations, even propagating across the magnetic field and having maximum Joule dissipation, cannot be suppressed at any value of the magnetic field if $\Gamma \mathrm{Re}_m > 1$. On the basis of this condition, the range of wave numbers on which the magnetic field has no effect on the stabilizing action is written as

$$k^2 < (1-A)\varepsilon/c_p T \nu_m$$

Comparison of stability conditions (3.2) and (3.5) shows that when a weak magnetic field is applied ($b \ll 1$), the heat-releasing medium in the case where the condition $b\mu\nu_m > (\gamma - 1)\kappa$ is met becomes more stable with respect to acoustic oscillations, which is equivalent to expansion of the range of stable wavelengths at a given level of heat release.

Analysis of the way that the stability region depends on the parameter μ that characterizes the direction of propagation of oscillations relative to the magnetic field leads us to the obvious conclusion that as μ decreases there is a reduction in the stability region, i. e. from the standpoint of thermoacoustic stability, oscillations with the lowest values of the parameter μ are the most dangerous.

REFERENCES

1. Artamonov, K. I., "Thermoacoustic Stability of a High-Temperature Heat-Releasing Gas," DOKLADY AKADEMII NAUK SSSR, Vol 231, No 3, 1976.

2. McNeil, H. and Becker, M., "Acoustic Instabilities in a Constant Flux Gas Core Nuclear Rocket," AIAA JOURNAL, Vol 8, No 2. (Russian translation:

"Akusticheskaya neustoychivost' gazovogo reaktora yadernogo raketnogo dvigatelya s postoyannym neytronnym potokom," RAKETNAYA TEKHNIKA I KOSMONAVTIKA, Vol 8, No 2, 1970.)

3. Bastos-Netto, D., Nobre, D. N. and Sudano, J. P., "Acoustic Instabilities in Nonadiabatic Weakly Ionized Gases with Applied Magnetic Fields," AIAA JOURNAL, Vol 15, No 8, 1977.

4. Iyevlev, V. M., "Some Results of Studies on Gas-Phase Void Nuclear Reactors," IZVESTIYA AKADEMII NAUK SSSR: ENERGETIKA I TRANSPORT, No 6, 1977.

5. Shercliffe, G., "Kurs magnitnoy gidrodinamiki" [Course in Magnetohydrodynamics], Moscow, Mir, 1967.

6610
CSO: 1862/145

UDC 532.592

LONG-WAVE STABILITY OF JET FLOWS OF IDEAL FLUID

Moscow IZVESTIYA AKADEMII NAUK SSSR: MEKHANIKA ZHIDKOSTI I GAZA in Russian No 5, 1979 pp 170-175

[Article by K. I. Artamonov and Yu. S. Meleshkov, Moscow]

[Text] An examination is made of the "spatial" stability of jets for which the velocity profiles are linearly dependent on one coordinate. It is shown how the form of the velocity profile and the presence of solid walls influence the development of perturbations in jets.

In experimental research that has been published on reduction of mixing of coaxial jet flows it has been found that by organizing certain velocity profiles of the jets in the inlet section, one can produce nearly laminar flow over a considerable length [Ref. 1, 2]. Some experiments [Ref. 1-4] have revealed so-called coherent structures: large-scale waves in the jet mixing layer.

A linear stability theory can be taken as a basis for explaining some of the results of these studies such as the development of a single unstable harmonic on the initial section of the mixing layer with frequency corresponding to the maximum increment of perturbations [Ref. 5], lack of a pronounced wave pattern of the flow in a submerged jet as contrasted with an accompanying jet [Ref. 1, 2] and certain other facts.

In the above-mentioned experiments the profiles of mean velocity can be taken as consisting of several segments of linear change in velocity. It was shown in Ref. 6 that the eigenvalues of the problem of stability of jets with a smooth profile of velocity can be approximated by the eigenvalues of the problem with profile made up of segments of linear velocity behavior. Moreover, we can expect that for large-scale perturbations the action of forces of viscosity is so weak that the theory of stability of an ideal fluid is valid.

In all calculations of jet flows, perturbations increase with increasing distance from the inlet device, and therefore we will consider here perturbations that increase lengthwise (spatial instability) rather than perturbations that increase timewise ("temporal instability"), implying infinite length of the jets.

1. Consider a plane-parallel flow of incompressible ideal fluid. We will take its velocity as directed along the coordinate axis x, and dependent only on a

single transverse coordinate y. The equations for perturbations of velocity and pressure are well known, and take the form

$$\frac{\partial u_1}{\partial t}+U(y)\frac{\partial u_1}{\partial x}+U'(y)u_2=-\frac{1}{\rho}\frac{\partial p}{\partial x}$$
$$\frac{\partial u_2}{\partial t}+U(y)\frac{\partial u_2}{\partial x}=-\frac{1}{\rho}\frac{\partial p}{\partial y},\quad \frac{\partial u_3}{\partial t}+U(y)\frac{\partial u_3}{\partial x}=-\frac{1}{\rho}\frac{\partial p}{\partial z} \tag{1.1}$$
$$\frac{\partial u_1}{\partial x}+\frac{\partial u_2}{\partial y}+\frac{\partial u_3}{\partial z}=0$$

At the breakpoints of the mean velocity profile U(y) it is necessary to give the conditions for "matching" of solutions. One of these is equality of pressures on both sides of the matching plane. Therefore it is convenient to take another equation only for pressure instead of system (1.1). Eliminating perturbations of velocity u_1, u_2, u_3 from (1.1), we get

$$\left(\frac{\partial}{\partial t}+U(y)\frac{\partial}{\partial x}\right)\Delta p=2U'(y)\frac{\partial^2 p}{\partial x\,\partial y} \tag{1.2}$$

Another condition of matching on the boundary of two zones of smoothness of the mean velocity U(y) is the kinematic condition

$$u_1=\left(\frac{\partial}{\partial t}+U(y)\frac{\partial}{\partial x}\right)\sigma$$

where $\sigma(t, x, z)$ is the equation of the perturbed plane of the boundary of these two zones. The final form of the conditions of matching of pressure perturbations is

$$\left(\frac{\partial}{\partial t}+U^+\frac{\partial}{\partial x}\right)^2\sigma=-\frac{1}{\rho}\frac{\partial p^+}{\partial y}$$
$$\left(\frac{\partial}{\partial t}+U^-\frac{\partial}{\partial x}\right)^2\sigma=-\frac{1}{\rho}\frac{\partial p^-}{\partial y} \tag{1.3}$$
$$p^+=p^-$$

If the average velocities to either side of the matching plane are equal ($U^+=U^-$), then conditions (1.3) take the form

$$\frac{\partial p^+}{\partial y}=\frac{\partial p^-}{\partial y},\quad p^+=p^-$$

In virtue of the linearity of problem (1.2), (1.3), its solution for two-dimensional perturbations (the interconnection between two-dimensional and three-dimensional perturbations will be pointed out below) can be written as

$$p=\int_0^\infty A(\omega, y)\exp(i(kx-\omega t))\,d\omega$$
$$\sigma=\int_0^\infty \Sigma(\omega)\exp(i(kx-\omega t))\,d\omega \tag{1.4}$$

where A, Σ are the amplitudes of perturbations that depend on the the mean velocity profile, the conditions of matching of solutions and the perturbations in the inlet device.

If the perturbations are represented in form (1.4), then the solution of problem (1.2), (1.3) defines dispersion relation $k = k(\omega)$ and $A(\omega, y)$ by means of which the quantities of (1.4) are calculated. It should be noted that in many stability problems the imaginary part of $k(\omega) = r(\omega) - iq(\omega)$ reaches a maximum, and consequently integrals (1.4) at large x have a simple asymptotic estimate [Ref. 7]

$$\int_0^\infty A(\omega, y)\exp(i(kx-\omega t))\,d\omega \cong A(\omega_0, y)\left[\frac{\pi}{2|q''(\omega_0)|x}\right]^{1/2}\exp[q(\omega_0)x+i(r(\omega_0)x+\omega_0 t)]$$

where ω_0 is the frequency at which $q(\omega)$ reaches a maximum.

In other words, if $q(\omega)$ is a function with a maximum (and this is just the case that occurs in development of perturbations) in the mixing layer, then we can expect that regardless of the spectrum of perturbations at the inlet to the fluid flow, the downstream pressure perturbations will actually consist of a single harmonic with frequency ω_0, and it is this wave that is to be observed in the experiment. If $q = 0$, the neutral perturbations will consist of frequencies that correspond to stationary points (the stationary phase method [Ref. 7]).

The amplitude of three-dimensional perturbations (proportional to $\exp(i(kx + mz - \omega t))A = \mu(m, \omega)\alpha(m, \omega, y)$ with accuracy to a factor of $\mu(m, \omega)$ that depends on the perturbation spectrum at the inlet to the flow, is determined from the equations:

$$\frac{d^2a}{dy^2} - \frac{2U'k}{Uk-\omega}\frac{da}{dy} - \varkappa^2 a = 0, \qquad \frac{(\omega-U^+k)^2}{(\omega-U^-k)^2} = \frac{da^+}{dy}\Big/\frac{da^-}{dy}, \qquad a^+ = a^- \tag{1.5}$$

$$\varkappa^2 = k^2 + m^2$$

We see from the form of equations (1.5) that if we know the dispersion relation for two-dimensional perturbations ($m = 0$) $k = f(\omega)$, we can easily determine the dispersion relation for three-dimensional perturbations

$$k = \cos\gamma f(\omega/\cos\gamma)$$

where $k = \kappa\cos\gamma$, $m = \kappa\sin\gamma$, and therefore henceforth we will consider only two-dimensional perturbations.

2. In the case of a linear velocity profile $U = \alpha y + u_0$, equation (1.5) takes the form

$$\frac{d^2a}{dy^2} - \frac{2}{y-b}\frac{da}{dy} - k^2 a = 0, \qquad b = \frac{\omega - ku_0}{k\alpha} \tag{2.1}$$

Equation (2.1) has the simple solution

$$a = C_1\exp(k(y-b))[k(y-b)-1] + C_2\exp(-k(y-b))[k(y-b)+1] \tag{2.2}$$

Using solution (2.2), the conditions of matching and the boundary conditions (on solid walls $\partial p/\partial y = 0$, for unbounded flows $p \to 0$ as $y \to \pm\infty$), we can calculate the

dispersion relation $k = k(\omega)$ in any problem of stability with velocity profile $U(y)$ that consists of segments of linear behavior. Considering that all branches of the dispersion relation enter as complex-conjugate pairs, we will consider only the unstable branches $k(q<0)$ below.

3. First of all, let us consider the stability of a flow of ideal fluid with tangential velocity discontinuity where the velocity in one of the flows varies linearly (Fig. 1). This is the crudest model of flow of accompanying jets with velocity profile specially organized by input devices. The model is inexact for short-wave perturbations both because they are appreciably affected by forces of viscosity, and because substituting a discontinuity for the smooth velocity profile of the mixing layer introduces an error that increases with reduction in the wavelength of perturbations. In the vicinity of a linear velocity profile

$$\frac{da}{dy} = -k\frac{k(y-b)}{k(y-b)+1}a$$

while in the constant-velocity region $da/dy = ka$, $\mathrm{Re}\, k > 0$.

The dispersion relation in the given case takes the form

$$\omega = k\frac{u_1+u_2}{2} + \frac{\alpha}{4} \pm \frac{\alpha}{2}\left[\frac{1}{4} - \frac{(u_1-u_2)}{\alpha}k - \frac{(u_1-u_2)^2}{\alpha^2}k^2\right]^{1/2} \qquad (3.1)$$

where the velocity of the lower flow is equal to u_2, and that of the upper flow is equal to $u_1 + \alpha y$.

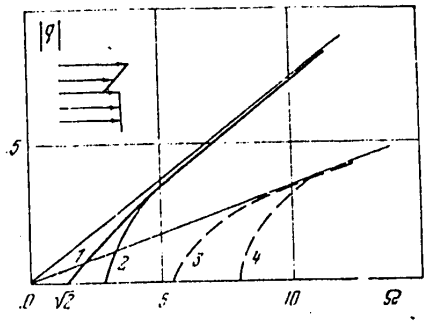

Fig. 1

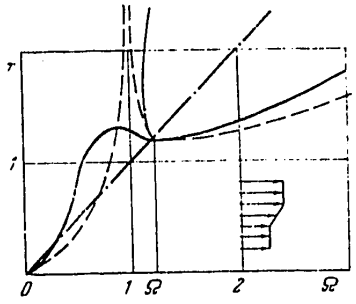

Fig. 2

For the dimensionless quantities

$$\Omega = \frac{2\sqrt{2}\omega}{\alpha}, \qquad K = \frac{2\sqrt{u_1^2+u_2^2}}{\alpha}k$$

equation (3.1) is resolved relative to K

$$K = \Omega\sin(\theta+\pi/4) - \cos\theta \pm [1-(\Omega\cos(\theta+\pi/4)+\sin\theta)^2]^{1/2}, \quad \cos\theta = \frac{u_1}{(u_1^2+u_2^2)^{1/2}} \qquad (3.2)$$

In the case of an ordinary tangential velocity discontinuity ($\alpha = 0$) the flow is unstable at all ω, and for a predetermined frequency the imaginary part of the wave number has the greatest value for a submerged jet ($\theta = 0, \pi/2$).

The dependence of the increment of perturbations on frequency is shown in Fig. 1, where curves 1 and 2 correspond to $\theta = 0$, $\pi/2$, while curves 3 and 4 correspond to the case where $\theta = \theta_1$, $\theta = \pi/2 - \theta_1$, $0 < \theta_1 < \pi/4$.

At low Ω the flow is stable, and at high Ω the dependence $K(\Omega)$ is the same as in the case of a tangential discontinuity. In the region of instability the greatest value of $|q|$ is reached in the case of a submerged jet $\theta = 0$. The value of the dimensionless wave number k falls at a given frequency ω with an increase in the quantity $\sqrt{u_1^2 + u_2^2}$. It is interesting to note that for dimensional frequency ω the region of stability can be expanded by increasing the slope of the velocity profile of the upper flow.

4. It is much closer to reality to model a mixing layer of two jets by a linear velocity profile (an example that even Rayleigh had considered [Ref. 8]). The dispersion relation for dimensionless quantities takes the form

$$\Omega = \frac{\omega h}{u + \alpha h/2}, \quad \delta = \frac{\alpha h/2}{u + \alpha h/2}, \quad K = kh \quad \Omega = K \pm \delta [(K-1)^2 - \exp(-2K)]^{1/2} \qquad (4.1)$$

where u is the velocity of the slower flow, and h is the width of the mixing layer.

The problem is to invert relation (4.1). At $\delta \ll 1$, i. e. at a sufficiently high velocity u,

$$K = \Omega \mp [(\Omega-1)^2 - \exp(-2\Omega)]^{1/2}\delta + O(\delta^2) \qquad (4.2)$$

This implies that at a sufficiently high velocity of the slower flow, the dispersion relations for the temporal and spatial instabilities coincide. The maximum value of the imaginary part of K is reached at $\Omega \cong 0.8$, and is equal to $\mathrm{Im}\, K \cong 0.4\delta$. A wave with just such parameters should be observed in an experiment at any inlet perturbation spectrum.

The spatial dispersion relation behaves quite differently as $\delta \to 1$, i. e. in the case of a submerged jet. When $\delta \to 1$ and $\Omega \to 1$, the real part of K approaches infinity, and the imaginary part approaches $\pi/2$. Fig. 2, 3 show the dependence

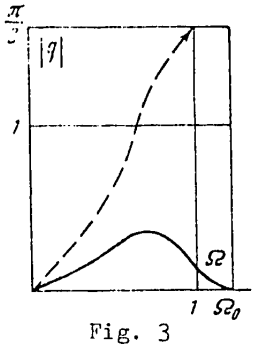

Fig. 3

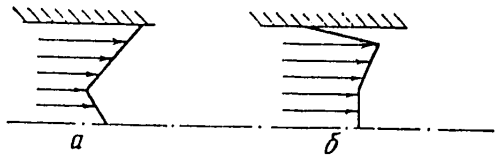

Fig. 4

of the wave number on frequency. The broken lines correspond to $\delta = 1$, the dot-dash lines--to $\delta = 0$, and the solid lines--to some intermediate case $0 < \delta < 1$. $\Omega_0 \cong 1.2$ is found from the equation $(\Omega_0 - 1)^2 - \exp(-2\Omega_0) = 0$.

Apparently the fact that a pronounced wave structure of perturbations shows up only at a fairly high velocity ratio of the jets can be attributed to the appreciable difference in the dispersion relation for a submerged jet and for accompanying jets. Actually, in order for the instability pattern to show up clearly, it is necessary that the increment of perturbations at the distance of about a wavelength should not be too large, as otherwise nonlinear interaction will strongly distort the wave pattern of flow even close to the inlet. In the mixing layer the wavelength of a maximally increasing perturbation approaches zero ($\mathrm{Re}\,K \to \infty$) with decreasing velocity ratio. This means that in the case of a submerged jet it is necessary to account for factors that were disregarded in the given model of stability of jet flows.

Most considerably distorted in a submerged jet is the wave structure of perturbations under the influence of nonlinear interactions and forces of viscosity, whose contribution increases with increasing Re K. In all cases the dimensional increments of perturbations decrease with expansion of the mixing layer, i. e. with increasing h.

5. Let us consider the stability of jet flows in channels. First let us examine flow with the velocity profile shown in Fig. 4a. This kind of flow arises in cases where a considerable gas flow must pass along the periphery with a low flowrate of the central jet, and from considerations of flow stability the velocity jump between jets must be eliminated. The velocity profiles of the peripheral and central jets are given respectively in the form $u+\alpha_1(y-h_1)$ and $u-\alpha_2(y-h_2)$, where h_1, h_2 are the widths of the jets. The dispersion relations for symmetric and antisymmetric modes respectively take the form

$$\omega = k\left(u + \frac{\alpha_1+\alpha_2}{k}\frac{\mathrm{th}\,kh_1\,\mathrm{th}\,kh_2}{\mathrm{th}\,kh_1+\mathrm{th}\,kh_2}\right)$$

$$\omega = k\left(u + \frac{\alpha_1+\alpha_2}{k}\frac{\mathrm{th}\,kh_1\,\mathrm{th}\,kh_2}{1+\mathrm{th}\,kh_1\,\mathrm{th}\,kh_2}\right)$$

Consequently, flows of such a type are absolutely stable. In real flows a boundary layer is formed on the walls of the channel, which requires consideration of a more complicated model of the mean velocity profile (see Fig. 4b). A complete study of flow stability at the walls is apparently impossible without consideration of the influence of the forces of viscosity, and therefore further results make sense only for long-wave perturbations. The dispersion relation in virtue of its awkardness will not be written out. Detailed calculations give the following result. Flow stability for perturbations of all wavelengths is possible only for a limited slope of the velocity profile in the wall region or when this region is sufficiently thin. If the velocities in all jets beginning with the wall region are given in the form $u+\alpha_2(h_2-h_3)-\alpha_1(y-h_2-h_3)$, $u+\alpha_2(y-h_3)$, u, where h_1, h_2, h_3 are the widths of the corresponding jets, then the stability criterion takes the form

$$\left(\frac{h_1}{h_2+h_3}\right)^{1/2} < \frac{h_2}{h_2+h_3}\frac{1}{(\alpha_1/\alpha_2+1)^{1/2}+h_3/(h_2+h_3)}$$

This criterion can be satisfied in the case of a boundary layer only with special organization of the flow on the wall.

In conclusion the authors thank A. A. Pavel'yev for furnishing experimental materials and for constructive discussion of the results of the work.

REFERENCES

1. Navoznov, O. I. and Pavel'yev, A. A., "Transition to Turbulence in Accompanying Jets," IZVESTIYA AKADEMII NAUK SSSR: MEKHANIKA ZHIDKOSTI I GAZA, No 6, 1969.

2. Navoznov, O. I., Pavel'yev, A. A. and Yatsenko, A. V., "Transition to Turbulence in Submerged and Accompanying Jets," IZVESTIYA AKADEMII NAUK SSSR: MEKHANIKA ZHIDKOSTI I GAZA, No 4, 1972.

3. Winant, C. D. and Browand, F. K., "Vortex Pairing: the Mechanism of Turbulent Mixing-Layer Growth at Moderate Reynolds Number," JOURNAL OF FLUID MECHANICS, Vol 63, Part 2, 1974.

4. Brown, G. L. and Roshko, A., "On Density Effects and Large Structure in Turbulent Mixing Layers," JOURNAL OF FLUID MECHANICS, Vol 64, Part 4, 1974.

5. Fneymuth, P., "On Transition in a Separated Laminar Boundary Layer," JOURNAL OF FLUID MECHANICS, Vol 25, No 4, 1966.

6. Gertsenshteyn, S. Ya., "On Convergence of the Rayleigh Method," DOKLADY AKADEMII NAUK SSSR, Vol 187, No 5, 1969.

7. Konson, E. T., "Asimptoticheskiye razlozheniya" [Asymptotic Expansions], Moscow, Mir, 1966.

8. Rayleigh, "Teoriya zvuka" [Theory of Sound], Vol 2, Moscow-Leningrad, Gostekhizdat, 1944.

6610
CSO: 1862/146

UDC 532.517.4

INFLUENCE OF INITIAL CONDITIONS ON FLOW OF AXISYMMETRIC ACCOMPANYING JETS

Moscow IZVESTIYA AKADEMII NAUK SSSR: MEKHANIKA ZHIDKOSTI I GAZA in Russian No 4, 1980 pp 18-24

[Article by O. I. Navoznov and A. A. Pavel'yev, Moscow]

[Text] An experimental study was done on flow on the initial section of axisymmetric jets of helium, air and Freon-12 in an accompanying flow of air for two different kinds of velocity profile at the nozzle tip close to the boundary of the jet. In one case the velocity profile on the nozzle tip was determined by boundary layers on the walls of the nozzle, and in the other case the velocity profile was set up artificially by a honeycomb made up of tubes of variable length. In the work measurements were made of the profiles of average and pulsation velocity, temperature, and the flow was also photographed. The studies showed that depending on initial conditions the intensity of mixing of jets on the initial section at Reynolds numbers defined with respect to the jet diameter $Re \geqslant 10^4$ may change from the level determined by molecular diffusion to the level typical of developed turbulent flow. The structure of the flow in the annular mixing layer also depends strongly on initial conditions. Observed ordered structures in the mixing layer are attributed to a section of development of perturbations close to the nozzle. The ordered structures are strongly influenced by the action of acoustic oscillations from an external source on the jet. In honeycomb formation of the initial profile the transition to developed turbulence may be determined both by the development of long-wave pertubrations and by the development of small-scale turbulence that arises with flow around the end face of the honeycomb.

1. At present there has not been enough experimental study of the influence of initial flow conditions -- initial distributions of average and pulsation velocities and scale of perturbations -- on the flow of accompanying jets, although there are some papers where initial mean velocity profile has been controlled [Ref. 1-5]. Close to the nozzle on the section of transition to developed turbulence the flow is characterized by an increase in initial perturbations. Depending on initial conditions, perturbations may develop in the flow with a scale both larger and smaller than the transverse dimension of the zone with velocity shear. The mutual influence of perturbations of different scales is of great interest.

According to linear stability theory the critical Reynolds numbers for jet flows are small or zero (for the mixing layer). Therefore at a low level of initial

perturbations, long-wave perturbations develop in the flow that lead to developed turbulence. However, ordered structures that are typical of the transition section may be retained even after transition to turbulence. By varying the initial conditions it is possible to determine to what extent the ordered structures in turbulent mixing layers are due to long-wave perturbations on the transition section.

An important result of the linear theory is the conclusion that at large Reynolds numbers the length on which the initial perturbations are intensified a predetermined number of times is proportional to the transverse size of the zone with velocity shear. In this connection it has been suggested that an increase in the transverse dimension of the zone with a smooth change of velocity on the boundary of flows with different velocities should lead to an increase in the length of the section of transition to turbulence. Since mixing intensity on the transition section is considerably lower than with developed turbulent flow, an increase in the length of the transition section leads to a reduction in intermixing of flows of different velocities at a given distance from the beginning of the flow.

Flow was experimentally studied on the initial section of accompanying axisymmetric jets of different velocity with two different forms of velocity profiles close to the boundary of the jets in the initial cross section. In the first case, the transverse dimension of the zone with nonmonotonic velocity behavior close to the boundary of the jets was determined by the thickness of the boundary layers on the nozzle wall separating the accompanying jets, and by the thickness of the edge of the nozzle. In the second case the velocity of the flow close to the boundary of the jets varied smoothly in a layer of finite thickness set up by a honeycomb. Far from this boundary the velocities in the jet and in the accompanying flow in both cases were constant.

Air, helium and Freon-12 were used as working fluids in the central jet. Air was used in the accompanying flow in all experiments. The working sections had identical systems for supply of the accompanying air, including a damping chamber with fine-mesh screens and a convergent channel, and differed in the construction of the feeder elements forming the initial velocity profile. The working sections were set up vertically with flow from the top down. The profiles of longitudinal average and pulsation velocities were measured by a DISA 55M hot-wire anemometer with 55E30 sensor, and the temperature profiles were measured by a Chromel-Copel thermocouple. The flow was photographed by the schlieren method at an exposure of 10^{-4} s.

2. This section describes the results of experiments in which the velocity profile on the nozzle tip close to the jet boundary was determined by boundary layers.

These experiments utilized the feed unit depicted in Fig. 1a, but instead of the honeycomb, two fine screens were installed in the central nozzle. The dimensions on the diagram are given in millimeters. The gas was supplied to the central nozzle by two pylons 1 of streamlined shape. The initial velocity profiles in the jet and in the accompanying flow were equalized by fine screens 2 with mesh size of 0.1 mm. To reduce the boundary layers on the inside and outside walls of the central nozzle, the last screens in the flow were placed as close as possible to the nozzle tip (24 mm from the tip). The edge of the nozzle was 0.2 mm thick.

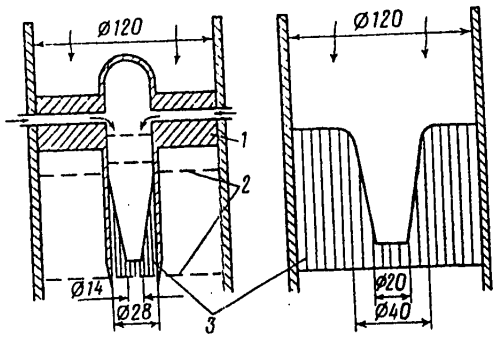

Fig. 1

In some experiments, a ring of wire 1 mm in diameter was placed in the accompanying flow on the outside wall of the nozzle at a distance of 11 mm from the tip to turbulize the boundary layer.

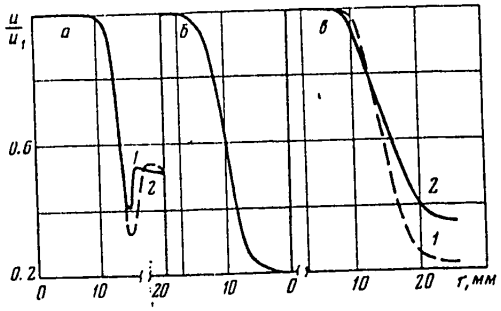

Fig. 2

Fig. 2a shows mean velocity profiles measured at a distance of 2 mm from the nozzle tip in the presence of turbulizing ring 2, and without it 1 at a velocity on the axis $u_1 = 30$ m/s. Velocity profiles at other velocities are close to those shown in Fig. 2a. The intensities of longitudinal pulsations of velocity on the nozzle tip in the center of the jet and in the accompanying flow did not exceed 1 and 0.8% respectively.

Accompanying jets of different densities were photographed to observe the flow structure under the above-described conditions. Fig. 3 [photos not reproduced] shows photographs of a helium jet in an accompanying flow of air at a velocity in the center of the jet of 12 m/s and at a velocity ratio of $m = u_2/u_1$, where u_2 is the velocity of the accompanying flow equal to 0.25 (Fig. 3a, c) and 0.5 (Fig. 3b, d) with a turbulizing ring (Fig. 3c, d) and without it (Fig. 3a, b). Fig. 3e shows a photograph of a jet of Freon-12 in an accompanying flow of air without a turbulizing ring at a jet velocity $u_1 = 2$ m/s and at $m = 0.5$. As can be seen from these photographs, flow in a jet without a turbulizing ring is characterized

by the presence of ordered structures. These structures are most clearly visible close to the nozzle, beginning at the very tip. This suggests that the origin of the ordered structures involves loss of stability. An increase in velocity leads to the appearance of small-scale turbulence, and against this background, developing structures can be seen as before. With increasing distance from the nozzle, these structures show up more clearly, the length on which the structures can be seen increasing with an increase in the ratio of the velocity of the accompanying flow to the velocity of the jet.

With the installation of a turbulizing ring, the flow pattern is strongly altered. Now the ordered structures can be distinguished only at a distance of less than two diameters from the nozzle tip, and at greater distances they are not apparent. A comparison of photographs of helium jets with and without a turbulizing ring shows that expansion of the jets changes insignificantly in this case. Thus the turbulizing ring alters the inner structure of the flow not only near the nozzle, but farther away, although this does not lead to any considerable change in the expansion of the jets. This indicates that the ordered structures seen on the photographs are a further development of perturbations observed on the section of transition to turbulence.

This is also confirmed by the fact that action of acoustic oscillations from an external source on the jet leads to a change in flow structure in the annular mixing layer, thix change depending on the frequency of the sound. Fig 3 also shows photographs of a helium jet ($u_1 = 12$ m/s) in an accompanying flow of air ($m = 0.5$) when acoustic vibrations of different frequencies act on the jet (b--0 Hz, f--500 Hz, g--2000 Hz) with the same amplitude produced by a dynamic loudspeaker set up to the side of the jet. The action of the sound leads to a change in the scale of the ordered structures and the rate of expansion of the jet. Both a reduction and an increase in the rate of expansion of the jet were observed depending on the frequency of the sound. Non-axisymmetric nature of the ordered structures can be seen in Fig. 3f. This is due to the non-axisymmetric nature of the perturbations that arise upon interaction of an acoustic wave with the edge of the nozzle. In general the action of acoustic oscillations on flow in a subsonic jet involves changes in the level and frequency of velocity pulsations that arise when acoustic oscillations interact with input devices, in the given case with the edge of the jet. The role of acoustic oscillatiosn thus reduces only to a change of initial conditions that determine the structure of the flow on the entire length of the initial section of the jet.

A change in flow structure on the initial section that is due as noted above to a change of initial conditions also has an effect on the distribution of average parameters in the jet, in particular the temperature. A characteristic feature of the temperature profile measured in an air jet without a turbulizing ring is the presence of three points of inflection. With installation of the ring, the temperature profile has a single point of inflection. The presence of three points of inflection in the temperature profile and a change in the shape of the profile with installation of the turbulizing ring are due to ordered structures in the annular mixing layer. The same temperature profiles with three points of inflection are also observed in a Freon jet with accompanying flow of air.

3. This section describes the results of experiments in which the initial velocity profile near the boundary of the jet is set up by a honeycomb.

The feed units shown in Fig. 1a and b were used in these experiments. In the feed unit shown in Fig. 1a, the jet and accompanying flow were fed separately, enabling investigation of the flows of different density. In the feed unit shown in Fig. 1b, only a uniform gas flow could be set up. In both units the honeycombs were assembled from pipes of different lengths with outside diameter of 1 mm and wall thickness of 0.05 mm. The reason for making the feed unit shown in Fig. 1b was that when the velocity was increased close to the wall in the unit of 1a, velocity pulsations arose with intensity depending on the nonuniformity of packing of the pipes of the honeycomb close to the nozzle wall. Fig. 2b shows the average velocity profile measured at a distance of 40 mm from the nozzle tip in the unit shown in Fig. 1a. Profile shape is practically independent of the velocity.

Fig. 4a, b, c show photographs of a helium jet in an accompanying flow of air on a unit (Fig. 1a) at velocities of the helium jet u_1 equal to 10, 12, and 18 m/s respectively, and at a ratio m of the velocity of the accompanying flow to the velocity in the center of the jet equal to 0.2. Since only a section of the jet with length of about 150 mm was accommodated on a frame, the photographs of Fig. 4 are made up of individual frames taken at different distances from the nozzle tip with one flow mode, but at different times. At the velocities indicated above the intensity of pulsations on the end face of the honeycomb did not exceed 1%.

The nature of flow in this case is sharply different from that observed in accompanying jets with boundary layers on the boundary of the jets (see Fig. 3). Molecular mixing is observed here on a considerable length. The length of this section depends on the jet velocity u_1, and decreases with increasing velocity. With an increase in velocity on the boundary of the jet, perturbations appear that are due to the nonmonotonic nature of the profile of velocity close to the nozzle wall.

The development of perturbations on the transition section was studied behind the feed unit shown in Fig. 1b. Fig. 2c shows mean velocity profiles at velocity u_1 on the axis of the jet *1*--10 m/s and *2*-- 20 m/s measured at a distance of 80 mm from the face of the honeycomb. The mean velocity profiles at these velocities differ noticeably from each other. The ratio of the velocity outside of the jet to the velocity on the axis of the jet increases from 0.25 at $u_1 = 10$ m/s to 0.35 at $u_1 = 20$ m/s. In either case the mean velocity profile changes insignificantly on the length of the profile.

Of greatest interest is the difference in lengthwise change of the profiles of longitudinal velocity pulsations. At a velocity of 10 m/s on the axis of the jet, pulsations increase both in the zone with velocity gradient, where they have a maximum, and in the core of the jet. At a velocity of 20 m/s on the axis of the jet, pulsations increase only in the zone with velocity gradient. Fig. 5 shows longitudinal velocity pulsations on the axis of the jet (broken lines) and at the point of their maximum (solid lines) as a function of distance from the end face of the honeycomb at velocities u_1 equal to 10 and 20 m/s (curves 1 and 2 respectively). The different behavior of pulsation intensity with respect to length is due to the fact that at a velocity of 10 m/s on the axis of the jet the intensity of pulsations behind the face of the honeycomb is low, and long-wave perturbations develop in the flow with scale that is commensurate with the

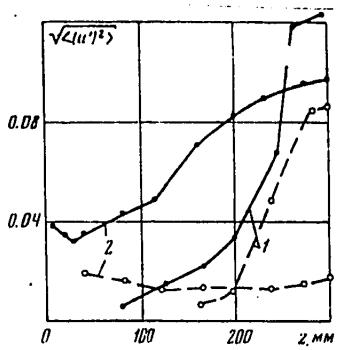

Fig. 5

size of the zone with velocity gradient, while at a velocity on the axis of the jet of 20 m/s the flow behind the end face of the honeycomb is turbulent, and small-scale turbulences develop in the flow, the initial scale of which is of the order of the size of a cell of the honeycomb. These results show the possibility of a transition to developed turbulence both with development of long-wave perturbations and with development of small-scale turbulence. The intensity of mixing on the transition section in either case is less than with developed turbulence.

Thus the results of this paper show that under different initial conditions on the initial section of accompanying axisymmetric jets flows may be realized that differ with respect to mixing intensity and structure. Let us note that a change of flow structure in the mixing layer produced by placing a turbulizing ring on the nozzle was accompanied by both an increase and a reduction in the width of the mixing layer at different velocities and distances from the nozzle tip. The change in width of the mixing layer reached 20%.

The ordered structures observed in this research are determined by the section of development of perturbations close to the nozzle since the flow structure far from the nozzle changes with a change in the flow mode on this section. It is possible that the ordered structures observed in Ref. 5 have the same origin.

These ordered structures, which are associated with waves of instability whose characteristics are determined by the velocity profile on the nozzle tip can interact with waves of instability whose characteristics are determined by the velocity profile on the initial section of the jet. Upon acoustic excitation of waves of the first type, interaction may lead to attenuation of waves of instability of the second type and to some reduction of intensity of velocity pulsations on the axis of the jet. This reduction was not observed if flow at the wall of the nozzle was turbulent and waves of instability of the first type did not develop.

Of particular interest is the possibility of reducing intermixing of accompanying flows of different velocity by setting up a velocity profile in the initial section

with a smooth change of velocity in a layer of finite thickness. A method of this kind can also be used for reducing friction in boundary layers at the wall, where according to linear stability theory an increase in the Reynolds number constructed with respect to the thickness of the boundary layer leads to a reduction in the range of wavelengths and incremental growth of perturbations. Therefore the artificial creation of a flow near the wall where velocity monotonically increases from zero at the wall to the velocity of the external flow in a layer of finite thickness, while the scale of the perturbations is much less than this thickness, may lead to an increase in the length over which the development of long-wave perturbations that are unstable according to linear theory will be less than in the case of flow with constant velocity in the initial section.

The small-scale perturbations that develop in flows of the type described above may lead to developed turbulence without an increase in long-wave perturbations as well. These small-scale perturbations may interact with long-wave perturbations, playing the part of additional viscosity. Stabilization or destabilization may be reached either due to the magnitude of the additional viscosity or due to its gradients. Interaction of this kind could explain the absence of an increase in velocity pulsations on the axis (see Fig. 5) at a velocity of 20 m/s.

The development of small-scale turbulence can be calculated by models of turbulence being developed at the present time [Ref. 6-9]. Analysis of the development of grid turbulence in a flow with constant velocity gradient carried out by means of the models described above [Ref. 8] had shown the possibility of an increase in turbulence energy in such a flow, which has subsequently been experimentally confirmed [Ref. 10].

The authors thank V. M. Iyevlev and K. I. Artamonov for assistance and for discussing the work.

REFERENCES

1. Navoznov, O. I. and Pavel'yev, A. A., "Mixing of Accompanying Gas Jets," IZVESTIYA AKADEMII NAUK SSSR: ENERGETIKA I TRANSPORT, No 2, 1968.

2. Navoznov, O. I. and Pavel'yev, A. A., "The Wake Behind a Plate Formed Upon Merging of Flows of Incompressible Fluid with Different Densities," IZVESTIYA AKADEMII NAUK SSSR: ENERGETIKA I TRANSPORT, No 6, 1969.

3. Navoznov, O. I. and Pavel'yev, A. A., "Transition to Turbulence in Accompanying Jets," IZVESTIYA AKADEMII NAUK SSSR: MEKHANIKA ZHIDKOSTI I GAZA, No 6, 1969.

4. Navoznov, O. I., Pavel'yev, A. A. and Yatsenko, A. V., "Transition to Turbulence in Submerged and Accompanying Jets," IZVESTIYA AKADEMII NAUK SSSR: MEKHANIKA ZHIDKOSTI I GAZA, No 4, 1972.

5. Brown, G. L. and Roshko, A., "On Density Effects and Large Structure in Turbulent Mixing Layers," JOURNAL OF FLUID MECHANICS, Vol 64, No 4, 1974.

6. Iyevlev, V. M., "Turbulentnoye dvizheniye vysokotemperaturnykh sploshnykh sred" [Turbulent Motion of High-Temperature Continuous Media], Moscow, Nauka, 1975.

7. Launder, B. E. and Spalding, D. B., "Lectures in Mathematical Models of Turbulence," L.-N. Y. Acad. Press, 1972.

8. Iyevlev, A. A., "Development of Grid Turbulence in a Flow with Constant Velocity Gradient," IZVESTIYA AKADEMII NAUK SSSR: MEKHANIKA ZHIDKOSTI I GAZA, No 1, 1974.

9. Lushchik, V. G., Iyevlev, A. A. and Yakubenko, A. Ye., "Three-Parameter Model of Shear Turbulence," IZVESTIYA AKADEMII NAUK SSSR: MEKHANIKA ZHIDKOSTI I GAZA, No 3, 1978.

10. Bekritskaya, S. I., "An Experimental Investigation of Small-Scale Turbulence in a Flow with Shear," IZVESTIYA AKADEMII NAUK SSSR: MEKHANIKA ZHIDKOSTI I GAZA, No 4, 1977.

6610
CSO: 1862/147

UDC 532.517.4.032

EXPERIMENTAL INVESTIGATION OF SMALL-SCALE TURBULENCE IN A SHEAR FLOW

Moscow IZVESTIYA AKADEMII NAUK SSSR: MEKHANIKA ZHIDKOSTI I GAZA in Russian No 4, 1977 pp 36-42

[Article by S. I. Bekritskaya, Moscow]

[Text] Turbulence characteristics are measured in a planar flow with velocity gradient. Turbulence development was observed as a function of the parameter of total deformation $\Gamma = (x_1/u_1)(\partial U_1/\partial x_1)$ up to a value of $\Gamma = 18$. An increase in turbulence energy accompanied by an increase in integral scale is attributed to the action of the mean shear on small-scale turbulence

1. The development of turbulence in flows with constant shear and a scale of pulsations that is small compared with the extent of the shear zone has been the subject of considerable research in recent years. The peculiarities of flows of this kind enable investigation of the interaction of initial turbulence with the mean velocity, and more precise definition of physical concepts of shear turbulence. Shear turbulence flows have been produced by a variety of techniques. In Ref. 1, shear flow was set up in the experimental facility by a single-plane grid of identical parallel bars located at different distances from each other in the direction of shear. In Ref. 2, constant shear was produced by a honeycomb with identical cells of different lengths that were varied across the channel in accordance with a definite law.

Turbulence characteristics were predetermined either by an input device, or by screens of various configurations placed downstream. In Ref. 3, turbulent shear flow was produced by a honeycomb with channels of constant length and variable hydraulic drag. The planar turbulent shear flow generator selected by the authors of Ref. 4 was the grid of Ref. 1 followed by a honeycomb with cells of constant length and size.

The authors of Ref. 5 used a honeycomb with channels of variable length and constant diameter to set up shear, and grids of equidistant bars to generate turbulence.

Measurements of turbulence characteristics in Ref. 1-5 showed that profiles produced behind the given input devices have slight lengthwise variability and

constant shear of the longitudinal mean velocity $\partial U/\partial x_1 = 5.5\text{-}15.6\ s^{-1}$. On the initial flow section in all these references there is a reduction in the pulsation components u_1, u_2, u_3, and then the process stabilizes and the turbulence energy $E = 0.5[\langle u_1^2\rangle + \langle u_2^2\rangle + \langle u_3^2\rangle]$ remains constant with respect to length. In some cases a subsequent increase was observed in the intensity of pulsations $\varepsilon_1 = \sqrt{\langle u_1^2\rangle}/U_1$ to 25% of the minimum level [Ref. 4, 5].

In the present study, velocity shear and initial turbulence characteristics are predetermined by a honeycomb (I) made up of tubes of the same diameter and with length l that varies in the direction of shear (see Fig. 1).

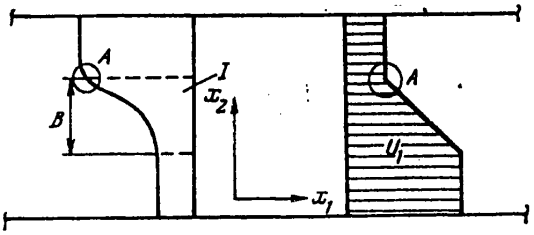

Fig. 1

Tube dimensions: diameter 1 mm (mesh M), thickness of tube walls 0.05 mm. The tubes were cemented in a hexagonal configuration. Geometric porosity of the end face $\psi = 0.815$. In the central part of a rectangular honeycomb of width $B = 50$ mm the length of the tubes was varied from 50 to 150 mm according to the law $lU = \text{const}$. The two end sections were made up of tubes of fixed (50 and 150 mm) length.

The working section (see Fig. 1) was a Plexiglas channel with smooth inside walls 870 mm long of lengthwise constant cross section (230 x 95 mm) with output of the stream into the atmosphere. A series of damping devices preceded the honeycomb. Before installation of the honeycomb in the working channel, the flow in the chamber preceding the honeycomb has constant mean velocity and constant intensity of pulsations (~1%) with respect to cross section. Air enters from a high-pressure line. Flowrate is controlled by a flowmeter washer, and temperature is regulated by an electric heat exchanger with respect to readings of a thermocouple in the chamber. Apertures are provided along the channel walls for taking static pressure readings; measurements were made by an inclined spirit manometer.

The principal measurements were made by instrumentation produced by the DISA company for heat-loss anemometry. The equipment included the 55M hot-wire anemometer with auxiliary and measurement modules, a linearizer and a correlator. Instruments of the (Bryul and K'yer) Company were used for frequency analysis. The Lyrec TR-61 tape recorder was used for recording signal specimens. A WX-451 two-coordinate chart recorder was used for graphic registration of measurement results. The technical specifications of these instruments and operating procedures are presented in detail in the operator's manuals. The company's standard direct sensors were used for measurements of mean velocities and longitudinal pulsations, and type 55A32 X-sensors were used for measuring transverse pulsations. The sensing elements of these devices are made of platinum-coated tungsten wire 5 μm in diameter and filament length of $L = 1.2$ mm; overheating in the working state -- 0.8.

The sensors were calibrated for mean velocity in the 55D41/42 gage tube. The sensors were displaced in the working section by a coordinate device remotely controlled by a drive module.

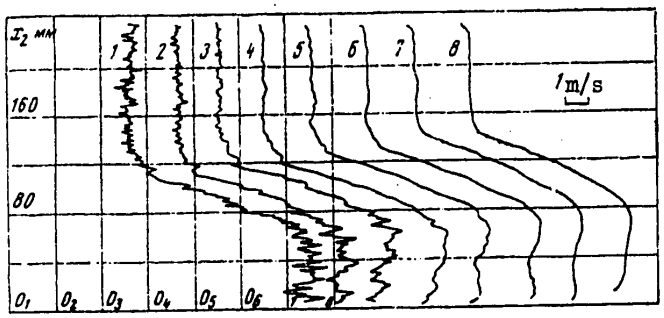

Fig. 2

2. Fig. 2 shows the signal recording for mean-velocity profile measurements in the plane equidistant from the side walls. Profiles 1-8 refer to cross sections $x_1 = 20$, 40, 80, 160, 320, 500, 650 and 800 mm. All profiles are taken in one regime. The increasing boundary layer on the walls leads to acceleration of the flow. The static pressure differential on segment $x_1 = 100$-700 mm for the regime shown in Fig. 2 (all subsequent measurements are referred to this regime) is 20% of the velocity head on the low-velocity side. The boundary layers do not reach the shear zone.

The mean-velocity profiles plotted with respect to coordinate x_3 in different zones -- in shear, on segments of constant higher and lower velocities -- show that in this direction the flow has invariable velocities except for the boundary regions at the walls. Toward the end of the channel the core of the flow that is free of wall influence has a transverse extent of no more than 70% of the channel dimension.

Mean-velocity measurements showed profile dependence not only on the length of the honeycomb tubes, but also on organization of the flow in the chamber preceding the honeycomb. For the given law of variation in tube length ($lU_1 = \text{const}$) the mean-velocity profile showed a dip of the wake type about 10 mm wide in region A (see Fig. 1). The result was rapid development of intense turbulence. This dip was eliminated by a smooth transition from tubes of shorter length to the section of tubes with a constant length of 150 mm; however, the profiles of Fig. 2 show an appreciable local increase in the gradient in region A as compared with the rest of the shear zone. Toward the end of the working section, the gradient is about the same (130 s^{-1}) over the width of the shear layer. There is a 2% error in measurement of mean velocity.

A square-pulse method was used to determine the upper limit of the working frequency band of the sensor-anemometer system. This limit is $8 \cdot 10^3$-$10 \cdot 10^3$ Hz for velocities of $U_1 = 3$-15 m/s. In this range the DISA Company guarantees an instrument error equivalent to a turbulence level of 0.013%. The error of the measurement voltmeter is 1%. Sensor filament length L and honeycomb mesh M are commensurate, and therefore the measurements yielded an understated value of the

pulsations. The correction was estimated by duplicating the measurements with another sensor having a filament 2.5 μm thick and 0.6 mm long. The readings of the two sensors were extrapolated to the case of a "point" sensor. The correction determined in this way decreased with increasing scale of pulsations.

Systematic measurements done on a special facility showed that pulsation intensity ε_1 on a honeycomb of the given design is independent of tube length in the range of 50-150 mm, and is a function of velocity at the output. When the velocity is changed from 2 to 7 m/s, there is a considerable rise in the level of pulsations, and after that there is litle change up to 25 m/s.

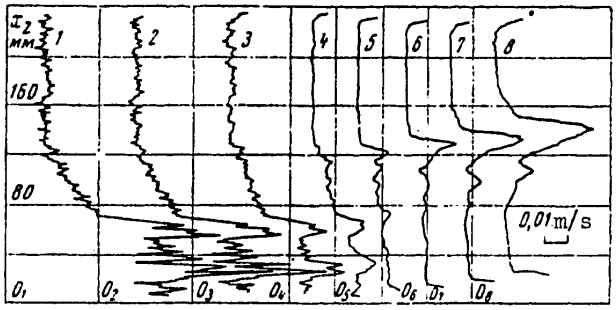

Fig. 3

Fig. 3 shows profiles of the absolute value of pulsations plotted in zone A synchronously with the mean-velocity profiles of Fig. 2 (curves 1-8 correspond to the same value of x_1 as in Fig. 2). The initial level of pulsations is uneven over the cross section, which is due to the difference in velocity. The small inhomogeneities (the "sawtooth" shape of the profile) are caused by peculiarities in flow formation on the honeycomb. Downstream the level of pulsations on segments of constant velocity falls off. Pulsations in the gradient zone at first degenerate over the entire layer. On the segment with gradient in region A on the section of x_1 from 160 to 320 mm the level of pulsations does not change, and then it increases. Toward the end of the working section an increase in pulsations is observed over the entire shear zone. At a distance of $x_1 = 800$ mm the maximum intensity is 6%, which is four times the minimum level in this zone. The increased intensity of pulsations close to the walls of the channel is separated from the zone of rising pulsations by sections of low intensity.

In the measurement of transverse pulsations, the sensitivity of the X-sensor was determined with respect to the error of the angle $\Delta\phi$ between the plane of the filament together with its mounts, and plane x x of the channel, and also with respect to the error $\Delta\alpha$ in setting the axis of the sensor parallel to coordinate x_1. Accounting for possible sources of measurement errors gives an error of 3%.

The measurements were done at points typical of different sections of the velocity profile in a number of cross sections lengthwise in the plane equidistant from the walls of the channel. In the initial cross sections $u_1 > u_2 > u_3$. Downstream the components u_2 and u_3 degenerate, remaining less than u_1. At distance

x_1 = 100-200 mm (faster in the zone of intense increase in pulsations) the quantity u_3 becomes greater than u_2, and downstream $u_1 > u_3 > u_2$ over the entire length. Transverse pulsations degenerate in the non-gradient zones. Fig. 4 shows the results of measurements of the intensity $\varepsilon_i = \sqrt{\langle u_i^2 \rangle}/U_1$ of pulsations: 1--ε_1, 2--ε_2, 3--ε_3. The points represent the results of individual measurements; however, the confidence of these values was confirmed by repeated measurements on one regime. It can be seen that the transverse pulsations increase in zone A analogously to the longitudinal component. At the end of the channel they are 2.5 times the minimum level that exists up to x_1 = 400 mm. In the end cross sections an increase in transverse pulsations is observed over the entire shear layer.

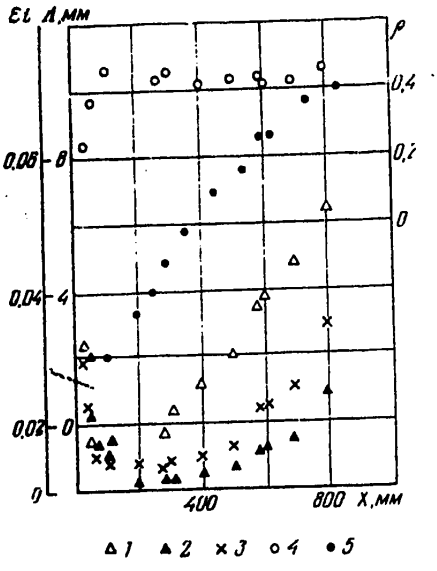

Fig. 4

Peculiarities of the correlator model enabled direct measurement of the correlation coefficients $\rho = \langle u_1 u_2 \rangle / \sqrt{\langle u_1^2 \rangle} \sqrt{\langle u_2^2 \rangle}$. Fig. 4 shows measurements of ρ (4) in region A.

The correlation coefficient immediately behind the honeycomb is small, correlation increases on the section of degeneration of pulsations, and ρ reaches a constant level of ~0.45 on the section of rising pulsations. The behavior of the correlation coefficient is analogous in the center of the shear zone; a difference is that the section where the constant level is reached is shifted toward greater distances x_1. An estimate of measurement accuracy gives an error of 4%.

The longitudinal pulsation component was used for determining the autocorrelation functions. Correlation analysis was done by time shift. The hot-wire anemometer signal was limited to a frequency of 10^4 Hz by low-frequency filters. A graphic plot of the correlation coefficient as a function of delay time ($\rho(\tau)$) was made by the WX-451 chart recorder. The measurement results were used in accordance with the Taylor hypothesis to determine the longitudinal integral scale of turbulence: $\Lambda_1 = NU_1 \int_0^T \rho(\tau) d\tau$ (N is the scale factor, T is the time range of analysis).

The smoothness of the function is evidence of a continuous frequency spectrum of pulsations. The area under the curves increases monotonically with increasing distance from the end face of the honeycomb. The constancy of quantity Λ_1 was verified in the transverse direction--with respect to x_3: the scales in plane x_1x_2 equidistant from the walls coincided with the values in plane x_1x_2 20 mm away from the middle plane.

The results of determination of Λ_1 in region A are shown in Fig. 4 (5). The scale increases in the shear zone more intensively than in the zones of constant velocity: in cross section x_1 = 250 mm the value Λ_1 in zone A is twice the corresponding value on the flat sections of the profile. By the cross section x_1 = 550 mm this difference has increased to the triple level. Then the intensity

of increase in scale in zone A slows down. By the cross section $x_1 = 800$, the value $A_1 = 10$ mm, which is 20% of the shear layer. The finite dimensions of the sensor lead to an overstatement of the measured scale as compared with its true value. Duplication of the measurements by a sensor with filament 2.5 μm thick and 0.6 mm long enabled estimation of the correction: for example at a distance $x_1 = 150$ mm the correction in zone A is 15%, and at a distance of 200 mm it has decreased to 5%.

Simultaneously with correlation analysis, the signal specimens were tape-recorded and then a three-octave analyzer was used to process the spectrum of the hot-wire anemometer signal. The spectra of the pulsations in all zones have a form typical of developed turbulent flow in the initial cross sections. The upper frequency limit of the spectrum in cross section $x_1 = 100$ mm lies in the vicinity of 5000 Hz. Downstream the spectra behave in the following way. On the nongradient sections there is a drop in the level of pulsations, and the frequency band of the spectrum changes slightly. In the shear zone, especially in region A, the level of pulsations increases with distance from the inlet, and the spectrum shifts markedly toward lower frequencies; by the end of the working section the upper frequency limit has reached 1500 Hz.

3. The results found in the experiments show that turbulent flow is set up in the working channel with initial profile that changes little with respect to channel length. The Reynolds number calculated from the velocity difference in the shear layer and with respect to the width of the layer $Re_0 = \Delta U_1 B/\nu = 2.7 \cdot 10^5$, but there is little expansion of the layer over the length of the working section, which is equal to 18 widths. The weak influence of transverse diffusion of turbulence is evidenced by local inhomogeneities of pulsation quantities over a considerable length. The boundary layers on the walls of the channel did not distort the region where the principal measurements were made. Apparently the increase in turbulence energy in the shear zone is the result of interaction of initial small-scale turbulence with mean-velocity shear. The pulsation spectra do not contain increasing perturbations of the isolated frequency. This shows that in the given case the development of turbulence cannot be a result of development of a disturbance with a scale equal to or greater than the width of the shear zone.

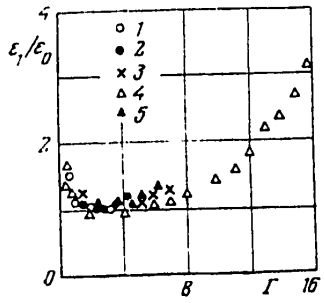

Fig. 5

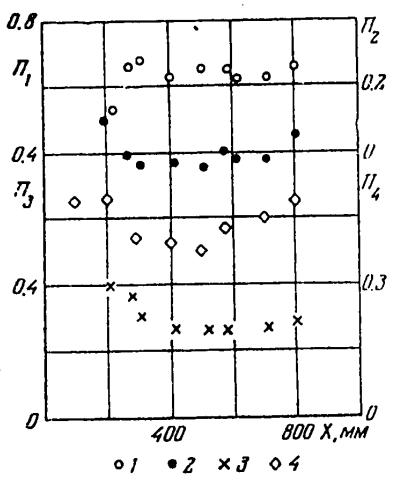

Fig. 6

One of the parameters that characterizes the development of perturbations in the given case is the dimensionless total deformation $\Gamma = (x_1/U_1)(\partial U_1/\partial x_2)$. In our experiment the values of Γ were uneven along the gradient: maximum values of Γ correspond to lower velocity; this nonuniformity increases in zone A due to a local increase in gradient. This explains the nonuniform increase in turbulence energy with respect to the width of the layer. A plot of the experimental results in the form of a curve of pulsation intensity as a function of parameter Γ (see Fig. 5) enables us to generalize the results to the entire shear layer (points 4 refer to zone A, and points 5 refer to the center of the shear layer). Small-scale turbulence degenerates until the quantity Γ reaches unity. Upon a further increase in Γ the degeneration of the pulsations slows down, and energy varies weakly for some time. At the same time an increase is observed in ρ. Beginning at a value of $\Gamma = 4$ the energy of pulsations increases; this is accompanied by an increase in the integral scale of turbulence pulsations and displacement of the spectrum toward the low-frequency region. At the end of the working channel, Γ in zone A reaches 18 (Γ^*), and the intensity of longitudinal pulsations rises to 6%, with scale reaching 20%. In the middle section of the shear zone the parameter Γ at the end of the channel is equal to 5.7, and pulsations increase by a factor of 1.5.

Fig. 5 shows the intensity of pulsations as the ratio of the local value ε_1 to the minimum value of pulsations in this zone ε_0. This enables comparison of the behavior of turbulence in different experiments (points 1-3 are taken from Ref. 3-5). The parameters that characterize the conditions of the experiments [Ref. 1, 3-5] are summarized in the table. In our experiments, Γ^* is 2-8 times the

Parameters	[3]	[3]	[4]	[5]	Present paper
U_1, m/s	16.4	12.4	5	16.4	7.5
$\partial U_1/\partial x_2$, s^{-1}	15	12.6	5.5	15.6	130
$(U_1 M/\nu)\cdot 10^{-3}$	11	24	2	11.4	0.5
$Re^*\cdot 10^{-3}$	0.23	0.47	0.08	1.77	0.12
Γ^*	2.7	3.3	5.4	7.2	18
Π_1	0.74	0.72	0.75	0.8	0.45
Π_2	0.35	0.34	0.32	0.31	0.26
Π_3	0.504	0.484	0.383	0.465	0.28
Π_4	0.638	0.575	0.505	0.605	0.505

value attained in the mentioned references. This explains the quite obvious increase in turbulence energy, a possibility that was doubted by the authors of Ref. 4 in their experiments, and which amounted to 25% in Ref. 5. In these papers, as in Ref. 1-3, shear flow occupies the entire cross section of the channel; boundary layers on the walls limit the length on which development of the initial flow can be traced, and this applies to a greater extent to zones with maximum Γ, situated at the wall on the side with lower velocity U_1.

Analysis of the results confirms the hypothesis expressed in Ref. 6, according to which small-scale turbulent flow with constant shear at a sufficient remove from the input device acquires a structure for which the following quantities are typically constant: parameter of turbulence deformation $\Pi_1 = \sqrt{E}/\Lambda_2(\partial U_1/\partial x_2)$ (characterizing the local effect of shear on turbulence on the scale of the eddies

that contain energy; Λ_2 is transverse scale), the local ratio of turbulent stress to energy $\Pi_2 = \langle u_1 u_2 \rangle / E$, the local anisotropy of pulsations with respect to the coordinate axes: $\Pi_3 = \langle u_2^2 \rangle / E$ and $\Pi_4 = \langle u_3^2 \rangle / E$. This state is possible only in developed turbulent flow in which the turbulent Reynolds number $Re = \sqrt{E}\Lambda_2/\nu$ is great enough ($>10^3$) that the effect of molecular viscosity on turbulence structure can be disregarded. The maximum value of Re* and the limiting values of the indicated parameters Π_1^*, Π_2^*, Π_3^*, Π_4^* attained in the experiments of Ref. 1-5 and in our research are summarized in the table. Scatter of the limiting values of the parameters can be attributed to inadequate Reynolds numbers Re* in most of the experiments. The behavior of the parameters Π_1, Π_2, Π_3, Π_4 as a function of total deformation Γ as plotted from the results of our research in region A is shown in Fig. 6. The quantity Λ_2 appearing in Re and Π_1 was not measured in our work, and was taken as $0.5\Lambda_1$ in the calculations. The basis for this was the scale measurements in Ref. 1, 3-5. Close to the input device, the ratio between scales is not satisfied, and the given parameters in this region (see Fig. 6) are not determined. The plotted curves show that the equilibrium state of shear turbulence was not reached in our experiments.

The author thanks A. A. Pavel'yev for continued cooperation in this work.

REFERENCES

1. Rose, W. G., "Results of an Attempt to Generate a Homogeneous Turbulent Shear Flow," J. FLUID MECH., Vol 25, Part 1, 1966.

2. Rose, W. G., "Interaction of Grid Turbulence with a Uniform Mean Shear," J. FLUID MECH., Vol 44, Part 4, 1970.

3. Champagne, F. H., Harris, V. G. and Corrsin, S., "Experiments on Nearly Homogeneous Turbulent Shear Flow," J. FLUID MECH., Vol 41, Part 1, 1970.

4. Mulhearn, P. J. and Luxton, R. E., "The Development of Turbulence Structure in a Uniform Shear Flow," J. FLUID MECH., Vol 68, Part 3, 1975.

5. Richards, H. K. and Morton, J. B., "Experimental Investigation of Turbulent Shear Flow with Quadratic Mean-Velocity Profiles," J. FLUID MECH., Vol 73, Part 1, 1976.

6. Pavel'yev, A. A., "Development of Grid Turbulence in a Flow with Constant Velocity Gradient," IZVESTIYA AKADEMII NAUK SSSR: MEKHANIKA ZHIDKOSTI I GAZA, No 1, 1974.

6610
CSO: 1862/168

UDC 532.517

THREE-PARAMETER MODEL OF SHEAR TURBULENCE

Moscow IZVESTIYA AKADEMII NAUK SSSR: MEKHANIKA ZHIDKOSTI I GAZA in Russian No 3, 1978 pp 13-25

[Article by V. G. Lushchik, A. A. Pavel'yev and A. Ye. Yakubenko, Moscow]

[Text] A model of shear turbulence is proposed that uses transport equations for three turbulence characteristics: energy E, friction stress $\langle u'v' \rangle$ and the function F with dimensionality coinciding with that of the quantity $E^m L^n$. Known equations were used for the first two quantities; special treatment was needed to construct the third equation. The constants in the equations were determined from analysis of the flow behind a grid with constant shear, and from the behavior of the solution in different regions of flow in a channel. The results of numerical solution are given for flow in the channel, and a comparison is made with available experimental data.

1. When calculating flows in which the turbulence characteristics at a given point depend on their values at other points of the flow, it becomes necessary to use transport equations for some of the turbulence characteristics. Equations for different moments of pulsation motion are ordinarily used in deriving these equations. A method of getting such equations is described for example in Ref. 1. All terms in equations for Reynolds stresses $\tau_{ij} = -\langle u_i u_j \rangle$ are expressed in terms of the Reynolds stresses and the scale of turbulence [see Ref. 1-6].

The equation for scale L or some combination of L with $E = 0.5\langle u'_\alpha v'_\alpha \rangle$ has been obtained by a variety of methods. However, the equations derived by different authors [Ref. 1-12] for scale without consideration of diffusion terms are close to one another. Considerable discrepancy shows up when diffusion terms are considered since the use of combinations $E^m L^n$ and the gradient form of the diffusion term makes the equations nonequivalent.

Different papers that have recently been published do not agree on the number of transport equations for turbulence characteristics, or on the type of combination $E^m L^n$. Many papers consider flows only at high Reynolds numbers, so that the effect of viscosity can be disregarded. These papers are surveyed in Ref. 1-6.

In our paper we use transport equations for three turbulence characteristics; these equations retain terms with viscosity, enabling calculation of flow in a channel directly from the wall. Analysis of flow in the channel enabled isolation of combinations E^mL^n and equations for them such that the behavior of the investigated quantities at different distances from the wall coincides satisfactorily with experimental data.

Selection of the number and form of controlling parameters that characterize turbulence, for which the transport equations are to be written, is obviously determined by the problem under consideration.

For problems in which the influence of initial and boundary conditions is considerable, according to research by A. N. Kolmogorov [Ref. 8] and Prandtl [Ref. 9] we deal with two parameters: the energy E and scale L of turbulence. This is due to the fact that the quantities E and L can be independent and arbitrarily assigned in the initial cross section. For example when a grid is installed at the inlet, the turbulence energy behind it is determined by the porosity of the grid, while scale is determined by mesh size.

Among the other tangential components of the Reynolds stress tensor $\tau_{ij} = -\langle u_i' u_j' \rangle$ (the normal components were unified by introducing turbulence energy E), the important one in boundary layer problems is $-\langle u'v' \rangle$, called the friction stress τ.

We can assume that for some problems we have local dependence of τ on E and L, and also on the mean-velocity profile ($\partial u/\partial y$ for the boundary layer) and on viscosity ν. Dimensional analysis shows that $\tau/E = \Psi(z, R_T)$. Here $z = L|\partial u/\partial y|/\sqrt{E}$ is the dimensionless gradient of mean velocity, and $R_T = \sqrt{E}L/\nu$ is the turbulence Reynolds number. Expansion of the function Ψ in a series with respect to powers of z gives the known expression for τ [Ref. 7]

$$\tau = \beta(z, R_T)\sqrt{E}L\frac{\partial u}{\partial y} \tag{1.1}$$

The function β in Ref. 8, 9 was taken as constant, and later as a function of R_T only [Ref. 10], and finally [Ref. 11] as shown above. In any case the function β must be assigned for determination of τ.

However, in some problems where the velocity profile is asymmetric or has maxima, and zeros of $\partial u/\partial y$ and τ do not coincide, and also in problems where the prehistory of the flow plays a significant part, the use of expression (1.1) for τ may lead to unsatisfactory results. In such cases it is advisable to use a transport equation for friction stress.

It should be noted that in characterizing turbulence structure by only two parameters (E and L), we are assuming that the other turbulence characteristics as a rule are unknown beforehand in the initial cross section. Moreover, the volume of the available experimental information is also inadequate for using these quantities to approximate processes of generation, dissipation, exchange and diffusion in the corresponding transport equations.

To close the equations for the Reynolds stress tensor (1.1), we use hypotheses proposed in Ref. 12, 13, after modifying them somewhat.

In constructing the equation for turbulence scale L, we use the constructive approach proposed in Ref. 7. If it is assumed that the change of scale at a given point of a plane-parallel flow with constant velocity gradient is determined by the quantities E, L, $\partial u/\partial y$ and ν (considering that τ also depends on these quantities), then we can write

$$u\frac{\partial L}{\partial x}=f\left(E,L,\frac{\partial u}{\partial y},\nu\right)=f_1(E,L)+f_2(\nu,L)+f_3\left(\frac{\partial u}{\partial y},L\right) \tag{1.2}$$

This representation means that scale changes due to the action of turbulence energy, viscosity and mean-velocity gradient are independent. Then from dimensional analysis we get

$$f_1\sim\sqrt{E},\quad f_2\sim\nu/L,\quad f_3\sim L\left|\partial u/\partial y\right| \tag{1.3}$$

Let us note that there are terms of this type in Rotta's equation for scale [Ref. 12] obtained by integrating the equations for the second two-point moments of velocity. The only difference is in the expression for f_3, for which Rotta has $(\tau/E)L\partial u/\partial y$.

Thus for the formulated problem at the present time there is a sound basis for using as a minimum the two-parameter (E,L)-model of turbulence with expression (1.1) for τ or a three-parameter (E,L,τ)-model of turbulence with the appropriate transport equations.

2. Consider steady-state turbulent flow that is plane-parallel on average with mean velocity $u=u(y)$ (directed everywhere along the x-axis), $\partial u/\partial y$ being constant along the x-axis. Turbulence is taken as homogeneous, and diffusion of turbulence is absent. With these assumptions, from the equations for $\langle u_i'u_j'\rangle$ with consideration of closing relations and dimensional analysis for the scale of turbulence (see section 1), we get the following equations for E, L and τ [Ref. 7]:

$$u\frac{\partial E}{\partial x}=-\left(c\sqrt{E}\,L+c_1\nu\right)\frac{E}{L^2}+\tau\frac{\partial u}{\partial y} \tag{2.1}$$

$$u\frac{\partial L}{\partial x}=\left(c_2\sqrt{E}\,L+c_3\nu\right)\frac{1}{L}-c_4L\left|\frac{\partial u}{\partial y}\right| \tag{2.2}$$

$$u\frac{\partial \tau}{\partial x}=-\left(c_5\sqrt{E}\,L+c_6\nu\right)\frac{\tau}{L^2}+c_7E\frac{\partial u}{\partial y} \tag{2.3}$$

To evaluate the constants c, c_1, c_2, c_3 in the equations for E and L, we consider the degeneration of turbulence in flow behind grids with $\partial u/\partial y=0$ [Rf. 14, 15]. On the initial stage of degeneration at large R_T when viscous terms can be disregarded, $\sqrt{E}L\approx\text{const}$, which defines a relation between c and c_2 of the form $c_2=0.5\,c$. Analysis of experimental data yields $c=0.3$-0.4. On the final stage of degeneration of grid turbulence at low R_T, where $E\sim x^{-5/2}$ and $L\sim x^{1/2}$, we get $c_3=0.2c_1$, and $c_1=5\pi/4$.

The constant c_5 in the equation for τ can be evaluated from analysis of experiments on uniform anisotropic turbulence [Ref. 16], giving $c_5=(2.5$-$3)c$.

The constant c_6 in the viscous term of the equation for τ cannot be determined from experiments for uniform grid turbulence.

Estimates for the constants c_4 and c_7 in the equations for L and τ can be obtained from analysis of the development of grid turbulence with mean-velocity gradient. In Ref. 7 it is assumed that in development of grid turbulence at large R_T in a flow with constant velocity gradient far from the grid a turbulence structure is set up such that the quantities $\tau^\circ = \tau/E$ and $z = L\left|\partial u/\partial y\right|/\sqrt{E}$ are constant and independent of distance. Since system of equations (2.1)-(2.3) is to describe this state of turbulence, by transforming the equations for E, L, τ into equations for z and τ°, we get

$$u\frac{\partial z}{\partial x} = \left[c + 0.7\frac{c_1}{R_T} - \left(c_4 + \frac{\tau^\circ}{2}\right)z\right]\frac{\partial u}{\partial y} \tag{2.4}$$

$$u\frac{\partial \tau^\circ}{\partial x} = \left[c_7 z - \left(c_3 - c + \frac{c_6 - c_1}{R_T}\right)\tau^\circ - z\tau^{\circ 2}\right]\frac{\sqrt{E}}{L} \tag{2.5}$$

Then, assuming $R_T \gg 1$ and setting the derivative with respect to x equal to zero in (2.4), (2.5), we get the following expressions for constants c_4 and c_7:

$$c_4 = \frac{c}{z_*} - \frac{\tau_*^\circ}{2}, \quad c_7 = \tau_*^{\circ 2} + \frac{c\tau_*^\circ}{z_*}\left(\frac{c_3}{c} - 1\right) \tag{2.6}$$

Here z_* and τ_*° are the limiting values of z and τ° established far from the grid.

From analysis of experimental data of Ref. 17 on development of grid turbulence close to uniform with lengthwise-constant velocity gradient, we can establish values of z_* and τ_*° that are 1.37-1.47 and 0.27-0.29 respectively for the two grids used in the experiment. It should be noted that the quantity $z_*\tau_*^\circ$ found in the experiment [Ref. 17] for the two grids is 0.4. This imposes a restriction on the value of c that is implied by solution of equation (2.1) for turbulence energy E in the limiting state ($z = z_* = \text{const}$, $\tau^\circ = \tau_*^\circ = \text{const}$, $R_T \gg 1$)

$$\frac{E}{E_0} = \exp\left[\frac{x - x_0}{uz_*}\frac{\partial u}{\partial y}(z_*\tau_*^\circ - c)\right]$$

From the solution we can see that when $c = z_*\tau_*^\circ \approx 0.4$ the turbulence energy will not increase with increasing x, which contradicts the results of measurements of Ref. 17. The required rate of increase is ensured by a value c = 0.3, which is the figure taken for subsequent estimates and calculations.

Substituting the values c = 0.3 and $c_5/c = 2.5$-3 in expressions (2.6) when $z_* = 1.37$-1.47 and $\tau_*^\circ = 0.27$-0.29, we get a range of variation of constants $c_4 = 0.05$-0.07 and $c_7 = 0.16$-0.21.

Thus from an analysis of experimental data on the development of grid turbulence in a flow with constant velocity gradient we get the following estimates for constants in equations (2.1)-(2.3):

$$c = 0{,}3,\ c_1 = 5\pi/4,\ c_2 = 0.5c,\ c_3 = 0.2c_1,\ c_4 = 0.05\text{—}0.07,\ c_5 = (2.5\text{—}3)c,\ c_7 = 0.16\text{—}0.21 \tag{2.7}$$

As we pointed out above, this analysis could not give an estimate for c_6, and therefore this constant will be estimated below in analysis of flow in a channel.

From the standpoint of replacing the equation for τ with relation (1.1) the relation for $\beta(z, R_T)$ is of interest with regard to its approximate determination

from equation (2.3) for τ in which the term R_T is not omitted as previously. Setting the derivative of τ with respect to x equal to zero, we get

$$\beta = \frac{2c_7}{\Pi + (\Pi^2 + 4c_7 z^2)^{1/2}}, \quad \Pi = c_5 - c + \frac{c_6 - c_5}{R_T} \tag{2.8}$$

Analysis of the function $\beta(z, R_T)$ of (2.8) shows that when $R_T \ll 1$, $\beta \approx (c_7/c_6)R_T$, and when $R_T \gg 1$ and $z \ll 1$, $\beta \approx c_7/(c_5 - c)$.

For subsequent analysis of equations in the case of nonuniform turbulence (e. g. with flow in a channel) where diffusion terms cannot be disregarded, it is advisable, as will be shown below, to use the combination $F = E^m L^n$ instead of the scale of turbulence L. In the non-diffusion approximation, using equations (2.1), (2.2) for E and L, we readily get an equation for F:

$$U\frac{\partial F}{\partial x} = -\left[\left(m - \frac{n}{2}\right)c\sqrt{E}L + \left(m - \frac{n}{5}\right)c_1\nu\right]\frac{F}{L^2} + \left(m\frac{\tau}{E}\frac{\partial u}{\partial y} - nc_4\left|\frac{\partial u}{\partial y}\right|\right)F \tag{2.9}$$

It is completely obvious that in the case of uniform turbulence systems of equations (2.1)-(2.3) and (2.1), (2.3), (2.9) are equivalent, and the function F has no advantages over the scale of turbulence L. On the other hand, when diffusion terms are included in the equations with approximation that is quite rough, the difference will be considerable.

3. New terms must be included in equations (2.1), (2.3) to account for turbulence characteristics. In this paper we use the gradient representation of diffusion terms that has already become widely accepted, according to which the diffusion of some turbulence characteristic that we will denote by Φ is written as

$$\frac{\partial}{\partial y}\left[(a_\Phi\sqrt{E}L + \alpha_\Phi\nu)\frac{\partial \Phi}{\partial y}\right]; \quad \Phi = E, \tau, F; \quad a_\Phi, \alpha_\Phi = \text{const} \tag{3.1}$$

Consider steady-state flow in a channel where convective terms can be disregarded. The equations for E and τ (in plane geometry) will take the following respective forms:

$$\frac{\partial}{\partial y}\left[(a_E\sqrt{E}L + \alpha_E\nu)\frac{\partial E}{\partial y}\right] - c\frac{E^{3/2}}{L} - c_1\nu\frac{E}{L^2} + \tau\frac{\partial u}{\partial y} = 0 \tag{3.2}$$

$$\frac{\partial}{\partial y}\left[(a_1\sqrt{E}L + \alpha_1\nu)\frac{\partial \tau}{\partial y}\right] - c_3\frac{\sqrt{E}}{L}\tau - c_4\nu\frac{\tau}{L^2} + c_7E\frac{\partial u}{\partial y} = 0 \tag{3.3}$$

To evaluate the constants in the diffusion terms and the constant in the viscous term of the equation for τ, we consider three different regions of flow in the channel: viscous sublayer, logarithmic layer and core of the flow.

In the first region, characterized by direct proximity to the wall, the flow velocity depends linearly on distance from the wall, and the principal terms of equations (3.3), (3.4) will be viscous. On the basis of the known experimental fact [Ref. 18, 19] that $E \sim y^2$, (3.2) implies

$$L = (c_1/2a_E)^{1/2}y = ky \tag{3.4}$$

From equation (3.3) for τ, setting $\tau \sim y^p$, we can get a relation between constants c_6 and α_τ of the form

$$c_6 = 0.5p(p-1)c_1\alpha_\tau/\alpha_E \tag{3.5}$$

With respect to power p it is known that $p = 3$-4. For $p = 3$, according to (3.5), we get $c_6 = 3c_1\alpha_\tau/\alpha_E$. As to the value $p = 4$, the use of estimate (3.5) for c_6 will be incorrect since in this case in equation (3.3) for τ it is necessary to consider the term $c_7 E\partial u/\partial y$ that is of the same order of magnitude (y^2) as the viscous terms. In this case we get the following estimate for c_6:

$$c_6 = 6\alpha_\tau/\alpha_E + 0.5c_7\alpha_E E_0/\tau_0 \tag{3.6}$$

Here E_0 and τ_0 are coefficients in the power laws of variation of E and τ in the viscous sublayer at the wall, written in universal coordinates.

If we assume constants $\alpha_E = \alpha_\tau = 1$, the law of variation $\tau \sim y^3$ gives $c_6 = 3c_1$. For $\tau \sim y^4$, using experimental data of Ref. 18, 19 for evaluating E_0, empirical relations of Deissler and Van Driest for τ, according to which $\tau_0 \approx 2.4 \cdot 10^{-4}$, and also the estimates of (2.7) for constants c_1 and c_7, we get $c_6 \approx 7c_1$. The scale of turbulence in the viscous sublayer at the wall will vary as $L \approx 1.4y$.

Let us note that constants α_E and α_τ may have other values in different versions of notating the dissipative terms in equations for the Reynolds stress tensor.

The region of the logarithmic layer is characterized by the fact that the flow velocity therein varies in accordance with a logarithmic law

$$u_+ = \frac{1}{\varkappa}\ln y_+ + C, \quad u_+ = \frac{u}{u_*}, \quad y_+ = \frac{yu_*}{\nu} \tag{3.7}$$

Here $u_* = \sqrt{\tau_w/\rho}$ is dynamic velocity, $\kappa = 0.4$ is the Kármán constant, $C = 5.2$-5.5, and the turbulence energy E and friction stress τ are nearly constant [Ref. 18, 20]. The latter means that the diffusion terms in the equations for E and τ can be disregarded, and this is confirmed by measurements of the components of turbulence energy balance in this region [Ref. 18].

From equation (3.2) for E in which only terms with generation and dissipation are retained (at $R_T \gg 1$), we find that

$$L = \frac{cE^{3/2}}{\tau\,\partial u/\partial y} = c\varkappa\frac{(\sqrt{E}u_*)_l}{(\tau/E)_l} = k_l y \tag{3.8}$$

Here the subscript l denotes the value of the quantity in the logarithmic layer.

In equation (3.3) for τ we should retain terms with generation and complete dissipation since (as was shown above) $c_6 > c_1$, and the term $c_6\nu v/L^2$ at R_T typical of the logarithmic layer will be of the same order as terms $c_5\tau\sqrt{E}/L$ and $c_7 E\partial u/\partial y$. From equation (3.3) in the logarithmic layer, using the expression for L obtained above, we can evaluate the constant c_6

$$c_6 = c^2\varkappa\frac{(E/u_*^2)_l}{(\tau/E)_l}\left[\frac{c_7}{(\tau/E)_l^2} - \frac{c_5}{c}\right]y_+ \tag{3.9}$$

Substituting the values of the constants in the expressions for c_6 and L, as well as the quantities τ and E in the logarithmic layer from experiments of Ref. 18, 20, we get $L \approx 1.1y$, $c_6 \approx 0.55y_+$. For $y_+ = 50$–100 corresponding to the region of the logarithmic layer, we get $c_6 \approx (7\text{–}14)c_1$.

Thus the value of constant c_6 from estimates in the logarithmic layer was greater than the value $3c_1$ corresponding to the law of variation of τ in the viscous sublayer at the wall y^3. This means that the equation (3.3) for τ with the given set of constants corresponds to a law of variation of τ with power close to 4.

In the region of developed flow in a channel, the viscous terms in both equations (3.2) and (3.3) can be disregarded. As to the diffusion terms, although they are small, they do play a considerable part in the general balance [Ref. 18], particularly close to the axis of symmetry. The results of measurements of the distribution of E and τ in channels [Ref. 18] shows that in the midsection of the channel ($0.3 \leqslant y/h \leqslant 0.6$, where h is channel radius or half-width) the relation $\tau/E = \text{const}$ is satisfied with fair accuracy. Using this principle we can establish the relation between constants a_E and a_τ in equations (3.2) and (3.3), viz.: $a_\tau = (c_5/c)a_E$. In doing this, we can also get an expression for the ratio of τ to E in the core of the flow in terms of the constants c, c_5, c_7 appearing in the equations: $\tau/E = (cc_7/c_5)^{1/2}$. Upon substitution of the values of these constants (see section 2) in this expression we get $\tau/E \approx 0.26$, which corresponds to the experimental data. This indicates correct choice of the constants c, c_5, c_7 obtained from analysis of the development of grid turbulence in a flow with constant velocity gradient.

Thus from analysis of experimental data on developed flow in a channel we have obtained the following estimates for the constants in the diffusion terms of equations (3.2), (3.3) for E and τ, and for the constant c_6:

$$a_E = a_\tau = 1, \quad a_\tau = (c_5/c)a_E = (2.5\text{–}3)a_E, \quad c_6 = (7\text{–}14)c_1 \tag{3.10}$$

The constant a_E must be determined by trial and error from conditions of agreement of the results of the calculation with experimental data on flow in a channel.

4. The use of representation (3.1) for the diffusion terms in the equations for E and τ, generally speaking, is known, and currently available calculations as well as the above analysis of equations for E and τ in different parts of the channel indicate correct description of the main features of flows with variable velocity gradient in the presence of walls.

As to the function $F = E^m L^n$, the equations for F in nonuniform flows become nonequivalent at different m and n. In this connection we are faced with the question of which combination for F is preferable from the standpoint of notating the diffusion term in form (3.1).

To answer this question, let us analyze the equation for F, which in the case of developed flow in a channel will take the following form:

$$\frac{\partial}{\partial y}\left[(a_t\sqrt{E}L+a_\nu\nu)\frac{\partial F}{\partial y}\right]-\left(m-\frac{n}{2}\right)c\frac{\sqrt{E}}{L}F-\left(m-\frac{n}{5}\right)c_1\nu\frac{F}{L^2}+\left(m\frac{\tau}{E}-nc_1\right)F\frac{\partial u}{\partial y}=0 \tag{4.1}$$

Let us consider combinations for $F = E^m L^n$ that have been used previously (see for example the survey in Ref. 3): L, L^2, $E^{1/2}L$, $E^{1/2}L^{-1}$, EL^{-2}, $E^{1/2}L^{-1}$, E^2L^{-1}, and also the dissipation of turbulence energy ε, which in equation (2.1) for E is represented as $\varepsilon = cE^{1/2}L^{-1} + c_1\nu EL^{-2}$, i. e. essentially a combination of the expressions for F enumerated above.

We will conduct our analysis for the same regions of the flow in a channel as in section 3 in examining the equations for E and τ. The principal requirement will be a positive value of the constants a_F and α_F, and also absence of singularities in the viscous terms in consideration of the flow in the viscous sublayer at the wall.

In the core of the flow, as noted above, there is approximate equilibrium between processes of turbulent diffusion and dissipation (its turbulent part). Retaining the corresponding terms in equations (3.2), (4.1) for E and F, and setting the coefficient of turbulent diffusion $D \sim \sqrt{E}L$ in the paraxial region (which is proportional to the coefficient of turbulent viscosity $\nu_T = \beta\sqrt{E}L$, where $\beta = \text{const}$ in this region) equal to a constant in accordance with Ref. 21, we establish the relation between constants a_F and a_E

$$a_F = a_E(2m+1)/(2m-n) \tag{4.2}$$

We can see from (4.2) that the condition $a_F > 0$ when $m \geq 0$ implies the inequality $n < 2m$. Among the combinations of F enumerated above, the only ones that satisfy this inequality are EL and those with $n < 0$, i. e. with L in the denominator. Other combinations (any with $m = 0$, $n > 0$) and $E^{1/2}L$, which corresponds to zero diffusion in the paraxial region, will give an incorrect description of the diffusion processes near the axis at $a_F > 0$, and consequently of the behavior of the turbulence characteristics as well. This situation can be changed by introducing the corresponding empirical functions in the diffusion term or by writing additional terms, which unduly complicates the equation for F.

In the logarithmic layer, as noted above, the diffusion term in the turbulence energy equation can be disregarded.

This cannot be done in the equation for F, since the scale of turbulence in the logarithmic layer according to (3.8) is not constant. From equation (4.1) with the use of expression (3.8) for L, as well as law (3.7) for the velocity profile in the logarithmic layer, we can get an expression for a_F

$$a_F = -\frac{1}{n}\frac{1}{c\varkappa^2}\frac{(\tau/E)_l}{(E/u_*^2)_l}\left[\frac{1}{2}\left(\frac{\tau}{E}\right)_l - c_4\right] \tag{4.3}$$

An interesting peculiarity of the resultant expression for a_F is that it does not depend on exponent m in the combination $F = E^m L^n$, i. e. in this flow region the sign of exponent n is the controlling factor. Actually, since in accordance with experimental data [Ref. 18, 20] $(\tau/E)_l \approx 0.23$ in the logarithmic layer, while estimates for uniform turbulence (section 2) give $c_4 \approx 0.06$, i. e. $0.5(\tau/E)_l - c_4 > 0$, the sign of a_F depends on the sign of exponent n. From (4.3) it is clear that when $n > 0$, the constant $a_F < 0$. To get $a_F > 0$ it is necessary either to change the constant c_4 in the equation for F ($c_4 > 0.5(\tau/E)_l \approx 0.12$), or to introduce an empirical function in the diffusion term, or to add new terms to the equation for F.

Thus the combinations for F in which L is in the numerator, i. e. $n>0$, are unsuitable from this standpoint. Since combinations with $n<0$ do not give rise to this difficulty, and they satisfy relation (4.2) for α_F obtained in the paraxial region, we will consider below only the combinations for F with L in the denominator.

Retaining only viscous terms in equation (4.1) for F, and using for L expression (3.4) derived from analysis of the equation for E in the viscous sublayer (under condition $E \sim y^2$), we can evaluate the order of the term that describes viscous dissipation F

$$\left(m-\frac{n}{5}\right)c_1\nu\frac{F}{L^2}\sim y^{2m+n-2} \tag{4.4}$$

From (4.4) we can see that the condition of abatement or finiteness of the dissipative term as the wall is approached ($y\to 0$) implies the inequality $m\geqslant 1-0.5n$. At $n<0$ this means that combinations like $E^{1/2}L^{-1}$ and EL^{-2} will have a singularity unless corrections are introduced at the walls. For combinations like $E^{1/2}L^{-1}$ and $E^{3/2}L^{-1}$ that satisfy the inequality $m\geqslant 1-0.5n$, the dissipative term does not have a singularity at the wall.

For further analysis of the two groups of combinations that do and do not satisfy the inequality $m\geqslant 1-0.5n$, we take the following: $f=E^{3/2}L^{-1}$ and $\omega=EL^{-2}$. The first is a quantity that is proportional to dissipation of turbulence energy ε at $R_T\gg 1$ ($\varepsilon=cf$), and the second is the characteristic value of the square of the turbulence frequency introduced by A. N. Kolmogorov [Ref. 8].

When the substitution $L=E^{3/2}/f$ is used, the equations for E and f in the viscous sublayer will have the form (the prime indicates the derivative with respect to the y coordinate)

$$\alpha_E\nu E''=c_1\nu\frac{f^2}{E^2},\qquad \alpha_f\nu f''=1.7c_1\nu\frac{f^3}{E^3} \tag{4.5}$$

Equation (4.5), under condition that $E\sim y^2$, implies $\alpha_f=1.7\alpha_E$. Using the relation between constants α_f and α_E, we can get the solution of equations (4.5) for E and f in the viscous sublayer (all quantities are dimensionless)

$$E=\frac{c_1}{\alpha_E}\frac{p^2}{2}(y^2+qy),\qquad f=\frac{c_1}{\alpha_E}\frac{p^3}{2}(y^2+qy) \tag{4.6}$$

Here p and q are constants; the two other constants are determined from the boundary conditions: $E=f=0$ at $y=0$.

It can be seen from (4.6) that the solution for E in the viscous sublayer contains a linear term in addition to the quadratic term that corresponds to experimental data. In the general case the constant q that should be determined by assignment of the boundary condition on the other boundary (the axis of symmetry in a channel) will not necessarily be equal to zero. Therefore, in order to guarantee that we single out the solution sith $E\sim y^2$, it is necessary to use relation (3.4) for L in equation (3.2) for E within the limits of the viscous sublayer (i. e. in term $c_1\nu E/L^2$, which is the principal term there) in addition to the relation for α_f.

It should be noted that generally speaking relation (3.4) cannot be used in the case of another combination for F, e. g. E^2L^{-1} or E^3L^{-2} since in this case $F/E \neq \text{const}$, as in solution (4.6).

The equations for E and ω close to the wall take the form

$$\alpha_E \nu E'' = c_1 \nu E/L^2, \quad \alpha_\omega \nu \omega'' - c\omega^2 = 1.4 c_1 \nu \omega / L^2 + c_4 \omega u' \tag{4.7}$$

When $L \sim y$ and $E \sim y^2$, the quantity ω/L^2 in the term with viscous dissipation has a singularity at $y = 0$. This singularity can be avoided if the dissipative term in the equation for ω is represented in the form $1.4c_1\nu(\omega - \omega_0)/L^2$. Here ω_0 is the value of ω on the wall, which is determined from the equation for E

$$\omega_0 = \frac{1}{2} \frac{\alpha_E}{c_1} \frac{E'^2}{E} \tag{4.8}$$

Let us note that when $E' = 0$, we have $\omega_0 = 0$ and both representations for the dissipative term are identical. The constant α_ω in the diffusion term of the equation for ω may be estimated in the following way. Setting terms with viscosity equal in the equation (4.7) for ω at the wall, and representing ω as $\omega = \omega_0 + \omega_1 y^p$, we find that the minimum whole-number value of p is 2, and $\alpha_\omega = 1.4\alpha_E$.

Thus from analysis of flow in a channel for combinations $f = E^{3/2}/L$ and $\omega = E/L^2$ we get the following estimates of the constants in the diffusion term of equation (4.1) for F:

$$\alpha_F = \alpha_E = 0.05 \div 0.1 \ (F = f, \omega); \quad \alpha_f = 1.7\alpha_E; \quad \alpha_\omega = 1.4\alpha_E$$

If we consider flows only at high turbulence Reynolds numbers R_T, where the viscous terms in the equations can be disregarded, then obviously we cannot give preference to any combination for F with $n < 0$. As applied to flow in a channel, this means that the boundary conditions must be assigned outside of the viscous sublayer (for example in the logarithmic layer). The possibilities of such an approach were realized in Ref. 22, where calculations of a wide class of flows were done for the combination $E^{3/2}/L$, and completely satisfactory results were obtained.

5. The system of equations of motion and for the quantities E, τ, f or ω for developed flow in a channel takes the following form:

$$\frac{1}{R} \frac{du}{dy} = r - \tau, \quad y = 1 - r \tag{5.1}$$

$$\frac{1}{r^i} \frac{d}{dy}\left(r^i D_E \frac{dE}{dy}\right) - \left(\frac{c_1}{R.L^2} + c\frac{\sqrt{E}}{L}\right) E = -\tau \frac{du}{dy} \tag{5.2}$$

$$\frac{1}{r^i} \frac{d}{dy}\left(r^i D_\tau \frac{d\tau}{dy}\right) - i\frac{D_\tau}{r^2}\tau - \left(\frac{c_6}{R.L^2} + c_5 \frac{\sqrt{E}}{L}\right)\tau = -c_1 E \frac{du}{dy} \tag{5.3}$$

$$\frac{1}{r^i} \frac{d}{dy}\left(r^i D_f \frac{df}{dy}\right) - \left(\frac{1.7c_1}{R.L^2} + 2c\frac{\sqrt{E}}{L}\right) f = -\left(\frac{3}{2}\frac{\tau}{E} + c_4\right) f \frac{du}{dy} \tag{5.4}$$

$$\frac{1}{r^i} \frac{d}{dy}\left(r^i D_\omega \frac{d\omega}{dy}\right) - \left\{\frac{1.4c_1}{R.L^2}\left[\omega - \frac{1}{2}\frac{\alpha_E}{c_1 E}\left(\frac{dE}{dy}\right)^2\right] + 2c\frac{\sqrt{E}}{L}\right\}\omega = -\left(\frac{\tau}{E} + 2c_4\right)\omega \frac{du}{dy} \tag{5.5}$$

Here $L=E^{3/2}/f$ or $L=(E/\omega)^{1/2}$; $D_\Phi=a_\Phi\sqrt{E}L+a_\Phi/R_*$, $\Phi=E, \tau, f, \omega$; $i=0$ corresponds to a flat channel, and $i=1$ corresponds to an axisymmetric channel.

System (5.1)-(5.5) is written in dimensionless form. The half-width h or radius r of the channel is taken as the characteristic length, and the characteristic velocity is the dynamic velocity $u_*^2=|d\bar{P}/d\bar{x}|h/2$, $R_*=\bar{h}\bar{u}_*/\nu$ is the Reynolds number defined with respect to u_*.

The boundary conditions in the given case will have the following form.

On the axis of the channel (y = 1) from the condition of symmetry

$$E'(1)=f'(1)=\omega'(1)=0, \quad \tau(1)=0 \tag{5.6}$$

On the wall of the channel (y = 0), depending on which function (f or ω) is used in the calculation, the boundary conditions are assigned differently. In the case of system (E, τ, f)

$$E(0)=\tau(0)=f(0)=0 \tag{5.7}$$

The constants in equations (5.2) and (5.4) for E and f are chosen in such a way that as the wall is approached ($y\to 0$), $E\sim y^2$ and $f\sim y^2$. In the case of system (E, τ, ω), the following boundary condition is assigned to ensure the required order to which turbulence energy E vanishes:

$$E(0)=E'(0)=\tau(0)=0 \tag{5.8}$$

The quantity $\omega(0)=\omega_0$ is found only after solution of the problem.

In accordance with the estimates made in sections 2-4, the following constants were taken in equations (5.2)-(5.5):

$$\begin{gathered} c=0.3, \quad c_1=5\pi/4, \quad c_4=0.04, \quad c_5=3c, \quad c_6=9c_1, \quad c_7=0.2 \\ \alpha_E=\alpha_1=1, \quad \alpha_f=1.7\alpha_E, \quad \alpha_\omega=1.4\alpha_E, \quad \alpha_\tau=(c_5/c)\alpha_E, \quad \alpha_E=\alpha_f=\alpha_\omega=0.06 \end{gathered} \tag{5.9}$$

Constants c_4, c_6 and α_E, for which the estimates were quite approximate, were selected from the condition of best coincidence of the results of calculation with experimental data [Ref. 18, 20] within the range set by the estimates.

System of equations (5.2)-(5.4) or (5.5) with boundary conditions (5.6), (5.7) or (5.8) respectively at the values of constants (5.9) was numerically solved. A sweep method with iteractions was used for system (E, τ, f), and a matrix sweep method with iterations was used in the case of system (E, τ, ω). In the latter case the equations for E and ω were simultaneously solved since boundary conditions (5.8) on the wall of the channel were assigned only for turbulence energy E, and ω_0 is determined from solution of the problem. After each iteration, the mean velocity distribution was found by integrating equation of motion (5.1) with boundary condition u(0) = 0. A nonuniform grid was required because of the small parameter R_*^{-1} on the leading derivative in the equations. The step along the y coordinate was rather close at the wall ($\Delta y = 0.976\cdot 10^{-5}$), and then increased with approach to the axis of symmetry ($\Delta y = 0.04$). The number of iterations fluctuated from 40 to 90. The quantity R_* was used as the parameter in the calculations.

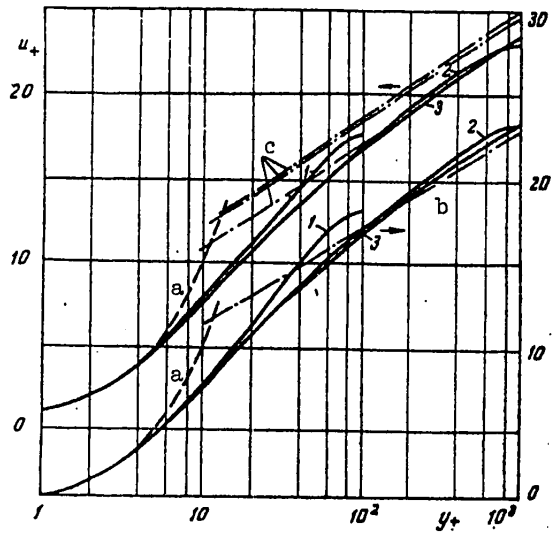

Fig. 1

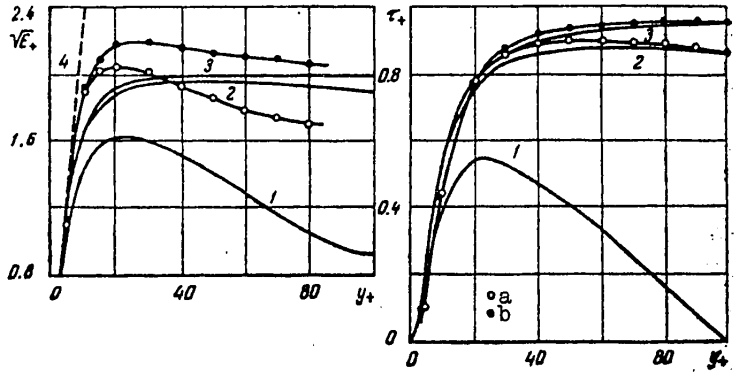

Fig. 2

Then from the resultant solution the mean discharge rate U was determined and used to calculate the Reynolds number $R = 2hU/\nu$ (or $R = 2r_0U/\nu$).

The calculations were done both for a circular pipe and for a flat channel. The results of the calculation and comparison with experimental data [Ref. 18, 20] are shown in Fig. 1-5. The calculations were done with respect to the two systems of equations ((E, τ, f) and (E, τ, ω)) and the results were close. Therefore the graphs give the results of calculation only for the system (E, τ, ω). Since experimental data have been extensive for a circular pipe in the region near the wall [Ref. 18], calculation was compared with experiment in more detail for this case than for a flat channel.

Fig. 1 shows velocity profiles with flow in a circular pipe (lower curves) and in a flat channel: a--$u_+ = y_+$; b--$u_+ = 5.75 \ln y_+ + 5.5$; c--$u_+ = K \ln y_+ + C$ for $R_* = 2300$,

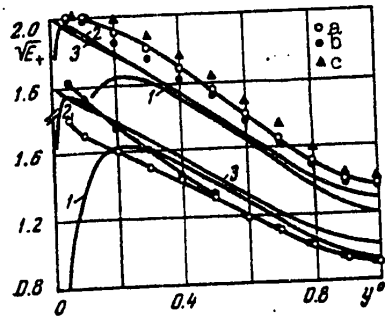

Fig. 3

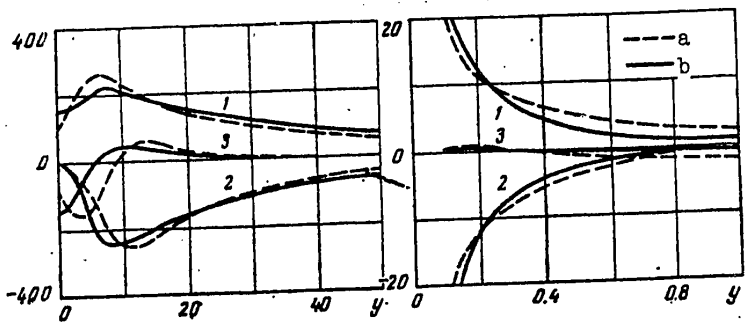

Fig. 4

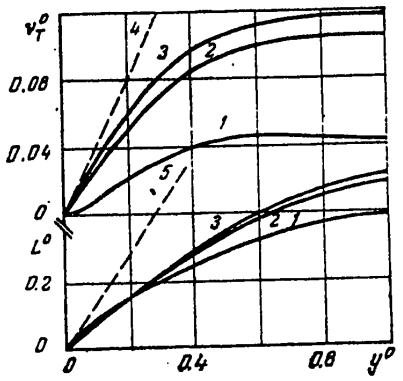

Fig. 5

4800, 8200 from experimental data of Ref. 20. Calculated curves 1, 2, 3 on Fig. 1-3, 5 correspond to $R_* = 10^2$, 10^3, 10^4. Fig. 2 shows the behavior of turbulence energy $\sqrt{E_+} = \sqrt{E}/u_*$ and turbulent friction $\tau_+ = \tau/u_*^2$ in the wall region of a circular pipe: a, b--$R_* = 1150$, 8750 (experimental data of Ref. 18), 4--$E_+ = 0.05y_+^2$. Shown on Fig. 3 (lower curves) is the behavior of turbulence energy in the core of the

flow in a circular pipe (notation the same as in Fig. 2). Fig. 4 shows the balance of turbulence energy in a circular pipe: 1--dissipation; 2--generation; 3--diffusion; a--experiment [Ref. 18] at $R_* = 1150$; b--calculation at $R_* = 10^3$. As an illustration, Fig. 5 shows the results of calculation for a circular pipe with respect to the coefficient of turbulent viscosity $\nu_T^0 = \nu_T/u_* r_0$ ($\nu_T = \tau/(\partial u/\partial y)$) and the scale of turbulence $L^\circ = L/r_0$, which are widely used in a variety of semi-empirical theories (4--$\nu_T^0 = 0.4y^\circ$, 5--$L^\circ = 1.4y^\circ$). As we can see, their behavior conforms completely satisfactorily to generally accepted ideas. Fig. 5 (upper curves) shows the behavior of turbulence energy in the core of the flow in a flat channel: a, b, c--$R_* = 2300$, 4800, 8200 (experiments of Ref. 20).

Summing up our verification of the proposed turbulence model, we can note the following. The model of turbulence for all three quantities (E, L, τ) enables a description of the development of grid turbulence in a flow with constant (including zero) mean velocity gradient [Ref. 7]. The model successfully explains and describes such a nontrivial result [Ref. 17] as the increase in turbulence energy at great distances from the grid in a flow with constant velocity gradient. Results are also satisfactory in the part of the calculation of turbulence characteristics in channel flow, where conventional models (for example Ref. 23) cannot describe plane and axisymmetric flows unless the constants are changed in the equations. Flow calculations in a plane channel done in Ref. 24 using the proposed turbulence model are generalized in our paper to the case of flow in a circular pipe.

Thus we have reason to hope that flows that are combinations of the classes enumerated above, for which the proposed model has been verified, will also be described within the framework of this model.

The authors thank V. M. Iyevlev and participants in seminars of G. N. Abramovich and G. A. Lyubimov for discussing the work.

REFERENCES

1. Monin, A. S. and Yaglom, A. M., "Statisticheskaya gidromekhanika" [Statistical Hydromechanics], Part 1, Moscow, "Nauka", 1965.

2. Bradshaw, P., "The Understanding and Prediction of Turbulent Flow", AERON. JOURNAL, Vol 76, No 739, 1972.

3. Launder, B. E. and Spalding, D. B., "Lectures in Mathematical Models of Turbulence", London-N. Y., Academy Press, 1972.

4. Mellor, G. L. and Herring, H. J., "Survey of the Mean Turbulent Field Closure Models", AIAA JOURNAL, Vol 11, No 5, 1973.

5. Iyevlev, V. M., "Turbulentnoye dvizheniye vysokotemperaturnykh sploshnykh sred" [Turbulent Motion of High-Temperature Continuous Media], Moscow, "Nauka", 1975.

6. Abramovich, G. N., Krasheninnikov, S. Yu. and Sekundov, A. N., "Turbulentnyye techeniya pri vozdeystvii ob"yemnykh sil i neavtomodel'nosti" [Turbulent Flows Under the Action of Body Forces and Non-Self-Similarity], Moscow, "Mashinostroyeniye", 1975.

7. Pavel'yev, A. A., "Development of Grid Turbulence in a Flow with Constant Velocity Gradient", IZVESTIYA AKADEMII NAUK SSSR: MEKHANIKA ZHIDKOSTI I GAZA, No 1, 1974.

8. Kolmogorov, A. N., "Equations of Turbulent Motion of an Incompressible Fluid", IZVESTIYA AKADEMII NAUK SSSR: SERIYA FIZICHESKAYA, Vol 6, No 1-2, 1942.

9. Prandtl, L., "Über ein penes Formelsystem für die ausgebildete Turbulenz", NACHR. GES. GOTTINGEN, MATH. PHYS., H. 6, 1945.

10. Glushko, G. S., "Turbulent Boundary Layer on a Flat Plate in an Incompressible Fluid", IZVESTIYA AKADEMII NAUK SSSR: MEKHANIKA, No 4, 1965.

11. Glushko, G. S., "Some Particulars of Turbulent Flows of Incompressible Fluid in Transverse Shear", IZVESTIYA AKADEMII NAUK SSSR: MEKHANIKA ZHIDKOSTI I GAZA, No 4, 1974.

12. Rotta, J., "Statistische Theorie nichthomogener Turbulenz", Z. PHYSIK, 1951, Bd 129, Nr 5, Bd 131, Nr 1.

13. Davydov, B. I., "Statistical Dynamics of an Incompressible Turbulent Fluid", DOKLADY AKADEMII NAUK SSSR, Vol 127, No 4, 1959.

14. Batchelor, G. K. and Townsend, A. A., "Decay of Turbulence in the Final Period", PROC. ROY. SOC. LONDON, SER. A, Vol 194, No 1039, 1948.

15. Batchelor, G. K. and Townsend, A. A., "Decay of Isotropic Turbulence in the Initial Period", PROC. ROY. SOC. LONDON, SER. A, Vol 193, No 1035, 1948.

16. Uberoi, M. S., "Equipartition of Energy and Local Isotropy in Turbulent Flows", J. APPL. PHYS., Vol 28, No 10, 1957.

17. Richards, H. K. and Morton, J. B., "Experimental Investigation of Turbulent Shear Flow with Quadratic Mean-Velocity Profiles", J. FLUID MECH., Vol 73, Part 1, 1976.

18. Laufer, J., "The Structure of Turbulence in Fully Developed Pipe Flow", NACA REPT., No 1174, 1954.

19. Khabakhpasheva, Ye. M., Mikhaylov, Ye. S., Perepemiza, B. V. and Yefimenko, G. I., "Experimental Investigation of the Structure of Wall Turbulence", in: "Pristennoye turbulentnoye techeniye" [Turbulent Wall Flow], Part 2, Novosibirsk, Institute of Thermal Physics, Siberian Department, USSR Academy of Sciences, 1975.

20. Comte-Belleau, J., "Turbulentnoye techeniye v kanale s parallel'nymi stenkami" [Turbulent Flow in a Channel with Parallel Walls], Moscow, "Mir", 1968.

21. Khintse, N. O., "Turbulentnost'" [Turbulence], Moscow, Fizmatgiz, 1963.

22. Hanjalic, K. and Launder, B. E., "A Reynolds Stress Model of Turbulence and its Application to Thin Shear Flows", J. FLUID MECH., Vol 52, Part 4, 1972.

23. Sekundov, A. N., "Application of Differential Equation for Turbulent Viscosity to Analysis of Plane Non-Self-Similar Flows", IZVESTIYA AKADEMII NAUK SSSR: MEKHANIKA ZHIDKOSTI I GAZA, No 5, 1971.

24. Lushchik, V. G., PAVEL'YEV, A. A. and Yakubenko, A. Ye., "Model of Shear Turbulence", Fourth All-Union Conference on Theoretical and Applied Mechanics, Abstracts of the Papers, Kiev, "Naukova dumka", 1976.

6610
CSO: 1862/169

- END -